

University of Windsor

Scholarship at UWindor

Electronic Theses and Dissertations

Theses, Dissertations, and Major Papers

2004

Supramolecular complexes containing pyridine N-oxides.

Dennis J. Hoffart
University of Windsor

Follow this and additional works at: <https://scholar.uwindsor.ca/etd>

Recommended Citation

Hoffart, Dennis J., "Supramolecular complexes containing pyridine N-oxides." (2004). *Electronic Theses and Dissertations*. 3672.

<https://scholar.uwindsor.ca/etd/3672>

This online database contains the full-text of PhD dissertations and Masters' theses of University of Windsor students from 1954 forward. These documents are made available for personal study and research purposes only, in accordance with the Canadian Copyright Act and the Creative Commons license—CC BY-NC-ND (Attribution, Non-Commercial, No Derivative Works). Under this license, works must always be attributed to the copyright holder (original author), cannot be used for any commercial purposes, and may not be altered. Any other use would require the permission of the copyright holder. Students may inquire about withdrawing their dissertation and/or thesis from this database. For additional inquiries, please contact the repository administrator via email (scholarship@uwindsor.ca) or by telephone at 519-253-3000ext. 3208.

Supramolecular Complexes

Containing

Pyridine *N*-Oxides

By

Dennis J. Hoffart

A Thesis

Submitted to the Faculty of Graduate Studies and Research

through the Department of Chemistry and Biochemistry

in Partial Fulfillment of the Requirements for

the Degree of Master of Science at the

University of Windsor

Windsor, Ontario, Canada

August, 2004



Library and
Archives Canada

Bibliothèque et
Archives Canada

Published Heritage
Branch

Direction du
Patrimoine de l'édition

395 Wellington Street
Ottawa ON K1A 0N4
Canada

395, rue Wellington
Ottawa ON K1A 0N4
Canada

Your file *Votre référence*
ISBN: 0-612-96379-9
Our file *Notre référence*
ISBN: 0-612-96379-9

The author has granted a non-exclusive license allowing the Library and Archives Canada to reproduce, loan, distribute or sell copies of this thesis in microform, paper or electronic formats.

L'auteur a accordé une licence non exclusive permettant à la Bibliothèque et Archives Canada de reproduire, prêter, distribuer ou vendre des copies de cette thèse sous la forme de microfiche/film, de reproduction sur papier ou sur format électronique.

The author retains ownership of the copyright in this thesis. Neither the thesis nor substantial extracts from it may be printed or otherwise reproduced without the author's permission.

L'auteur conserve la propriété du droit d'auteur qui protège cette thèse. Ni la thèse ni des extraits substantiels de celle-ci ne doivent être imprimés ou autrement reproduits sans son autorisation.

In compliance with the Canadian Privacy Act some supporting forms may have been removed from this thesis.

Conformément à la loi canadienne sur la protection de la vie privée, quelques formulaires secondaires ont été enlevés de cette thèse.

While these forms may be included in the document page count, their removal does not represent any loss of content from the thesis.

Bien que ces formulaires aient inclus dans la pagination, il n'y aura aucun contenu manquant.

Canada

© Dennis J. Hoffart 2004

All Rights Reserved

Abstract

In the first section, the coordination chemistry of a new, divergent, *N,O* ligand was investigated. Several metal complexes of 4,4'-bipyridine *N*-monoxide, **2a**, were characterised by X-ray crystallography, including Cu^I, Cu^{II}, Pd^{II}, Cd^{II}, Hg^{II}, and Eu^{III}. The observed non-covalent interactions and coordinative preferences of **2a** were contrasted with those of 4,4'-bipyridine and 4,4'-bipyridine *N,N'*-dioxide. Each of the compounds has a unique molecular topology that can be applied to the generation of ordered, pre-designed solids. Examples of this methodology are given with respect to the Cu^I, Cu^{II}, and Hg^{II} metal complexes.

Chapter three is concerned with the design and synthesis of multi-dimensional, polyrotaxane architectures. A new [2]pseudorotaxane, **3b** ⊂ DB24C8, was used as a divergent ligand to connect metal nodes into extended coordination frameworks. Three distinct polyrotaxane networks were synthesised, one two-dimensional net containing Cd^{II} in which one-dimensional polyrotaxane strands are pillared in the second dimension by **3b**. Two different three-dimensional topologies were generated using five different lanthanide cations. Structures containing Sm^{III}, Eu^{III}, Gd^{III}, Tb^{III} are isomorphous and adopt an α -polonium type lattice. The slightly smaller lanthanide, Yb^{III}, generates the previously unreported $\begin{pmatrix} 3 \\ 4,6 \\ 6 \end{pmatrix}$ three-dimensional net.

The final chapter describes the integration of an electrostatic component into the formation of [2]pseudorotaxanes. A derivative of DB24C8, **4d**, was synthesised in which there are pendant $-\text{SO}_3^-$ groups on each benzo ring. The association constants of several threads were measured with **4d**. It was shown that through the introduction of an electrostatic contribution to the recognition process that [2]pseudorotaxanes could be formed in a competitive solvent such as acetic acid. The X-ray crystal structure of **3b** \subset **4d** is presented and confirms the interpenetrated nature of the [2]pseudorotaxane.

Dedication

*This work is dedicated to my
Grandfather.*

He is a great fish and I must convince him, he thought. I must never let him learn his strength nor what he could do if he made his run. If I were him I would put in everything now and go until something broke. But, thank God, they are not as intelligent as we who kill them; although they are more noble and more able.

Ernest Hemingway

Excerpt from *The Old Man and the Sea*

Acknowledgements

It has been a long time coming and I would not have made it, if it was not for all the help and encouragement along the way. First and foremost, I would like to thank my supervisor, Steve Loeb. When I arrived in Windsor, Steve challenged me with a goal and I would like to thank him for letting me choose my own path, indirect as it was.

I would also like to thank the members of the Loeb group, past and present, especially: Jorge Tiburcio, Dave Tramontozzi, Roopa Patel, Sarah Vella, Derek Beauchamp, Iavor Mihalkov, Chantelle Bondy, Greg Davidson, Natalie Suhan, Clare Sullivan, Jeff Bonelli, and Jason Jolicoeur. Thanks!

Special thanks go out to Dr. Jorge Tiburcio for all of his help and suggestions along the way. I would also like to thank Dr. James Gauld for his editing expertise. Special thanks are due to Mike Fuerth and S. Zhang for their respective expertise in NMR spectroscopy and mass spectroscopy. Also, I would like to thank all of my housemates along the way: Jorge Tiburcio, Steve Clemens, and Joe DiMartino for “keepin’ it real”.

Last but not least, I would like to thank my family and Erica Robinson for all of their love and support. I couldn’t have done it without you!

Table of Contents

Abstract	<i>iv</i>
Dedication	<i>vi</i>
Acknowledgements	<i>viii</i>
List of Figures	<i>xiii</i>
List of Tables	<i>xvii</i>
List of Abbreviations and Symbols	<i>xix</i>
Chapter One - Introduction	1
1.1 Supramolecular Chemistry	1
1.2 Supramolecular Interactions	2
Chapter Two – 4,4'-Bipyridine <i>N</i>-Monoxide	4
2.1 Introduction	4
2.1.1 4,4'-Bipyridine	4
2.1.2 4,4'-Bipyridine <i>N,N'</i> -Dioxide	7
2.1.3 Divergent <i>N,O</i> Ligands	9
2.1.4 Scope	10
2.2 Experimental	11
2.2.1 General Comments	11
2.2.2 General Methods for X-ray Crystallography	11

2.2.3	Preparation of 4,4'-Bipyridine <i>N</i> -Monoxide (2a)	13
2.2.4	Preparation of [Cu ^I (2a) ₃][BF ₄] (2b)	14
2.2.5	Preparation of [Cu ^I (2a) ₄][PF ₆] (2c)	15
2.2.6	Preparation of [Cu ^{II} (2a) ₄ (H ₂ O) ₂][PF ₆] ₂ (2d)	16
2.2.7	Preparation of [Pd ^{II} (2a) ₄] ₃ [BF ₄] ₂ [OTf] ₄ (2e)	17
2.2.8	Preparation of [Cd ^{II} (2a) ₂ (H ₂ O) ₄][OTf] ₂ (2f)	18
2.2.9	Preparation of [Hg ^{II} (2a) ₂][ClO ₄] ₂ (2g)	19
2.2.10	Preparation of [Eu ^{III} (2a) ₄ (H ₂ O) ₄][OTf] ₃ (2h)	20
2.3	Results and Discussion	21
2.3.1	Synthesis	21
2.3.2	Supramolecular Interactions and Coordination Modes of 2a	22
2.3.3	Molecular Topologies for Use as Secondary Building Units	29
2.4	Conclusions	33
 Chapter Three – Multi-Dimensional Polyrotaxanes		35
3.1	Introduction	35
3.1.1	Interlocked and Interpenetrated Molecules	35
3.1.2	Metal-Capped Rotaxanes	38
3.1.3	Polyrotaxanes	39
3.1.4	Functional Materials	47
3.1.5	Scope	48
3.2	Experimental	48
3.2.1	General Comments	48

3.2.2	General Methods for X-ray Crystallography	49
3.2.3	Preparation of Bromoethylbipyridinium <i>N</i> -Monoxide [Br] (3a)	50
3.2.4	Preparation of Bis(Bipyridinium <i>N</i> -Monoxide) Ethane [OTf] ₂ (3b)	51
3.2.5	Preparation of [Cd ^{II} (3b) ₂ (DB24C8)][OTf] ₆ (3c)	52
3.2.6	Preparation of [M ^{III} (3b) ₃ (DB24C8) ₃][OTf] _{8.5} [Cl] _{0.5} (M ^{III} = Sm ^{III} (3d), Eu ^{III} (3e), Gd ^{III} (3f), Tb ^{III} (3g))	53
3.2.7	Preparation of [Yb ^{III} (3b) ₃ (DB24D8) ₃][OTf] ₈ [Cl] (3h)	54
3.3	Results and Discussion	55
3.3.1	Synthetic Design and Considerations	55
3.3.2	Synthesis of a [2]Pseudorotaxane and its Components	58
3.3.3	Two Dimensional Polyrotaxane Based on a Cd ^{II} Cation	61
3.3.4	Three-Dimensional Polyrotaxanes Based on Sm ^{III} , Eu ^{III} , Gd ^{III} , Tb ^{III} Cations	64
3.3.5	Three Dimensional Polyrotaxane Based on a Yb ^{III} Cation	68
3.4	Conclusions	73
 Chapter Four – Electrostatics in Pseudorotaxane Formation		74
4.1	Introduction	74
4.1.1	Supramolecular Cation Complexation	74
4.1.2	Sulfonated Crown Ethers	76
4.1.3	Zwitterionic Rotaxanes	77
4.1.4	Scope	78
4.2	Experimental	79
4.2.1	General Comments	79

4.2.2	General Methods for X-ray Crystallography	79
4.2.3	Preparation of 4,4'(5')-Dibenzylalcohol-24-crown-8 (4a)	80
4.2.4	Preparation of 4,4'(5')-Dibromomethyl dibenzo-24-crown-8 (4b)	81
4.2.5	Preparation of the disodium salt of 4,4'(5')-Disulfomethyl dibenzo-24-crown-8 (4c)	82
4.2.6	Preparation of the tetramethylammonium salt of 4,4'(5')-Disulfodibenzo-24-crown-8 (4d)	83
4.2.7	Formation of [2]Pseudorotaxanes	84
4.3	Results and Discussion	84
4.3.1	Synthesis of Sulfonated Crown Ethers	84
4.3.2	Solution Behaviour of [2]Pseudorotaxanes	86
4.3.3	Solid State Structure of 3b \subset 4d	93
4.4	Conclusions	97
	References	99
	Curriculum Vitae	105

List of Figures

Figure 1.1	Macrocyclic hosts for cation complexation.	1
Figure 1.2	Relative energies associated with non-covalent bonding interactions.	3
Figure 2.1	4,4'-Bipyridine (4,4'-bpy) and its structural analogues.	5
Figure 2.2	Protonated 4,4'-bipyridine (4,4'-H ₂ bpy ²⁺).	6
Figure 2.3	Connection modes observed for 4,4'-bipyridine <i>N,N'</i> -dioxide.	8
Figure 2.4	Examples of some divergent <i>N,O</i> ligands.	10
Figure 2.5	Observed supramolecular connection modes in the metal complexes of 2a .	22
Figure 2.6	Example π -stacking interactions observed in the metal complexes of 2a .	23
Figure 2.7	The intermolecular hydrogen bond array of four C–H...O and four O–H...O hydrogen bonds connects molecules of 2d in the solid state.	25
Figure 2.8	O–H...N hydrogen bond pair observed in the extended structure of 2h .	26
Figure 2.9	Observed metal coordination modes for 2a .	28
Figure 2.10	X-ray crystal structures of the four distinct molecular topologies formed by the self-assembly of 2a and a metal centre.	30
Figure 2.11	Generation of ordered, multi-dimensional architectures through the use of secondary building units.	31
Figure 2.12	Incorporation of a linear SBU into a two-dimensional square net.	32
Figure 2.13	Extended networks comprised of trigonal and square planar SBUs.	33
Figure 3.1	Cartoon depiction of a [2]rotaxane and a [2]catenane.	36

Figure 3.2	Synthesis of a [2]rotaxane via the “threading” methodology.	37
Figure 3.3	[2]Pseudorotaxane formation using functionalised bis(pyridinium) ethane cations and 24C8 and the benzo and naphtho derivatives of 24C8.	38
Figure 3.4	Examples of metal capped [2]rotaxanes incorporating a cyclodextrin macrocycle.	39
Figure 3.5	Leigh’s synthetic protocol for the production of main chain, cross-linked, and pendant organic polyrotaxanes.	41
Figure 3.6	Hydrothermal synthesis of a two and three-dimensional polyrotaxane using Tb ^{III} .	43
Figure 3.7	Polyrotaxanes previously synthesised in the Loeb group.	44
Figure 3.8	Ball and stick representations of some pyridine <i>N</i> -oxide metal complexes.	45
Figure 3.9	Geometric comparison of 4,4'-bipyridine, 4,4'-bipyridine <i>N,N'</i> -dioxide, DED and, 3b .	46
Figure 3.10	Comparison of the steric presence of 3b \subset DB24C8 and DED \subset DB24C8.	47
Figure 3.11	Relative sizes of the cations used in the construction of multi-dimensional polyrotaxanes.	55
Figure 3.12	The synthetic protocol for the preparation of polyrotaxanes.	57
Figure 3.13	Ball and stick and space-filling models of 3b \subset DB24C8.	58
Figure 3.14	Ball and stick model of the Cd ^{II} coordination sphere showing the <i>trans</i> arrangement of the ligands.	61
Figure 3.15	Space-filling views of 3d .	62
Figure 3.16	Line drawing of 3d depicting the pillared nature of the polyrotaxane.	63
Figure 3.17	Ball and stick representation of the Sm ^{III} centre with six coordinated [2]rotaxanes..	65
Figure 3.18	Space-filling model depicting a single, cubic unit of the Sm ^{III} structure.	66

Figure 3.19	Line drawing showing the two-fold interpenetrated nature of the Sm ^{III} , Eu ^{III} , Gd ^{III} , and Tb ^{III} polyrotaxane networks.	67
Figure 3.20	Comparison of the metal–metal distances in the DED and 2b polyrotaxanes.	67
Figure 3.21	Diffusion tube used in the preparation of 3h .	68
Figure 3.22	Ball and stick illustration of the coordination environment around the Yb ^{III} centre.	69
Figure 3.23	Space-filling model of Yb ^{III} coordination sphere.	70
Figure 3.24	Plane tessellations observed in the Yb ^{III} polyrotaxane, structural motif.	72
Figure 3.25	Line drawing of showing the interpenetrated nature of 3h and the propagation of the $\begin{pmatrix} 3 \\ 4,6 \\ 6 \end{pmatrix}$ net.	72
Figure 4.1	Cation selectivity as a function of cavity size in various crown ethers.	75
Figure 4.2	The incorporation of electrostatic components onto the crown ether moiety greatly increases the stability of the cation complex.	75
Figure 4.3	Relative lanthanide complex stabilities as a function of cavity size and charge for some sulfonated crown ethers.	76
Figure 4.4	Two examples of zwitterionic rotaxanes.	78
Figure 4.5	Synthesis of 4c .	85
Figure 4.6	Synthesis of 4d .	86
Figure 4.7	Synthetic protocol for the preparation of [2]pseudorotaxanes used in this study.	87
Figure 4.8	Graphical representation of the change in chemical shift of the α -pyridinium hydrogen as a function of crown ether concentration in CD ₃ COOD _{aq} at 500 MHz.	88
Figure 4.9	The acid/base equilibrium that exists between acetic acid and a pyridine.	90

Figure 4.10	^1H NMR spectra showing the uncomplexed crown (top) and thread (bottom) and $\text{Bz}_2\text{DED} \subset \mathbf{4d}$ (middle) at 500 MHz in $\text{CD}_3\text{COOD}_{aq}$.	91
Figure 4.11	Van't Hoff plot a plot of the thermodynamic parameters for the [2]pseudorotaxane formation of $\text{Bz}_2\text{DED} \subset \mathbf{4d}$.	93
Figure 4.12	Ball and stick depiction of $\mathbf{3b} \subset \mathbf{4d}$.	95
Figure 4.13	Comparison of the solid state structures of $\mathbf{3b} \subset \text{DB24C8}$ and $\mathbf{3b} \subset \mathbf{4d}$.	96
Figure 4.14	Packing diagrams of $\mathbf{3b} \subset \mathbf{4d}$.	97

List of Tables

Table 2.1	¹ H NMR spectroscopic data (D ₂ O, 300 MHz) for 2a .	13
Table 2.2	Crystal data and details of structure solution and refinement for 2b .	14
Table 2.3	Crystal data and details of structure solution and refinement for 2c .	15
Table 2.4	Crystal data and details of structure solution and refinement for 2d .	16
Table 2.5	Crystal data and details of structure solution and refinement for 2e .	17
Table 2.6	Crystal data and details of structure solution and refinement for 2f .	18
Table 2.7	Crystal data and details of structure solution and refinement for 2g .	19
Table 2.8	Crystal data and details of structure solution and refinement for 2h .	20
Table 2.9	Listing of π -stacking distances observed in complexes of 2b-2h .	24
Table 2.10	Listing of hydrogen bond distances and angles observed in complexes 2b-2h .	27
Table 3.1	¹ H NMR Spectroscopic Data (D ₂ O, 300 MHz) for 3a .	50
Table 3.2	¹ H NMR Spectroscopic Data (CD ₃ NO ₂ , 500 MHz) for 3b .	51
Table 3.3	Crystal data and details of structure solution and refinement for 3c .	52
Table 3.4	Crystal data and details of structure solution and refinement for 3d .	53
Table 3.5	Crystal data and details of structure solution and refinement for 3h .	54
Table 3.6	Selected hydrogen bond distances and angles in 3b \subset DB24C8.	59
Table 3.7	Crystal data and details of structure solution and refinement for 3b \subset DB24C8.	60
Table 3.8	Selected angles from 3h .	70
Table 4.1	¹ H NMR Spectroscopic Data (CDCl ₃ , 500 MHz) for 4a .	80

Table 4.2	¹ H NMR Spectroscopic Data (CDCl ₃ , 500 MHz) for 4b .	81
Table 4.3	¹ H NMR Spectroscopic Data (D ₂ O, 500 MHz) for 4c .	82
Table 4.4	¹ H NMR Spectroscopic Data ((CD ₃) ₂ SO, 500 MHz) for 4d .	83
Table 4.5	Comparison of association constants for [2]pseudorotaxanes containing 4d and DB24C8.	89
Table 4.6	Crystal data and details of structure solution and refinement for 3b ⊂ 4d .	94
Table 4.7	Hydrogen bond distances and angles in 3b ⊂ 4d .	95

List of Abbreviations and Symbols

\subset	union
(PhPy) ₂ Et	<i>bis</i> -1,2-(4-phenyl(4-pyridinium)ethane
°C	degrees centigrade
15C5	15-crown-5
18C6	18-crown-6
21C7	21-crown-7
24C8	24-crown-8
Å	Ångstrom
Bz ₂ DED	benzylated <i>bis</i> -1,2-(4-pyridyl(4-pyridinium)ethane
d	doublet
DB24C8	dibenzo-24-crown-8
DED	<i>bis</i> -1,2-(4-pyridyl(4-pyridinium)ethane
DFDB24C8	diformyldibenzo-24-crown-8
Et	ethyl
F _c	calculated structure factor
F _o	observed structure factor
FW	formula weight
g	grams
hrs	hours
Hz	hertz
<i>i</i> Pr ₂ O	<i>isopropyl ether</i>
<i>J</i>	coupling constant

J	joules
K	kelvin
kJ	kilojoules
m	multiplet
Me	methyl
MeNO ₂	nitromethane
MHz	megahertz
min	minutes
mL	millilitres
mmol	millimoles
mol	moles
NLO	non-linear optical
NMR	nuclear magnetic resonance
OTf	trifluoromethane sulfonate
Ph	phenyl
ppm	parts per million
py	pyridine
R	agreement factor
R _w	weighted agreement factor
s	singlet
t	triplet
T	temperature
TGA	thermogravimetric analysis

TMS	tetramethylsilane
V	unit cell volume
var	variables
Z	number of molecules in the unit cell
δ	chemical shift in ppm
μ	absorption coefficient
ρ	density

Chapter One - Introduction

1.1 Supramolecular Chemistry

The way in which molecules interact with each other is the basis of life, from enzyme – substrate complexes to the base pairs present in our own DNA. The branch of chemistry dedicated to determining and understanding these interactions is termed supramolecular chemistry.

The beginning of supramolecular chemistry is generally credited to Charles Pedersen, Jean-Marie Lehn, and Donald Cram for their syntheses of crown ethers in 1967, cryptands in 1969, and spherands in 1973 respectively.¹⁻⁴ It was for this work that they shared the 1987 Nobel prize in Chemistry (Figure 1.1).

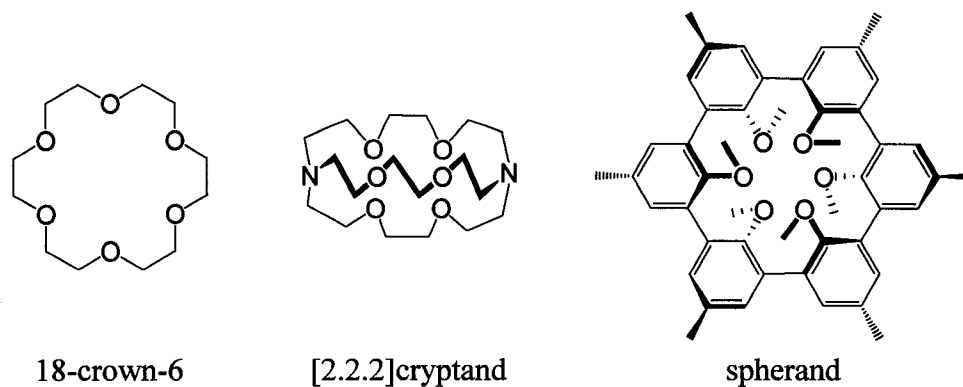


Figure 1.1
Macrocyclic hosts for cation complexation.

Although supramolecular chemistry as a specific science is relatively new, some of the ideas and concepts originate from the end of the nineteenth century; ideas such as Alfred Werner's *coordination chemistry* in 1893, Emil Fischer's idea of *lock and key* in 1894, and Paul Ehrlich's model of a *receptor* in 1906.¹ Based on concepts such as these, and also those of *self-assembly* and *molecular recognition*, supramolecular chemistry has evolved into a field of study that may be described as "chemistry of the intermolecular bond" or as "chemistry beyond the molecule".¹

1.2 Supramolecular Interactions

Intermolecular interactions are generally weaker than covalent bonds. However, the strength of the associations is cumulative and thus the stability of a supramolecular complex is dependent upon the number and strength of the individual interactions. Various examples of non-covalent interactions ordered by relative energies are illustrated in Figure 1.2. The examples given are as follows:¹

- 1) Ion-ion: The electrostatic attraction between the *tris*(diazabicyclooctane)³⁺ cation and the hexacyanoferrate³⁻ anion.
- 2) Ion-dipole: The Na⁺ cation interacts with the δ^- oxygen atoms of an 18-crown-6 macrocycle.
- 3) Hydrogen bond: The δ^- oxygen atoms interact with the δ^+ hydrogen atoms in a carboxylic acid dimer.
- 4) Dipole-dipole: The δ^- charge on the carbon atom of a ketone interacts with the δ^+ charge on the oxygen atom of another ketone.
- 5) π -stacking: Two examples are shown, face to face, and edge to face interactions of two benzene molecules. The edge to face is sometimes regarded as a weak hydrogen bond.

- 6) Van de Waals: The example shown is the weak electrostatic association of two polarisable noble gas atoms.

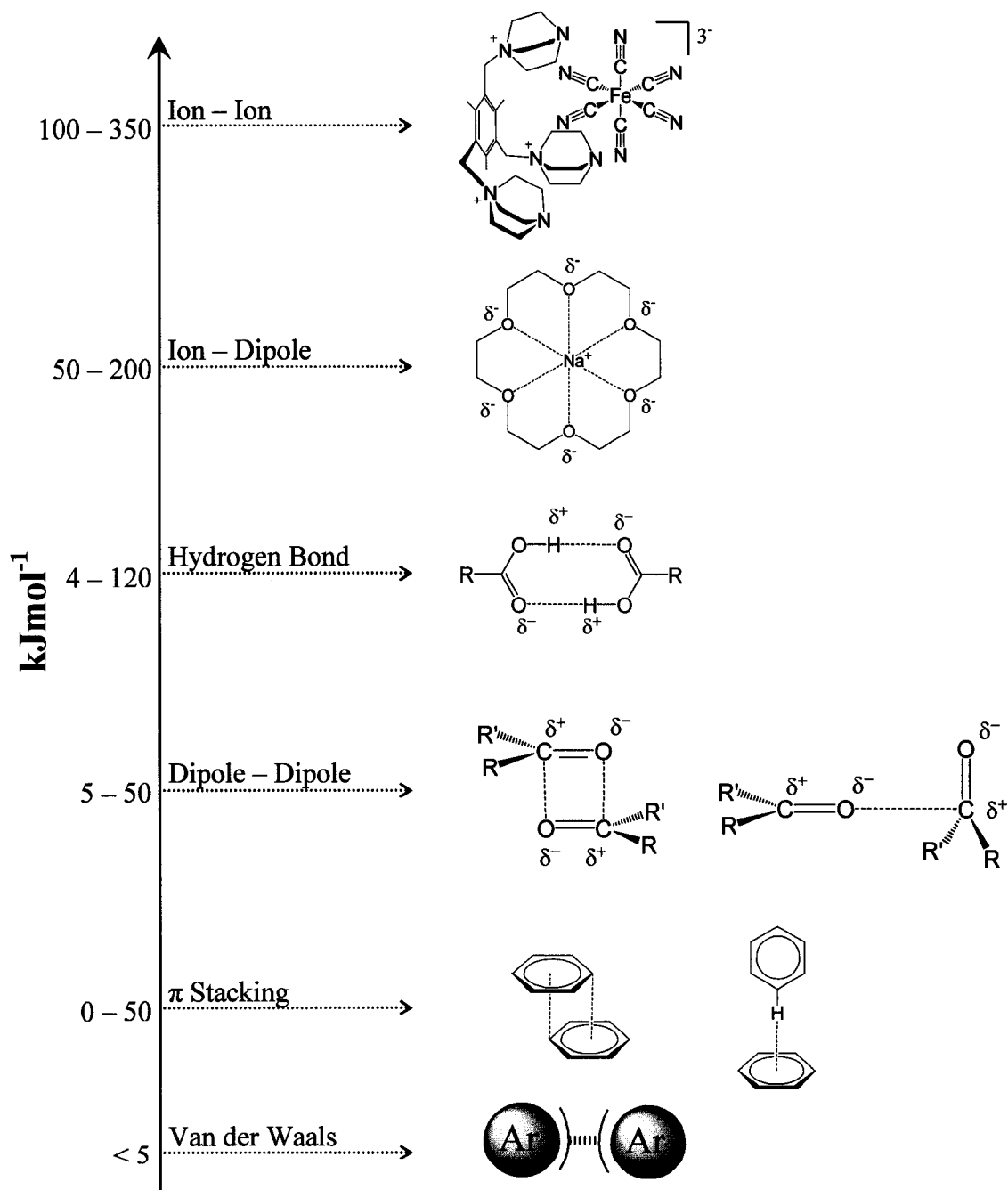


Figure 1.2

Relative energies associated with non-covalent bonding interactions.¹

Chapter Two - 4,4'-Bipyridine N-Monoxide

2.1 Introduction

Although the synthesis of new materials has long been recognized as the most essential element in advancing technology, it generally remains more of an art than of a science – in that the discovery of new compounds has mostly been serendipitous, using methods referred to by critics as 'shake and bake', 'mix and wait' and 'heat and beat'. For much of the twentieth century, this worked well for the synthesis of important solid-state materials, and we expect that it will continue to yield interesting compounds. However, it is becoming increasingly urgent to produce materials designed to perform highly specific and cooperative functions.

Omar Yaghi⁵

2.1.1 4,4'-Bipyridine

The use of 4,4'-bipyridine and its analogues in coordination chemistry and crystal engineering is ubiquitous. For example, a search of the Cambridge Structural Database (CSD) for 4,4'-bpy results in almost 560 hits, in which close to 500 are of 4,4'-bpy involved in μ^2 coordination.⁶ The utility of 4,4'-bpy as a divergent, linear spacer manifests itself in the number and diversity of related compounds that have been used to mimic its coordination behaviour.⁷⁻⁹ Some examples are shown in Figure 2.1. The

variation of these ligands as 4,4'-bpy mimics, is intended to tailor the physical properties of the generated complexes whilst retaining the predictable coordination modes of 4,4'-bpy.

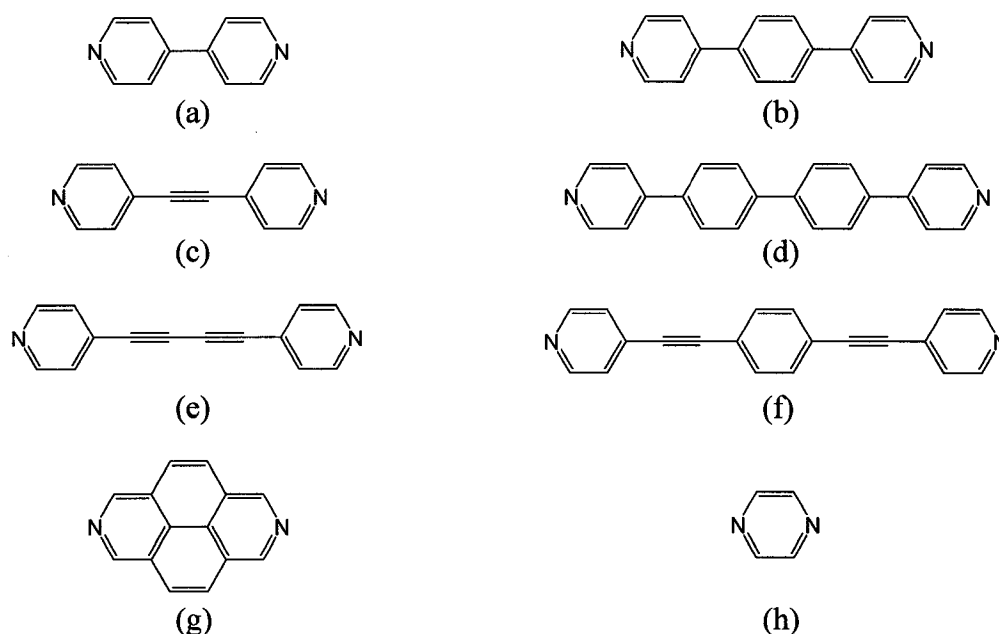


Figure 2.1

(a) 4,4'-Bipyridine (4,4'-bpy) and its structural analogues: (b) 1,4-bis(4-pyridyl)phenylene (4,4'-pyph), (c) 1,2-bis(4-pyridyl)acetylene (4,4'-pyac), (d) 4,4'-bis(4-pyridyl)biphenylene (4,4'-pybiph), (e) 1,4-bis(4-pyridyl)-1,3-butadiene (4,4'-pybut), (f) 1,4-bis(4'-pyridylethynyl)phenylene (4,4'-pyphac) (g) 2,7-diazapyrene (diaz), (h) pyrazine (pyrz).^{7,8}

The structural topology of 4,4'-bpy complexes is strongly dependent on several factors:⁹

- 1) Metal : ligand stoichiometry.
- 2) Connection mode of 4,4'-bpy: Bridging, mono-dentate, or un-coordinated.
- 3) Stereochemical preference of metal.
- 4) Presence of coordinated solvent molecules or other ancillary ligands.
- 5) Role of anions: Coordinated or un-coordinated).
- 6) Presence of guest / template molecules.

From a supramolecular perspective, 4,4'-bpy as a ligand is interesting due to the varied connection modes. It can act as a bridging ligand in a μ^2 coordination mode, or it can coordinate to a single metal, leaving the other terminal nitrogen atom available for hydrogen bonding.⁹ It is noted that there are some reported structures¹⁰ in which 4,4'-bpy does not coordinate a metal, but instead is connected solely through hydrogen bonds and π -stacking interactions.

Metal:ligand stoichiometry is arguably the largest factor in the coordination chemistry of 4,4'-bpy. A 1:1 ratio generates one-dimensional coordination polymers, for example, linear or zig-zag,⁹ while a ratio of 1:1.5 can yield an assortment of structural topologies, including molecular ladder and honeycomb nets.^{7,9} Two-dimensional square grids and three-dimensional diamondoid nets are the result of a 1:2 stoichiometry.^{7,9} Finally, a three-dimensional cubic array is afforded by an octahedral metal and 4,4'-bpy in a ratio of 1:3.⁹

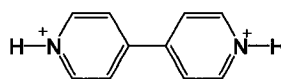


Figure 2.2

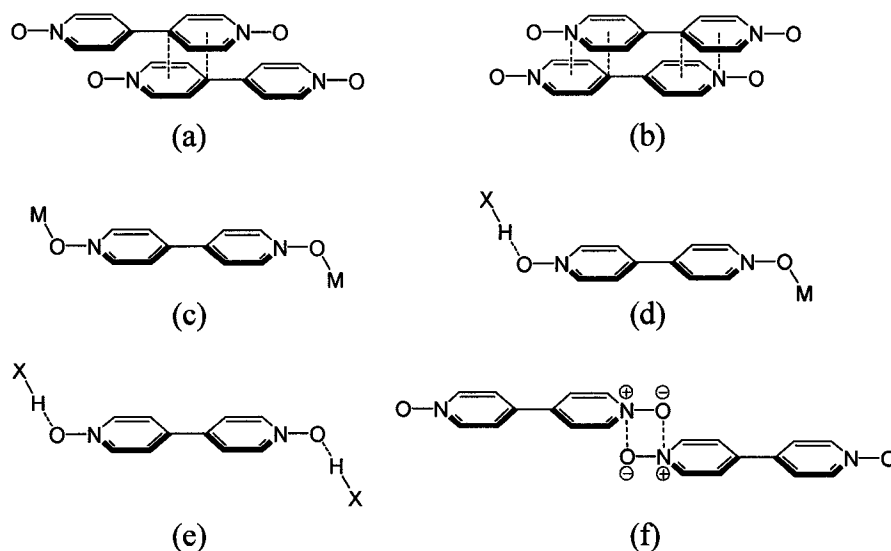
Protonated 4,4'-bipyridine (4,4'-H₂bpy²⁺)¹¹.

An extension of 4,4'-bpy that is worthy of note is the ligand generated upon protonation (Figure 2.2).¹¹ This ligand is incapable of metal coordination due to the fact that the lone pairs on the nitrogens are unavailable. Instead, the ligand forms metal complexes through second sphere coordination, typically via hydrogen bonding to an appropriate heteroatom of a metal bound ligand, for example, H₂O, NH₃, or Cl⁻. Acting in this

fashion, the complexes are solely organised through hydrogen bond interactions. Interestingly, some complexes based on 4,4'-H₂bpy²⁺ display fascinating photophysical properties.^{9,11}

2.1.2 4,4'-Bipyridine *N,N'*-Dioxide

A simple modification of 4,4'-bpy that has only recently been used in a similar fashion, is 4,4'-bipyridine *N,N'*-dioxide (4,4'-bpno). In contrast to the plethora of 4,4'-bpy compounds, there are approximately 40 reported crystal structures in the CSD containing 4,4'-bpno.⁶ Although pyridine *N*-oxide ligands are known to form complexes with all transition metals,¹² a majority of 4,4'-bpno structures incorporate a lanthanide cation¹³⁻¹⁸ due to the fact that water will often displace a pyridine *N*-oxide from a transition metal complex.¹²

**Figure 2.3**

Connection modes observed for 4,4'-bipyridine *N,N'*-dioxide^{9,16,19} (a) 'single ring' π -stacking, (b) 'double ring' π -stacking, (c) μ^2 metal coordination, (d) metal coordination and X-H...O hydrogen bonding, (e) μ^2 X-H...O hydrogen bonding, (f) $N^{\delta+}\dots O^{\delta-}$ ion dipole interaction. (X = electronegative heteroatom)

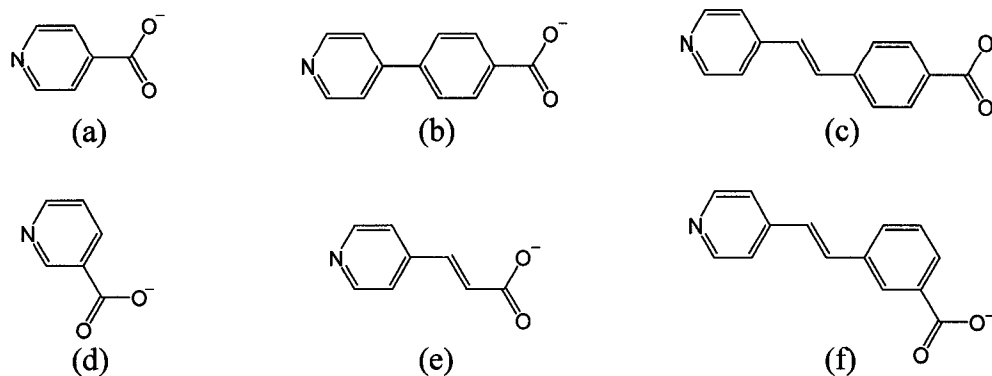
Like 4,4'-bpy, 4,4'-bpno is a divergent, linear ligand that is capable of μ^2 coordination, coordination to a single metal centre through a single donor atom or, in a non-coordinating mode, act as a hydrogen bond acceptor. The two lone pairs on each of the oxygen atoms allow for a large variety of supramolecular connection motifs, some examples of which are shown in Figure 2.3. Not shown are combinations of these interactions in which all four lone pairs on the ligand are involved in some form of intermolecular interaction. Despite its linear topology, 4,4'-bpno is incapable of acting as a perfect linear spacer due to the spatial disposition of the lone pairs and as a result, two different bridging coordination modes have been observed.²⁰ A *cis* or *syn* bonding conformation arises when each oxygen donates to a metal centre using lone pairs which are related by a mirror. A *trans* or *anti* conformation arises when the lone pairs involved

in coordination are related by C_2 symmetry or an inversion centre. The consequences of this feature manifest themselves in the generation of distinct architectures.¹³⁻²⁰

2.1.3 Divergent *N,O*-Ligands

Chemically and topologically similar to both 4,4'-bpy and 4,4'-bpno is the asymmetric molecule, 4,4'-bipyridine *N*-monoxide, **2a**. This divergent *N,O* ligand has largely been ignored in the literature. Indeed, **2a** has only been reported as a synthetic method to activate the *ortho* position of a pyridyl ring in 4,4'-bpy to electrophilic aromatic substitution.²¹

Some examples of other asymmetric, divergent *N,O* ligands that have been used in the synthesis of solid state *NLO* materials are highlighted in Figure 2.4. In combination with a tetrahedral metal centre, diamondoid nets are generated. Due to the asymmetry of the ligands, the nets are acentric and depending upon the degree of interpenetration, crystallise in polar space groups.²²⁻²⁴

**Figure 2.4**

Examples of some divergent *N,O* ligands: (a) isonicotinate, (b) 4-(4-pyridyl)benzoate (c) 4-(2-(4-pyridyl)ethenyl)benzoate, (d) nicotinate, (e) 4-pyridylacrylate, (f) 3-(2-(4-pyridyl)ethenyl)benzoate.²²⁻²⁷

2.1.4 Scope

This chapter describes the synthesis and X-ray structures of the first metal complexes of 4,4'-bipyridine *N*-monoxide, and compared analogous complexes involving 4,4'-bipyridine and 4,4'-bipyridine *N,N'*-dioxide. Particular attention is given to the supramolecular interactions that exist between adjacent metal complexes in the solid state. In addition, the potential application of these metal complexes as secondary building units to the construction of multidimensional coordination networks is discussed.

2.2 Experimental

2.2.1 General Comments

4,4'-Bipyridine and *meta*-chloroperoxybenzoic acid were purchased from Aldrich Chemicals and were used as received. All metal salts were purchased from Aldrich Chemicals except $[\text{Hg}^{\text{II}}][\text{ClO}_4]_2$ and $[\text{Pd}^{\text{II}}][\text{BF}_4]_2$ which were purchased from Strem and were used as received. All deuterated solvents were purchased from Cambridge Isotope Laboratories. All solvents were purchased from EM Science. 4,4'-Bipyridine N-monoxide was synthesized via modification of a published procedure.²¹ ^1H NMR spectra were recorded on a Brüker Avance 300 or 500 instrument locked to the deuterated solvent at 300.1 or 500.1 MHz respectively. All peak positions are listed in ppm relative to TMS.

2.2.2 General Methods for X-ray Crystallography

Crystals were frozen in paratone oil inside a cryoloop to prevent loss of solvent. A matrix was run and a unit cell determined prior to collection. A full hemisphere was collected in each case. Reflection data were integrated from frame data obtained from hemisphere scans on a Brüker Apex diffractometer with a CCD area detector with Mo- K_α radiation ($\lambda = 0.71073 \text{ \AA}$). Diffraction data and unit cell parameters were consistent with assigned space groups. The structures were solved by Patterson or direct methods, completed by subsequent Fourier syntheses and refined with full-matrix least-squares

methods against $|F^2|$ data. All non-hydrogen atoms were refined anisotropically. All hydrogen atoms were calculated and treated as idealised contributions. Scattering factors and anomalous coefficients are contained in the SHELXTL 5.03 software package (Sheldrick, G.M., Madison, WI).²⁸ All crystallographic figures were prepared using DIAMOND.²⁹

2.2.3 Preparation of 4,4'-Bipyridine N-Monoxide (2a)

2a was prepared by modification of a previously reported method.²¹ To a solution of 4,4'-bipyridine (10.0 g, 64.0 mmols) in CHCl₃ (200 mL) was added a solution of 57–86% mcpba (12.9 g, 64.0 mmol max) in CHCl₃ (500 mL) and stirred for 3 days after which four portions of mcpba (2.0 g, 9.9 mmol max) in CHCl₃ (150 mL) each were added every 24 hrs. After stirring for a total of 17 days, the crude mixture was filtered and the solvent removed *in vacuo*. The brown solid was extracted with hot water (3 x 200 mL) to give a mixture of the mono and dioxide species. The water was removed to give a light tan solid which was further extracted with a mixture of EtOAc and MeOH (9:1) (3 x 50 mL) to yield pure 4,4' bipyridine N-monoxide. Yield 6.0 g (55%).

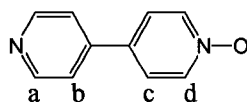


Table 2.1

¹H NMR spectroscopic data (D₂O, 300 MHz) for **2a**.

Proton	δ (ppm)	Multiplicity	# of Protons	J (Hz)
a	8.317	d	2	7.10
b	7.796	d	2	7.10
c	7.598	d	2	6.14
d	8.524	d	2	6.14

2.2.4 Preparation of $[\text{Cu}^{\text{I}}(\mathbf{2a})_3][\text{BF}_4]$ (**2b**)

One equivalent of $[\text{Cu}^{\text{I}}][\text{I}]$ was ion exchanged with one equivalent of $[\text{Ag}^{\text{I}}][\text{BF}_4]$ in MeCN to give $[\text{Cu}^{\text{I}}(\text{MeCN})_4][\text{BF}_4]$. $[\text{Cu}^{\text{I}}(\text{MeCN})_4][\text{BF}_4]$ (9.1 mg, 0.03 mmol) was combined with three equivalents of **2a** (15.0 mg, 0.09 mmol) in MeCN (1 mL). Large yellow crystals were grown by slow vapour diffusion of $i\text{Pr}_2\text{O}$ into the MeCN solution. Yield (14.4 mg) 72.0%.

Table 2.2

Crystal data and details of structure solution and refinement for **2b**.

Formula	$\text{C}_{30}\text{H}_{24}\text{BCuF}_4\text{N}_6\text{O}_3$	Collection Temp [K]	173(2)
Formula Weight	666.90	ρ_{calcd} [g cm^{-3}]	1.620
Crystal System	Monoclinic	μ ($\text{MoK}\alpha$) [mm^{-1}]	0.873
Space Group	$C2/c$	Min/max trans	0.8335/1.0000
a [\AA]	26.532(3)	Unique data	21645
b [\AA]	15.3203(12)	R(int)	0.0221
c [\AA]	14.1113(11)	R1 [$I > 2\sigma I$]	0.0355
α [$^\circ$]	90	R1 [all data]	0.0437
β [$^\circ$]	107.534(3)	wR2 [$I > 2\sigma I$]	0.0953
γ [$^\circ$]	90	wR2 [all data]	0.1009
V [\AA^3]	5469.5(8)	Data/variables	4817/406
Z	8	Goodness-of-fit	1.035

2.2.5 Preparation of [Cu^I(2a)₄][PF₆] (2c)

[Cu^I(MeCN)₄][PF₆] (8.1 mg, 0.02 mmol) was combined with four equivalents of **2a** (15.0 mg, 0.09 mmol) in MeCN (1 mL). Red plates were grown by slow vapour diffusion of *i*Pr₂O into the MeCN solution. Yield (11.3 mg) 56.8%.

Table 2.3

Crystal data and details of structure solution and refinement for **2c**.

Formula	C ₄₀ H ₃₄ CuF ₆ N ₈ O ₅ P	Collection Temp [K]	100(2)
Formula Weight	915.26	ρ _{calcd} [g cm ⁻³]	1.555
Crystal System	Triclinic	μ (MoKα) [mm ⁻¹]	0.685
Space Group	<i>P</i> -1	Min/max trans	0.4150/1.0000
a [Å]	7.797(1)	Unique data	18971
b [Å]	14.593(3)	R(int)	0.0906
c [Å]	18.419(3)	R1 [I > 2σI]	0.0618
α [°]	89.763(3)	R1 [all data]	0.0920
β [°]	76.129(3)	wR2 [I > 2σI]	0.1440
γ [°]	74.384(3)	wR2 [all data]	0.1552
V [Å ³]	1955(1)	Data/variables	18982/551
Z	2	Goodness-of-fit	0.955

2.2.6 Preparation of $[\text{Cu}^{\text{II}}(\mathbf{2a})_4(\text{H}_2\text{O})_2][\text{PF}_6]_2$ (**2d**)

$[\text{Cu}^{\text{I}}(\text{MeCN})_4][\text{PF}_6]$ (22.3 mg, 0.06 mmol) was combined with four equivalents of **2a** (41.2 mg, 0.24 mmol) in H_2O (1 mL) and heated in air until the solution turned a deep blue colour. Large blue crystals were observed to form upon cooling to room temperature. Yield (29.6 mg) 45.7%.

Table 2.4

Crystal data and details of structure solution and refinement for **2d**.

Formula	$\text{C}_{40}\text{H}_{36}\text{CuF}_{12}\text{N}_8\text{O}_6\text{P}_2$	Collection Temp [K]	173(2)
Formula Weight	1078.25	ρ_{calcd} [g cm^{-3}]	1.492
Crystal System	Tetragonal	μ ($\text{MoK}\alpha$) [mm^{-1}]	0.621
Space Group	$P4nc$	Min/max trans	0.8572/1.0000
a [\AA]	17.183(8)	Unique data	18131
b [\AA]	17.183(8)	R(int)	0.0492
c [\AA]	8.128(6)	R1 [$I > 2\sigma I$]	0.0616
α [$^\circ$]	90	R1 [all data]	0.0774
β [$^\circ$]	90	wR2 [$I > 2\sigma I$]	0.1270
γ [$^\circ$]	90	wR2 [all data]	0.1364
V [\AA^3]	2400(2)	Data/variables	2112/190
Z	2	Goodness-of-fit	1.119

2.2.7 Preparation of [Pd^{II}(2a)₄]₃[BF₄]₂[OTf]₄ (2e)

[Pd^{II}(MeCN)₄][BF₄]₂ (9.7 mg, 0.02 mmol), [Gd^{III}][OTf]₃ (13.2 mg 0.02 mmol) and **2a** (15.0 mg, 0.08 mmol) were combined in H₂O (1 mL). Large colourless blocks of the mixed anion, Pd^{II} complex formed upon slow concentration of the solution. Yield (22.4 mg) 83.3%.

Table 2.5Crystal data and details of structure solution and refinement for **2e**.

Formula	C ₃₁ H _{31.5} B _{0.5} F ₅ N ₆ O ₁₄ Pd _{0.75} S	Collection Temp [K]	173(2)
Formula Weight	924.39	ρ_{calcd} [g cm ⁻³]	1.557
Crystal System	Triclinic	μ (MoK α) [mm ⁻¹]	0.508
Space Group	<i>P</i> -1	Min/max trans	0.8637/1.0000
a [Å]	20.6240(18)	Unique data	63606
b [Å]	21.3105(19)	R(int)	0.0602
c [Å]	22.366(2)	R1 [I > 2 σ I]	0.0755
α [°]	63.191(2)	R1 [all data]	0.0999
β [°]	64.445(2)	wR2 [I > 2 σ I]	0.2026
γ [°]	82.821(2)	wR2 [all data]	0.2268
V [Å ³]	7885.5(12)	Data/variables	27680/2098
Z	8	Goodness-of-fit	1.022

2.2.8 Preparation of $[\text{Cd}^{\text{II}}(\mathbf{2a})_2(\text{H}_2\text{O})_4][\text{OTf}]_2$ (**2f**)

One equivalent of $[\text{Cd}^{\text{II}}][\text{Cl}]_2$ was ion exchanged with two equivalents of $[\text{Ag}^{\text{I}}][\text{OTf}]$ in H_2O . $[\text{Cd}^{\text{II}}][\text{OTf}]_2$ (22.6 mg, 0.04 mmol) and **2a** (15 mg, 0.08 mmol) were then combined in MeCN (1 mL). Slow diffusion of $i\text{Pr}_2\text{O}$ into the MeCN solution produced small colourless blocks. Yield (24.9 mg) 64.4%.

Table 2.6

Crystal data and details of structure solution and refinement for **2f**.

Formula	$\text{C}_{46}\text{H}_{54}\text{Cd}_2\text{F}_{12}\text{N}_{10}\text{O}_{28}\text{S}_4$	Collection Temp [K]	173(2)
Formula Weight	1776.03	ρ_{calcd} [g cm^{-3}]	2.201
Crystal System	Monoclinic	μ ($\text{MoK}\alpha$) [mm^{-1}]	0.879
Space Group	$P2(1)/n$	Min/max trans	0.8504/1.0000
a [\AA]	12.0573(11)	Unique data	17570
b [\AA]	13.8727(13)	R(int)	0.0329
c [\AA]	20.2089(19)	R1 [$I > 2\sigma I$]	0.0372
α [$^\circ$]	90	R1 [all data]	0.0458
β [$^\circ$]	96.012(2)	wR2 [$I > 2\sigma I$]	0.0991
γ [$^\circ$]	90	wR2 [all data]	0.0934
V [\AA^3]	3361.7(5)	Data/variables	5909/460
Z	2	Goodness-of-fit	1.035

2.2.9 Preparation of $[\text{Hg}^{\text{II}}(\mathbf{2a})_2][\text{ClO}_4]_2$ (**2g**)

$[\text{Hg}^{\text{II}}][\text{ClO}_4]_2$ (50.0 mg, 0.11 mmol) was dissolved in MeCN (0.5 mL) and slowly diffused into a solution of **2a** (38.0 mg, 0.22 mmol) in MeCN (0.5 mL). Pale, yellow crystals grew at the **2a** – Hg^{II} solution interface. Yield (62.2 mg) 70.7%.

Table 2.7

Crystal data and details of structure solution and refinement for **2g**.

Formula	$\text{C}_{20}\text{H}_{16}\text{C}_{12}\text{HgN}_4\text{O}_{10}$	Collection Temp [K]	173(2)
Formula Weight	743.86	ρ_{calcd} [g cm^{-3}]	2.212
Crystal System	Monoclinic	μ ($\text{MoK}\alpha$) [mm^{-1}]	7.198
Space Group	$P2(1)/c$	Min/max trans	0.7234/1.0000
a [\AA]	7.8533(6)	Unique data	8749
b [\AA]	18.6106(13)	R(int)	0.0180
c [\AA]	7.9341(6)	R1 [$I > 2\sigma I$]	0.0193
α [$^\circ$]	90	R1 [all data]	0.0221
β [$^\circ$]	105.5990(10)	wR2 [$I > 2\sigma I$]	0.0457
γ [$^\circ$]	90	wR2 [all data]	0.0469
V [\AA^3]	1116.89(14)	Data/variables	1959/169
Z	2	Goodness-of-fit	1.082

2.2.10 Preparation of [Eu^{III}(2a)₄(H₂O)₄][OTf]₃ (2h)

[Eu^{III}][OTf]₃ (30.3 mg, 0.05 mmol) and **2a** (34.8 mg, 0.20 mmol) were combined in MeCN (1 mL) and the resultant powder was recrystallised from MeCN solution over several days to give large colourless blocks. Yield (48.1 mg) 73.9%.

Table 2.8

Crystal data and details of structure solution and refinement for **2h**.

Formula	C ₄₇ H ₄₆ EuF ₉ N ₁₀ O ₁₇ S ₃	Collection Temp [K]	173(2)
Formula Weight	1442.08	ρ_{calcd} [g cm ⁻³]	1.579
Crystal System	Monoclinic	μ (MoK α) [mm ⁻¹]	1.238
Space Group	<i>P2/c</i>	Min/max trans	0.9026/1.0000
a [Å]	9.8195(12)	Unique data	23783
b [Å]	16.899(2)	R(int)	0.0218
c [Å]	18.286(2)	R1 [I > 2 σ I]	0.0457
α [°]	90	R1 [all data]	0.0471
β [°]	92.084(2)	wR2 [I > 2 σ I]	0.1224
γ [°]	90	wR2 [all data]	0.1234
V [Å ³]	3032.3(6)	Data/variables	5346/407
Z	2	Goodness-of-fit	1.138

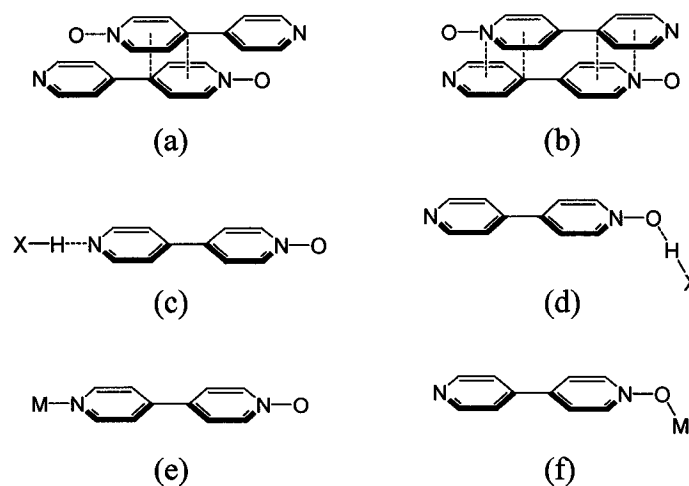
2.3 Results and Discussion

2.3.1 Synthesis

Generally the oxidation of pyridines is carried out under harsh conditions, typically in refluxing acetic acid with a strong oxidiser such as hydrogen peroxide. Milder oxidation conditions were utilised to maximise the yield of the mono *N*-oxide and try to limit the production of the *N,N'*-dioxide. Because the reaction proceeded at room temperature, the length of the reaction had to be increased to ensure maximum yields.

In contrast to the chemistry of 4,4'-bpy, metal–ligand stoichiometry was not as important a factor in determining the geometrical structure of the final product. This seems to be a general rule with one exception; a Cu^I–ligand ratio of 1:3 generates a trigonal planar structure while a Cu^I–ligand ratio of 1:4 yields a tetrahedral complex.

X-ray crystallography was the predominant method of characterisation for these materials as it gave the most pertinent structural information. These structures would not be expected to persist in solution.

2.3.2 Supramolecular Interactions and Coordination Modes of **2a****Figure 2.5**

Observed supramolecular connection modes in the metal complexes of **2a**. (a) 'single ring' π -stacking, (b) 'double ring' π -stacking, (c) X-H...N hydrogen bonding, (d) X-H...O hydrogen bonding, (e) *N*-oxide-metal coordination, (f) pyridine-metal coordination. Not included are all possible combinations of connection modes a-f.

As a supramolecular tecton, **2a** exhibits many of the connection modes of both 4,4'-bpy and 4,4'-bpno (Figure 2.5). Both of the aromatic rings of either aforementioned ligand are electronically equivalent whereas in **2a** the pyridyl ring has more electron density than the *N*-oxide ring. This allows for good π -overlap in an anti-parallel manner (Figure 2.6) with the *N*-oxide ring stacking over the pyridyl ring of another molecule of **2a** and *vice versa*.

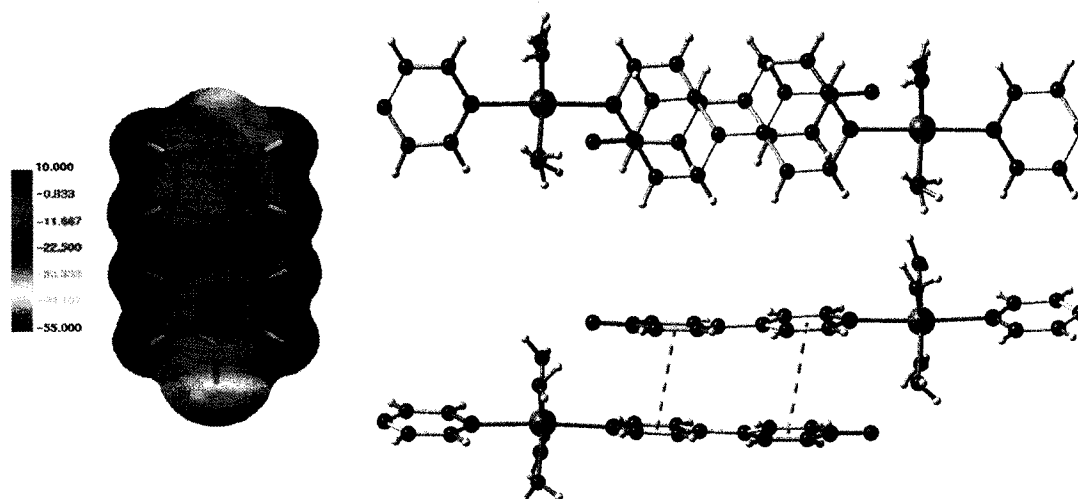


Figure 2.6

An example of π -stacking interactions observed in the metal complexes of **2a**. The electron density map³⁰ of **2a** shows the relatively electron rich pyridyl ring and the relatively electron poor *N*-oxide ring. Two views of the crystal structure of **2f** are shown depicting the anti-parallel π -stacking interactions. Extraneous ligands have been truncated. Key: bronze = Cd^{II}; blue = N, black = C; red = O; white = H. Solvent molecules and anions have been removed for clarity.

Table 2.9 summarizes the range of observed π -stacking distances which compare well with the typical distance of ~ 3.5 Å. The mode of π -stacking varies from compound to compound and can also vary within each of the complexes. In all of the complexes there is extensive π -stacking which most often is complementary. This means that both aromatic rings π -stack with the aromatic rings of another molecule of **2a** (Figure 2.6). However, other modes are also observed, such as ‘single ring’ π -stacking.

Table 2.9

Listing of π -stacking distances observed in complexes of **2b-2h**. A range of distances is given for each compound due to the extensive π -stacking observed in these compounds. Distances are measured from the centroid of one aromatic ring to the closest atom of the next ring.

Compound	Range of Distances (Å)	
2b	3.384(2)	3.679(3)
2c	3.30(46)	3.7(8)
2d	3.395(2)	3.443(2)
2e	3.281(2)	3.689(1)
2f	3.378(3)	3.687(3)
2g	3.614(4)	3.661(4)
2h	3.297(6)	3.683(6)

Both 4,4'-bpy and 4,4'-bpno often act as bridging ligands. However, because of the mismatch of donor atoms, **2a** generally coordinates through only a single atom to one metal centre. This leaves the other functionality available to engage in X–H...O or X–H...N hydrogen bonding. The **2d** structure exhibits an interesting array of hydrogen bonding; four molecules of **2a** from four separate molecules of **2d** form a square of four C–H...O hydrogen bonds and four O–H...O hydrogen bonds, two to a coordinated water molecule below the plane of the square and two to a separate coordinated water molecule above the plane, as depicted in Figure 2.7. The partial positive charge on the nitrogen atom of the *N*-oxide polarises the adjacent C–H bond, making the α -hydrogen more acidic and thus, a better hydrogen bond donor. In this way, each oxygen of the *N*-oxide accepts two hydrogen bonds.

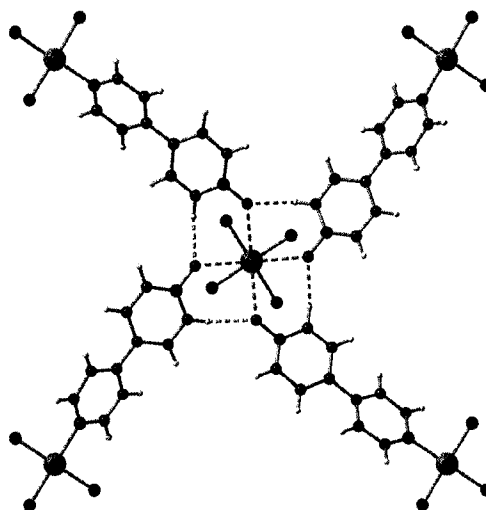


Figure 2.7

The intermolecular hydrogen bond array of four C–H...O and four O–H...O hydrogen bonds connects molecules of **2d** in the solid state. Extraneous ligands have been truncated for simplicity. Key: bronze = Cu^{II}; blue = N, black = C; red = O; white = H. Anions have been removed for clarity.

In metal complexes where the **2a** ligand is *N*-bound, the *N*-oxide is available for hydrogen bonding, likewise when the *N*-oxide is participating in metal coordination, the pyridyl nitrogen can act as a hydrogen bond acceptor. Often many of the supramolecular interactions featured in this section occur in concert; a good example of this can be seen in the **2h** structure illustrated in Figure 2.8.

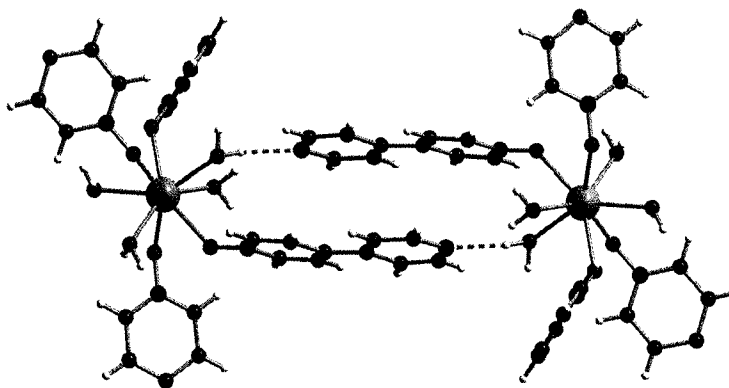


Figure 2.8

O–H...N hydrogen bond pair observed in the extended structure of **2h**. Molecules of **2a** not involved in O–H...N hydrogen bonding have been truncated. Key: bronze = Eu^{III}; blue = N, black = C; red = O; white = H. Anions and solvent molecules are omitted for clarity.

The strongest observed hydrogen bonds, judged by the bond distance, are the O...H–O and N...H–O interactions. This is to be expected as the electronegativities of carbon and hydrogen are similar, making the C–H bond relatively non-polar. However, it is the O...H–C interactions that typically align closest to the ideal angle of 180°. Table 2.10 summarizes the hydrogen bond distances and angles observed in all of the metal complexes of **2a**. A common feature of many of the **2a** structures is the formation of hydrogen bonds to coordinated water molecules, as shown in Figure 2.7 and Figure 2.8. In homoleptic compounds such as **2e**, however, where there are no coordinated water molecules, hydrogen bonding often occurs with non-coordinated water.

Table 2.10

Listing of hydrogen bond distances and angles observed in complexes **2b-2h**.
 Note: all distances listed are measured from the acidic hydrogen to the electronegative acceptor heteroatom.

Hydrogen Bonds	O...H-C		O...H-O			
		Distance (Å)	Angle (°)	Distance (Å)	Angle (°)	
2b	O1...H11A-C11	2.650(2)	119.49(15)			
	O1...H25A-C25	2.529(2)	140.69(16)			
	O2...H5A-C5	2.385(2)	144.86(16)			
	O2...H21A-C21	2.756(3)	129.76(14)			
	O3...H1A-C1	2.589(3)	143.01(16)			
	O3...H15A-C15	2.584(3)	116.82(15)			
2c	O1...H21A-C21	2.30(5)	163.88(2)			
	O1...H31A-C31	2.38(8)	164.43(2)			
	O2...H19A-C19	2.66(5)	143.96(2)			
	O2...H25A-C25	2.43(2)	148.15(2)			
	O3...H1A-C1	2.42(7)	172.96(2)			
	O3...H15A-C15	2.28(1)	155.95(2)			
	O4...H5A-C5	2.31(1)	143.04(2)			
	O4...H38A-C38	2.50(3)	164.64(2)			
2d	O1...O2W	3.142(1) ^a	-			
	O1...H9A-C9	2.243(1)	143.83(3)			
2e	O1...H11F-C115	2.237(3)	175.16(1)	O1...H29B-O29	2.167(2)	146.24(2)
	O2...H71A-C71	2.246(3)	166.48(1)	O2...H30C-O30	2.010(1)	163.43(3)
	O3...H45A-C45	2.395(1)	159.33(2)	O4...H28C-O28	2.478(2)	133.01(2)
	O3...H11C-C111	2.418(3)	162.04(1)	O5...H33B-O33	1.944(1)	152.41(2)
	O4...H1A-C1	2.278(1)	173.27(2)	O6...H28B-O28	1.908(2)	163.93(3)
	O5...H94A-C94	2.320(1)	150.16(2)	O8...H25C-O25	1.894(1)	155.35(2)
	O6...H31A-C31	2.309(1)	161.26(2)	O11...H27C-O27	1.992(2)	162.86(2)
	O7...H5A-C5	2.438(3)	171.23(1)	O12...H26C-O26	1.970(1)	163.18(2)
	O7...H10F-C105	2.377(3)	171.22(1)			
	O8...H91A-C91	2.418(1)	177.32(2)			
	O9...H11A-C11	2.380(3)	160.77(1)			
	O9...H41A-C41	2.355(1)	165.39(2)			
O10...H44A-C44	2.350(1)	153.03(2)				
O10...H10C-C101	2.203(2)	165.92(2)				
O11...H15A-C15	2.221(4)	174.09(1)				
O12...H55A-C55	2.219(4)	171.23(1)				
2f				O1...H4WB-O4	1.832(3)	164.75(17)
				O1...H6WB-O6	1.853(2)	174.52(18)
				O2...H3WB-O3	1.800(3)	170.23(19)
				O2...H4WA-O4	1.752(3)	175.04(19)
2f						
2h				N...H-O		
				Distance (Å)	Angle (°)	
				N2...H1W-O3	2.015(5)	143.05(27)
			N4...H4W-O4	1.927(6)	168.56(30)	

^a Distance measured is the donor-acceptor heteroatom distance.

Previously mentioned, **2a** can participate in selective metal coordination at either the pyridyl or *N*-oxide terminals. Depending upon the characteristics of the metal cation, coordination can occur at the pyridyl nitrogen, the *N*-oxide, or in some cases both. Although pyridine *N*-oxide complexes are known with almost all transition metals,¹¹ the late transition metals as used in this study prefer donation from the pyridyl portion of **2a** rather than from the *N*-oxide. In contrast, the oxophilic lanthanide cations prefer donation from the *N*-oxide. However, a metal such as Hg^{II}, which has similar characteristics of both transition metals and lanthanides, will coordinate to both donor groups (Figure 2.9).

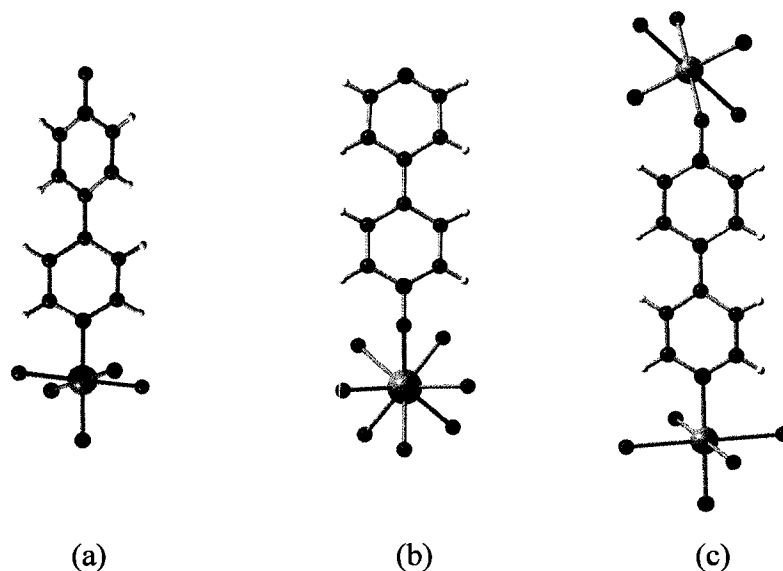


Figure 2.9

Observed metal coordination modes for **2a**. (a) **2d**, (b) **2h**, (c) **2g**. Only a single molecule of **2a** per metal centre is shown for simplicity. Key: bronze = Cu^{II} (a) Eu^{III} (b) Hg^{II} (c); blue = N, black = C; red = O; white = H. Anions and ancillary ligands are removed for clarity.

2.3.3 Molecular Topologies for Use as Secondary Building Units

Pre-formed metal complexes, or secondary building units (SBU's), with known geometrical conformations have been used in the generation of ordered, solid-state materials.³¹ In this respect, the mismatch of donor atoms on **2a** is synthetically advantageous as it allows for control of specific metal ligand interactions. Judicious choice of metal can yield complexes that are *entirely N* or *O*-bound, depending upon their coordination preferences. This mismatch also potentially enables for the introduction of both transition and lanthanide cations into the same framework, which can be used to specifically tune the physical properties of the material.³²

Towards the realisation of solid-state materials constructed from SBU's, a library of molecular topologies was compiled. Four distinct geometries: linear, trigonal planar, square planar, and tetrahedral were formed by coordination of the pyridyl nitrogen to a suitable transition metal cation (Figure 2.10).

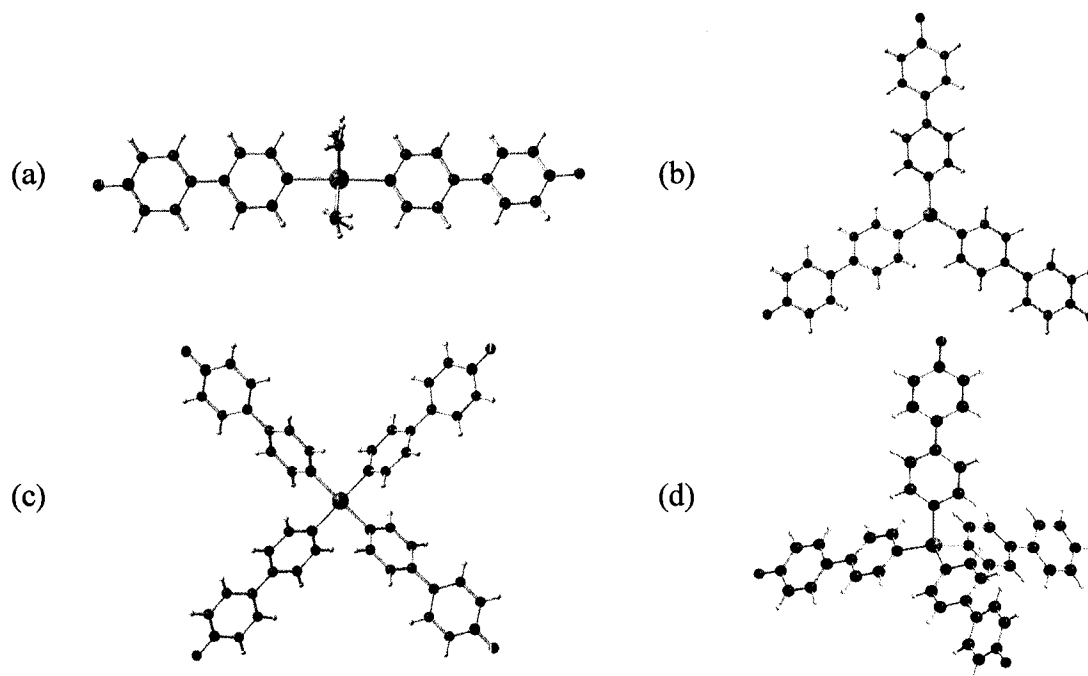
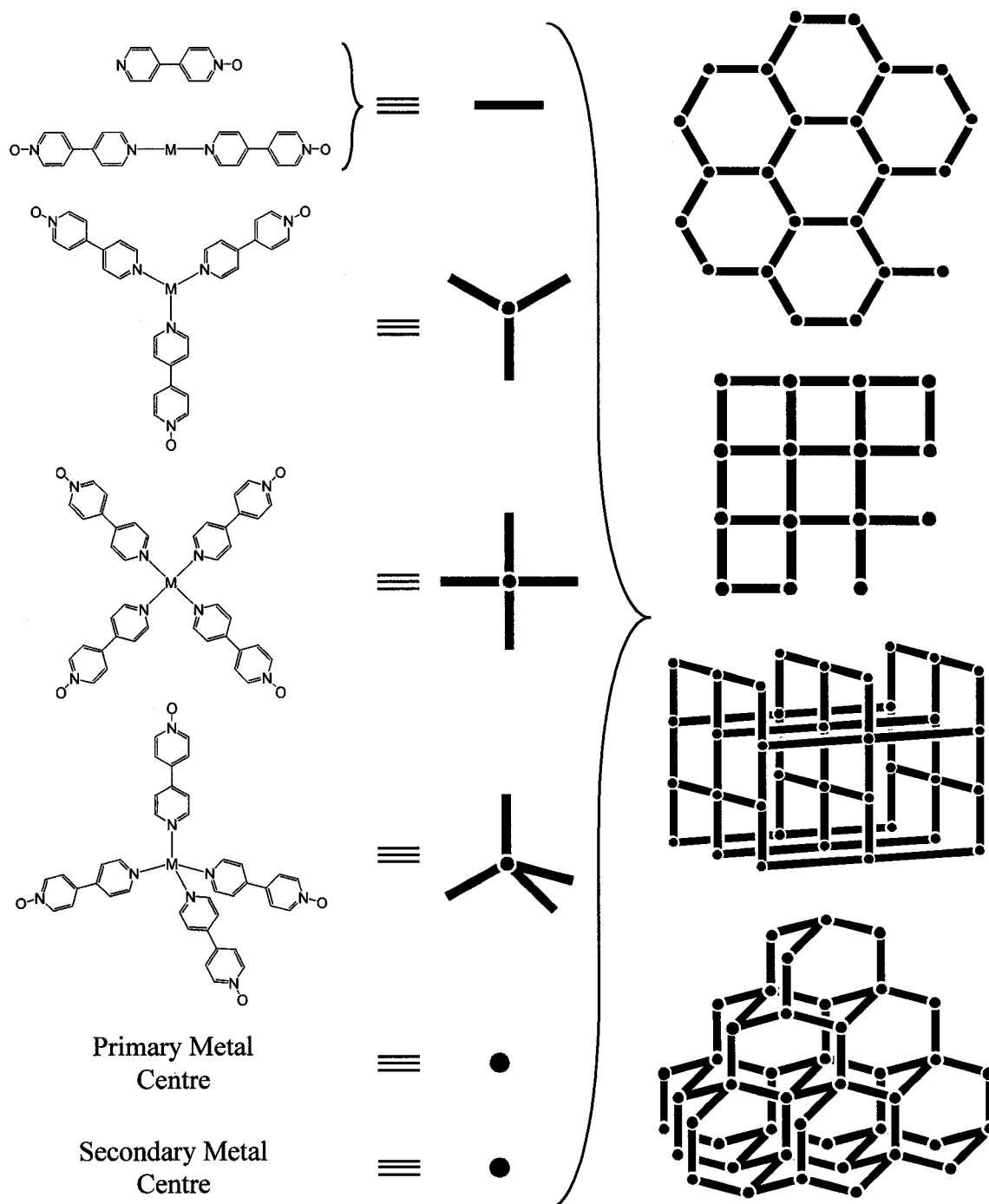


Figure 2.10

X-ray crystal structures of the four distinct molecular topologies formed by the self-assembly of **2a** and a metal centre. (a) linear: **2f**, (b) trigonal planar: **2b**, (c) square planar: **2e**, (d) tetrahedral: **2c**. Key: bronze = Cd^{II} (a) Cu^I (b) Pd^{II} (c) Cu^I (d); blue = N, black = C; red = O; white = H.

Possible network topologies as a result of combining pre-formed SBU's with a secondary metal cation are shown in Figure 2.11. It should be noted that the geometry of the network is dependent upon the spatial orientation of the SBU as well as the preferred coordination geometry of the secondary metal cation. Thus the geometry of the architectures depicted here are the sole result of the SBU topology. Consideration of both the geometrical preferences of the metal cation and the SBU can lead to distinct architectures not shown here.

**Figure 2.11**

Generation of ordered, multi-dimensional architectures through the use of secondary building units. Nets depicted on the right represent only a small number of possible topologies.

The crystal structure of **2g** is a good example of how a linear SBU can be used to construct a two-dimensional layered architecture. In this case, the building block is a Hg^{II} centre with two **2a** ligands coordinated in a *trans* fashion through the pyridyl functionality. The *N*-oxide functionality is then directed towards the centre of another linear component and participates in metal coordination to a secondary Hg^{II} centre (Figure 2.12).

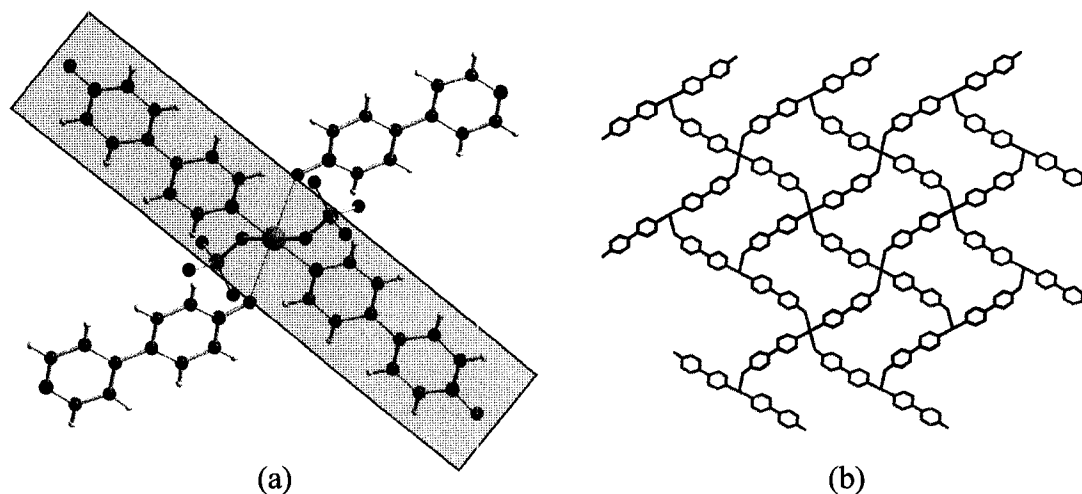


Figure 2.12

Incorporation of a linear SBU into a two-dimensional square net. (a) coordination environment of the Hg^{II} centre, highlighted is the linear SBU. (b) stick drawing of the square net, with the linear components highlighted in blue and red. Key: bronze = Hg^{II} ; blue = N, black = C; red = O; green = Cl; white = H. Hydrogens and anions have been omitted for clarity in (b).

Using the trigonal and square planar topologies of **2b** and **2d** respectively, two hydrogen-bonded networks were synthesised (Figure 2.13). As expected, a two-dimensional trigonal network was the result of combining the trigonal molecules of **2b**. Likewise, a square grid network was generated by **2d** through the hydrogen bonding array depicted in Figure 2.7. The trigonal units of **2b** connect through a series of bifurcated $\text{C-H}\cdots\text{O}$ hydrogen bonds between the *N*-oxide functionality and the protons α to the coordinated

pyridine. The topology of the network generated by **2d**, is reminiscent of the extended Hg^{II} structure in which the individual SBUs are connected by metal coordinate bonds. Conversely, molecules of **2d** interconnect solely through hydrogen bonds and π -stacking interactions. Similarly, the individual two-dimensional, trigonal sheets are held together in the solid state by a series of π -stacking interactions.

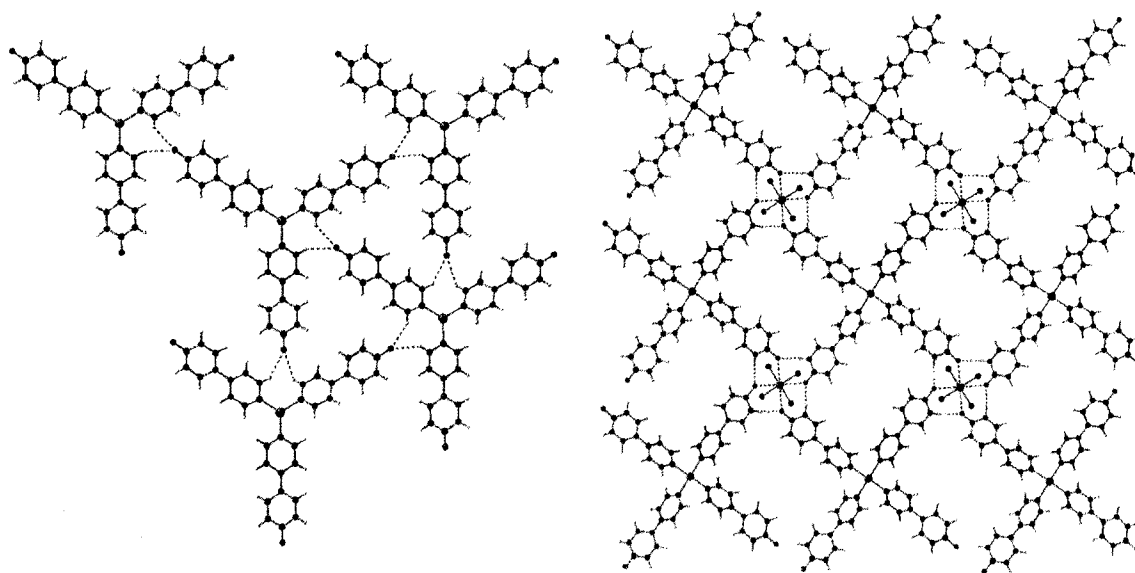


Figure 2.13

Extended networks comprised of trigonal and square planar SBUs. The terminal *N*-oxide functionality connects the SBUs through C–H...O and O–H...O hydrogen bonding arrays. Key: bronze = Cu^{I} (left) Cu^{II} (right); blue = N, black = C; red = O; white = H. Anions and extraneous ligands are omitted for clarity.

2.4 Conclusions

Through the mismatch of donor atoms on **2a**, several molecular species were designed such that hydrogen bond acceptor atoms in geometrically unique positions would be available. This distinctive feature allows the aforementioned compounds to be used as

molecular building units in the design and construction of complex, multi-dimensional solids. This feature is also shown to be useful in the synthesis of supramolecular solids in which the discrete molecular species are connected by non-covalent interactions, such as hydrogen bonding and π -stacking.

Similar in topology to 4,4'-bipyridine and 4,4'-bipyridine *N,N'*-dioxide, **2a** exhibits comparable non-covalent interactions. However, the major difference is that it is significantly easier to generate discrete molecular species using **2a** as it rarely engages in μ^2 coordination modes.

Chapter Three - Multi-Dimensional Polyrotaxanes

3.1 Introduction

Considerable effort is being devoted to the fabrication of nanoscale devices. Molecular machines, motors and switches have been made, generally operating in solution, but for most device applications (such as electronics and opto-electronics) a maximal degree of order and regularity is required. Crystalline materials would be excellent systems for these purposes, as crystals comprise a vast number of self-assembled molecules, with a perfectly ordered three-dimensional structure.

Gerard van Koten³³

3.1.1 Interlocked and Interpenetrated Molecules

Rotaxanes are one of three main classes of interlocked and interpenetrated molecules, the others being catenanes and knots. They are comprised of two independent components; a dumbbell shaped “thread” or “axle” and a macrocyclic “bead” or “wheel”, mechanically interlocked and only separable by the breaking of a covalent bond. A pseudorotaxane is similar to a rotaxane except that the two components are allowed to freely associate and dissociate in a dynamic equilibrium. An integer often precedes the term pseudorotaxane or rotaxane and indicates the number of individual components in the system. Thus, a

[2]rotaxane, the simplest example, consists of two interlocked components, and a [3]rotaxane would then consist of three components.

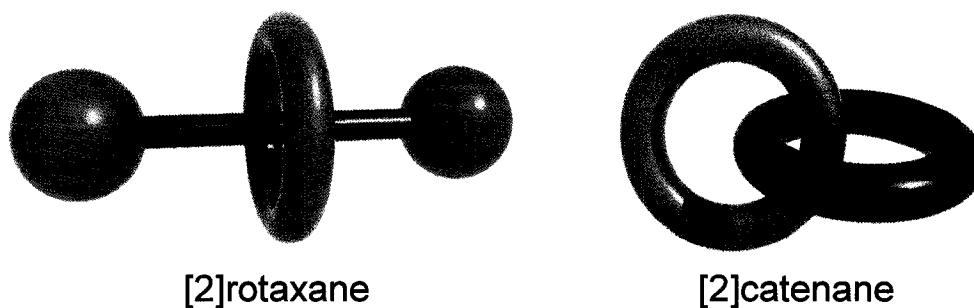


Figure 3.1

Cartoon depiction of a [2]rotaxane and a [2]catenane.

The first rotaxane was synthesised by Harrison and Harrison³⁴ in 1967 by the “statistical” method in which the thread component was covalently capped by large “stopper” groups while, by chance, penetrating through a macrocycle supported on a resin. After successive reactions (70 times) the final product was isolated in only 6 % yield.

Clearly, in order for applied research of rotaxanes to be fruitful a better synthetic approach was needed. Towards this end, supramolecular chemists applied their knowledge of self-assembly and molecular recognition. Through the combined use of hydrogen bond donors and acceptors, π - π stacking, ion-dipole interactions and other non-covalent intermolecular forces, rotaxanes can now be synthesised in near quantitative yields.^{35,36}

It has been shown that a pseudorotaxane can be readily converted into a rotaxane through a variety of methods.³⁷⁻³⁹ “Clipping” involves the formation of a macrocycle around a

pre-formed dumbbell shaped thread. “Slipping” is the association of both pre-formed components, in which the macrocycle when given enough kinetic energy is able to slip over the bulky end-groups of a pre-formed thread. “Threading”, the synthetic procedure employed in this study, is completed through the addition of large bulky stoppers to each end of the pseudorotaxane complex either covalently or through metal coordination (Figure 3.2).

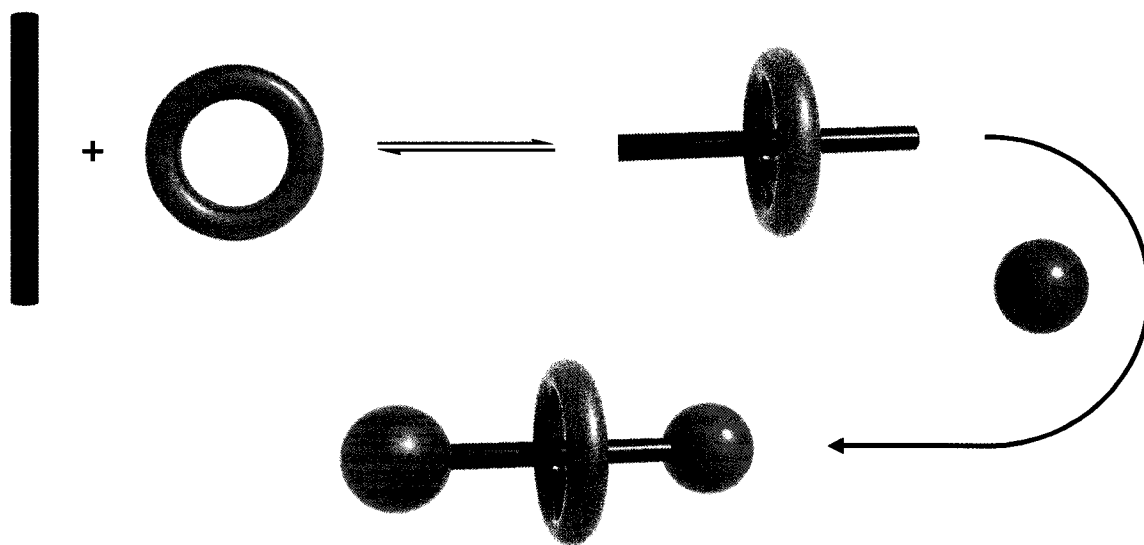


Figure 3.2

Synthesis of a [2]rotaxane via the “threading” methodology. A dynamic equilibrium exists between the [2]pseudorotaxane and the uncomplexed thread and macrocycle. A [2]rotaxane can be irreversibly formed by the addition of large, bulky stopper groups to each end of the [2]pseudorotaxane, thereby preventing the macrocycle from dethreading.

Wisner and Loeb⁴⁰ previously developed the *bis*-pyridinium ethane recognition site for the 24-membered cyclic polyether 24C8 and its benzo and naphtho derivatives (Figure 3.3). This motif has proven versatile as both components are readily functionalised. Numerous derivatives of pyridine are commercially available and are easily coupled together using 1,2-dibromoethane to form the 24C8 recognition site on the thread. Due to

the interest in crown ether chemistry, there are numerous synthetic protocols for the preparation of derivitised crown ethers, some of which are also commercially available.

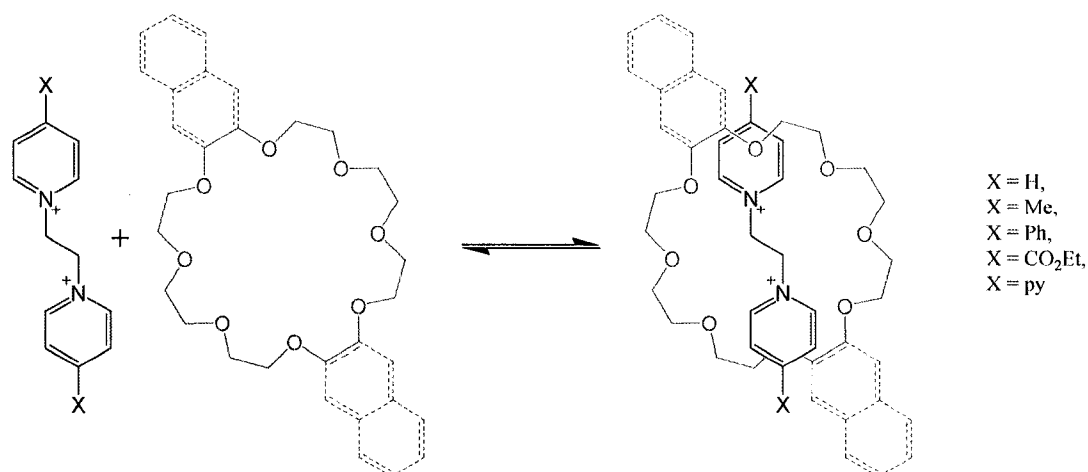
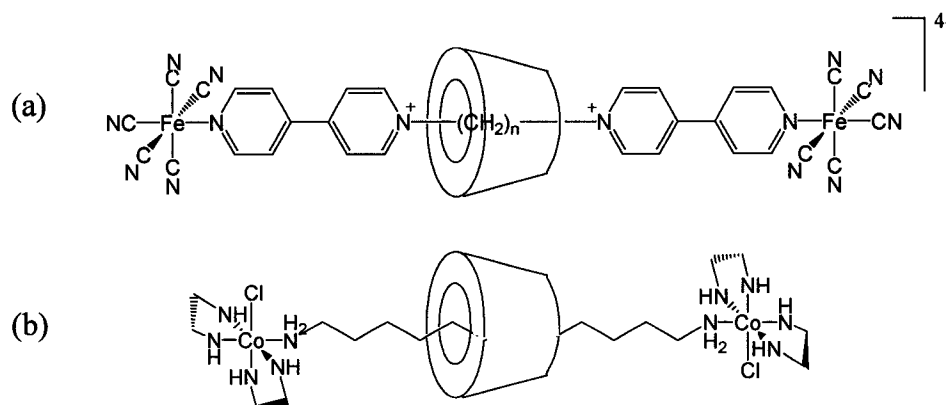


Figure 3.3

[2]Pseudorotaxane formation using functionalised bis(pyridinium) ethane cations and 24C8 and the benzo and naphtho derivatives of 24C8.⁴¹

3.1.2 Metal-Capped Rotaxanes

The capping of a pseudorotaxane to form a rotaxane is typically completed by covalently linking a large bulky stopper to each end of a pseudorotaxane. It has been proven that metal coordination to divergent Lewis basic donor atoms located on the terminals of the thread component is a facile method for the conversion of a pseudorotaxane into a rotaxane.⁴²⁻⁵³ Incorporation of a metal centre into the rotaxane motif has many interesting consequences; the metal fragment chosen can impart new photophysical, electronic, and magnetic properties to the system.

**Figure 3.4**

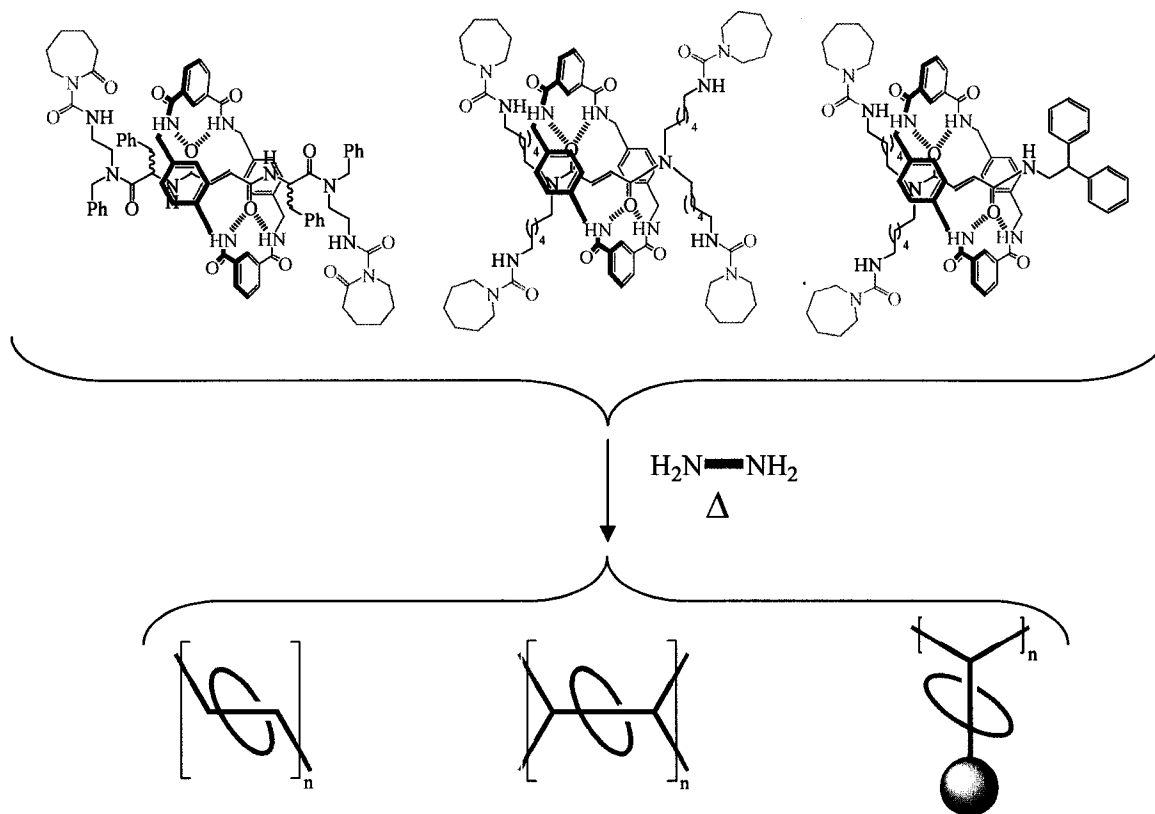
Examples of metal capped [2]rotaxanes incorporating a cyclodextrin macrocycle. (a)⁵¹, (b)^{48,49}

In the metal cation capping reaction (Figure 3.2 and Figure 3.4) the pseudorotaxane acts as a divergent ligand. One of the most ubiquitous uses of a divergent ligand in coordination chemistry is to generate coordination polymers where the metal cation acts as a node and the organic ligand acts as a spacer or linker. The geometry of the ligand and the coordination geometry of the node dictate the topology of the network. For instance, a tetrahedral ligand will tend to form diamondoid networks whereas a linear ligand connected to a octahedral node will generate a three dimensional cubic architecture.⁵⁴ Whereas judicious choice of ligand topology can dictate the framework morphology, the coordination tendencies of specific metals can also predispose a particular coordination compound to adopt a desired architecture.⁵⁴

3.1.3 Polyrotaxanes

There are a few basic approaches to the preparation of polyrotaxanes: (1) incorporation of a rotaxane into the monomeric unit of an organic polymerisation reaction,⁵⁵ (2) use of

a pseudorotaxane as a ligand and metal cations as stoppers in the construction of coordination polymers,⁵⁶⁻⁶⁰ and (3) a self-assembly process in which the macrocycle and thread are simultaneously formed upon coordination to a metal.^{61,62} By definition, a one-dimensional polyrotaxane is a molecule in which an infinite number of rotaxanes are aligned and connected through covalent or coordinate bonds to form a chain. Similarly, a two-dimensional polyrotaxane is an infinite number of one-dimensional chains connected through covalent or coordinate bonds to form a grid and a three dimensional polyrotaxane carries this line of reasoning one step further to produce a structure that extends indefinitely in the x , y , and z directions. Each of these approaches have advantages, and depending upon the intended application, one approach may be more useful or convenient. For example, Leigh⁵⁵ used blocked isocyanates to stopper [2]rotaxanes, which at elevated temperatures (> 150 °C) readily react with diamines or diols to produce main-chain, pendant, or cross-linked organic polymers in which a rotaxane assembly had been included (Figure 3.5).

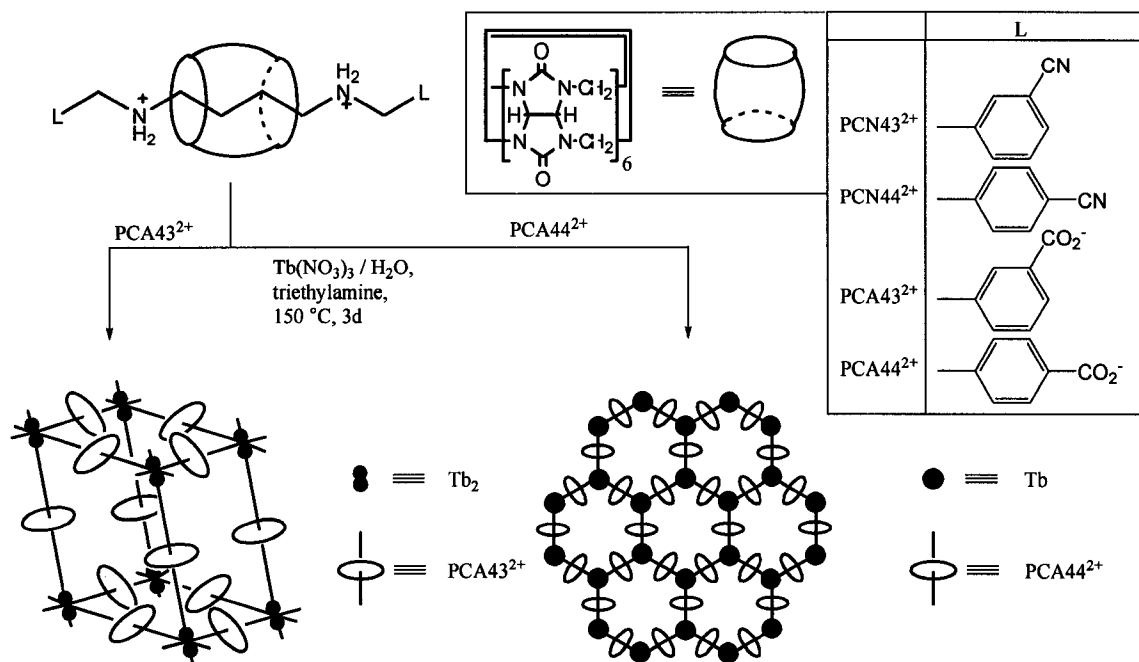
**Figure 3.5**

Leigh's synthetic protocol for the production of main chain, cross-linked, and pendant organic polyrotaxanes.⁵⁵

Kim and coworkers⁵⁶⁻⁶⁰ have applied the principles of self-assembly, molecular recognition and coordination chemistry to the design and synthesis of multi-dimensional polyrotaxanes. They have synthesised several one and two-dimensional architectures, as well as one example of a three-dimensional framework using a dialkylammonium thread and a cucurbit[6]uril, CB[6]. Through a series of supramolecular interactions, the most important of these interactions being a hydrophobic effect, the CB[6] "bead" threads onto a dialkylammonium thread. From a crystal engineering perspective, this is very attractive, the strong association ($K_a = \sim 10^5 - 10^6 \text{ M}^{-1}$) in water allows for a variety of synthetic conditions including a hydrothermal method, which would completely destroy

other pseudorotaxane complexes formed through hydrogen bonding interactions. Once a [2]pseudorotaxane coordinates to a metal centre, the metal acts as a stopper, and the ligand is now a [2]rotaxane.

By varying the metal cation, the associated anion, and the position of the donor group on the terminus of the pseudorotaxane, Kim produced several multi-dimensional polyrotaxanes. These include zigzag, square-wave, straight-chain and helical shaped one-dimensional polyrotaxanes,⁶⁰ two unique two-dimensional polyrotaxanes, a square grid and a hexagonal net. The latter displaying two-fold interpenetration, effectively filling the $\sim 38 \text{ \AA}$ diameter pores.⁵⁶ Under hydrothermal conditions, cyano functional groups on a [2]pseudorotaxane were converted to carboxylates in the presence of $\text{Tb}^{\text{III}}(\text{NO}_3)_3$, forming the first three-dimensional polyrotaxane (Figure 3.6).⁵⁹ Contrary to what is expected, the polyrotaxane did not have a large degree of porosity due to the inclusion of one uncoordinated [2]pseudorotaxane molecule per unit cell.

**Figure 3.6**

Hydrothermal synthesis of a two and three-dimensional polyrotaxane using Tb^{III}.⁵⁹

Previous work in the Loeb group has shown that one and two-dimensional polyrotaxanes are readily self-assembled from DED, DB24C8, and transition metal cations.⁶³ The one-dimensional polyrotaxanes are generated in the solid state by vapour diffusion of *i*Pr₂O into a solution of the [2]pseudorotaxane complex and a metal cation in MeCN. The metal node, in the example in Figure 3.7, has octahedral geometry with two [2]rotaxane ligands coordinated in a *trans* arrangement with the other ancillary ligands being two molecules of MeCN and two molecules of water. It was proposed that if the 1:1 [2]pseudorotaxane to metal cation stoichiometry was changed to 2:1 and the reaction was carried out in a non-coordinating solvent such as MeNO₂, the weakly coordinated MeCN ligands could be replaced by [2]rotaxane ligands. This was in fact the case and several two-dimensional, square grid, polyrotaxanes were characterised by X-ray crystallography and

TGA.⁶³ The Cu^{II} , Co^{II} , Ni^{II} , and Cd^{II} structures are isomorphous, with the Cd^{II} crystals being the easiest to prepare. The metal centres are now coordinated by four [2]rotaxane ligands with the additional coordination sites on the metal being occupied by a molecule of water and one $[\text{BF}_4^-]$ anion. There is significant void space in these structures as the grids do not interpenetrate. They align in an ABA alternating pattern with dimensions of $22.2 \text{ \AA} \times 22.2 \text{ \AA}$ (as measured between Cd^{II} centres). The channels are lined with the [2]rotaxane ligands and are filled with MeNO_2 solvent molecules and anions (15 solvent molecules per Cd^{II} centre). Figure 3.7 shows the structures of these one and two dimensional polyrotaxanes.⁶³

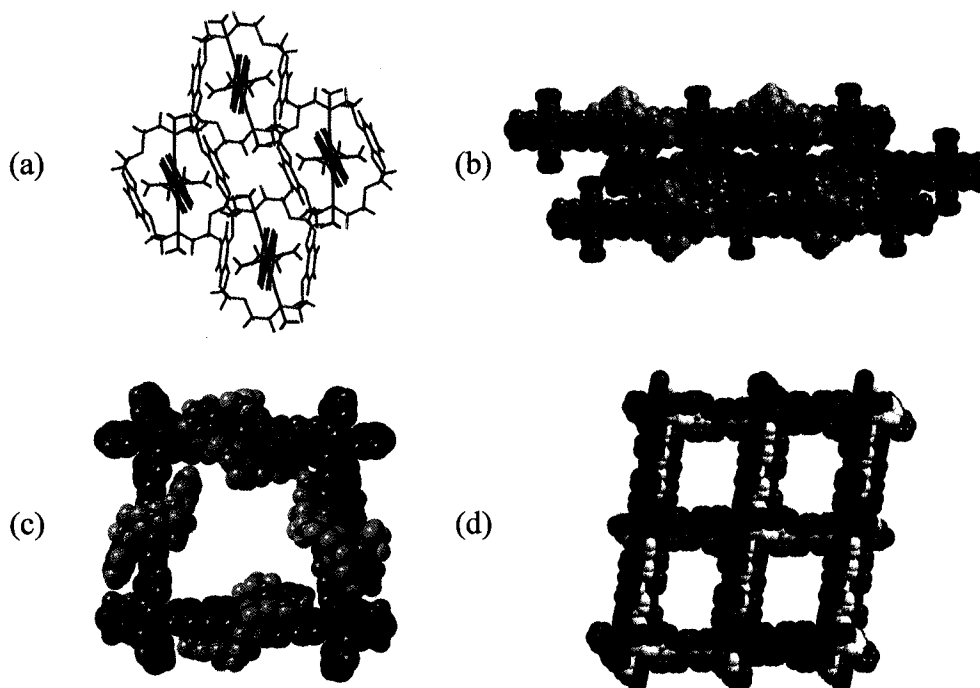


Figure 3.7

Polyrotaxanes previously synthesised in the Loeb group.⁶³ (a) Line drawing of the one dimensional Co^{II} polyrotaxane depicting the packing arrangement down the 001 axis. (b) space-filling diagram of the one dimensional Co^{II} polyrotaxane. (c) and (d) space-filling representations of the two dimensional Cd^{II} polyrotaxane showing the crown ether lined channels and the layering arrangement respectively. Where applicable, solvent molecules and anions have been removed for clarity.

All coordination sites on the octahedral metal centres are still not fully occupied by [2]rotaxanes (structures remain two dimensional), and thus it was thought that by simply replacing the coordinated water and anion the dimensionality could be extended. However, all efforts in this direction failed. It was thought that perhaps the steric demands of the crown ether prevented a coordination number of six. Three solutions to this problem were proposed: (1) a larger cation with an increased coordination number would allow for more ligands to be connected to the metal node, (2) removal of the steric presence of the crown ether by extending the length of the thread component, (3) a combination of both these tactics. Extension of the thread also has the advantage of possibly generating even larger cavities than had been observed for the two dimensional polyrotaxanes.

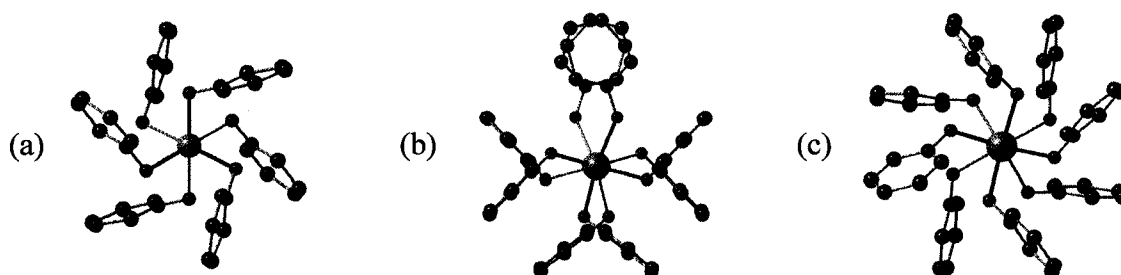


Figure 3.8

Ball and stick representations of some pyridine *N*-oxide metal complexes. (a) $[\text{Hg}(\text{PyNO})_6]^{2+}$, (b) $[\text{La}(\text{PyNO})_8]^{3+}$, (c) $[\text{Nd}(\text{PyNO})_8]^{3+}$.¹² Hydrogens have been omitted for clarity.

A modification of DED that increases its length without disrupting the crown ether recognition site would be to oxidise the terminal nitrogen on the pyridine functionality to the respective *N*-oxide. An N–O bond is typically $\sim 1.3 \text{ \AA}$ and thus the thread dimensions would be increased by $\sim 2.6 \text{ \AA}$ (Figure 3.9), effectively reducing the steric presence of the crown ether on the metal node (Figure 3.10). Pyridine *N*-oxides are known to be

sterically undemanding ligands and readily saturate the coordination sphere of most metals (Figure 3.8).¹² Another perceived advantage is that pyridine *N*-oxides are also excellent ligands for the oxophilic lanthanide cations.¹² These cations are physically larger than the transition metals and also display a coordination number of eight with pyridine *N*-oxide ligands, typically in a square anti-prism geometry. Thus a *N,N'*-dioxide derivative of the DED thread was synthesised; which allows for investigation of the aforementioned hypotheses. Just as the coordination tendencies of DED are reminiscent of 4,4'-bipyridine, the coordination modes observed for **3b** are similar to those for 4,4'-bipyridine *N,N'*-dioxide (Figure 3.).

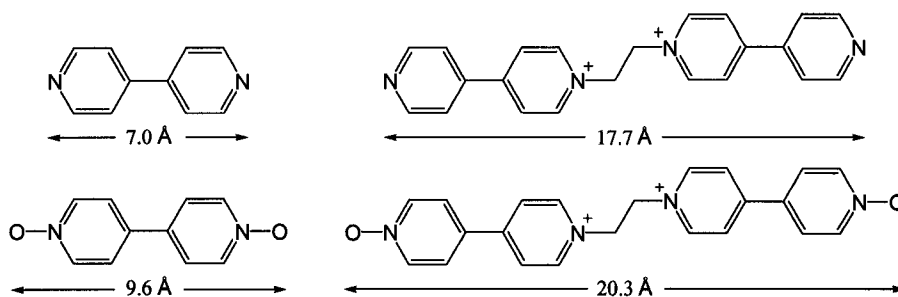


Figure 3.9

Geometric comparison of 4,4'-bipyridine, 4,4'-bipyridine *N,N'*-dioxide, DED and, **3b**.

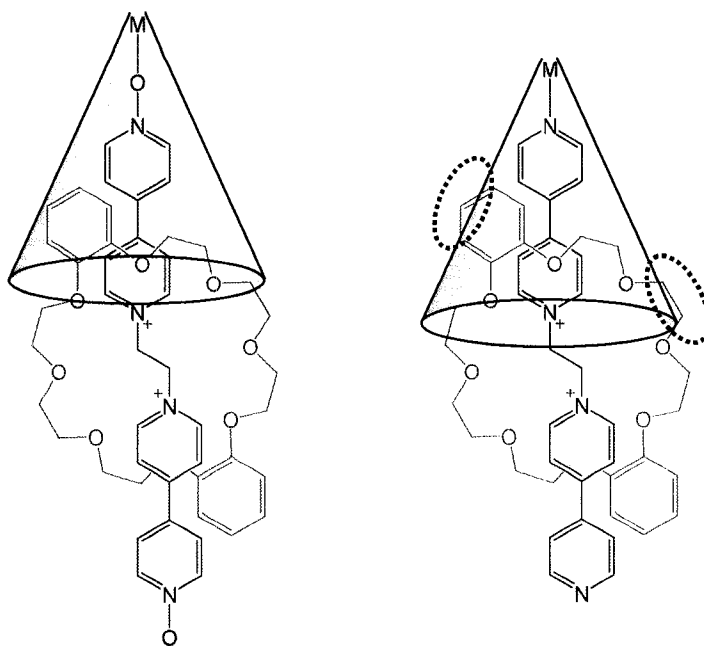


Figure 3.10

Comparison of the steric presence of **3b** \subset DB24C8 and DED \subset DB24C8. The same sized cone has been used in each diagram. Qualitatively it can be seen that DED \subset DB24C8 is bulkier and that the crown ether is positioned much closer to the metal centre.

3.1.4 Functional Materials

A major focus in the research of interlocked molecules is their incorporation into molecular machines and nanotechnology. For these molecules to be useful on a macroscopic level there needs to be a method of organising them in the solid state. One approach to the solution of this problem has been to use programmed self-assembly incorporating metal cations as nodes and pseudorotaxanes as linkers. Tailoring of the solid state properties of the material could be achieved by selective choice of the metal cation (e.g. coordination geometry, oxidation state, and magnetic properties) and also by chemical functionalisation of the distinct rotaxane components.

These metal-based polyrotaxanes are interesting in terms of the design and synthesis of porous solid state materials. Coordination networks have been shown to possess many applications including small molecule sorption/desorption, ion exchange resins, *in situ* catalysis, and gas/fuel storage.⁸ The dynamic nature of the pseudorotaxane ligand is attractive due to the possibility of tailoring the properties of the solid simply through the functionalisation of the crown ether while still maintaining the designed network topology.

3.1.5 Scope

This chapter describes the design and organisation of a new [2]pseudorotaxane into an ordered, three dimensional crystalline lattice. The solution behavior of **3b** \subset DB24C8 will be discussed along with the solid state structures of one two-dimensional polyrotaxane and five three-dimensional polyrotaxane structures.

3.2 Experimental

3.2.1 General Comments

1,2-Dibromoethane and all metal salts were purchased from Aldrich Chemicals except [Yb^{III}][OTf]₃ which was purchased from Strem and were used as received. All deuterated solvents were purchased from Cambridge Isotope Laboratories and used as received. All solvents were purchased from EM Science. ¹H NMR spectra were recorded on a Brüker

Avance 300 or 500 instrument locked to the deuterated solvent at 300.1 or 500.1 MHz respectively. All peak positions are listed in ppm relative to TMS. TGA were performed on a Mettler Toledo TGA/SDTA851^c Instrument under He(g) atmosphere at scan rate of 5 °C/min.

3.2.2 General Methods for X-ray Crystallography

Crystals were frozen in paratone oil inside a cryoloop to prevent loss of solvent. A matrix was run and a unit cell determined prior to collection. A full hemisphere was collected in each case. Reflection data were integrated from frame data obtained from hemisphere scans on a Brüker Apex diffractometer with a CCD area detector with Mo-K_α radiation ($\lambda = 0.71073 \text{ \AA}$). Diffraction data and unit cell parameters were consistent with assigned space groups. The structures were solved by Patterson or direct methods, completed by subsequent Fourier syntheses and refined with full-matrix least-squares methods against $|F^2|$ data. All non-hydrogen atoms were refined anisotropically. All hydrogen atoms were calculated and treated as idealised contributions. Scattering factors and anomalous coefficients are contained in the SHELXTL 5.03 software package (Sheldrick, G.M., Madison, WI).²⁸ All crystallographic figures were prepared using DIAMOND.²⁹

3.2.3 Preparation of Bromoethylbipyridinium *N*-Monoxide [Br] (3a)

2a (5.00 g, 29.0 mmols) was dissolved in 10 mL of 1:1 CHCl₃:MeCN and was added to 40 mL of 1,2-dibromoethane and this mixture refluxed for 24 hrs. The reaction solution was filtered hot and the isolated brown precipitate washed with CHCl₃ and dried in air at room temperature. Yield (9.60 g) 92 %.

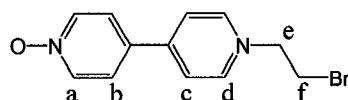


Table 3.1

¹H NMR Spectroscopic Data (D₂O, 300 MHz) for **3a**.

Proton	δ (ppm)	Multiplicity	Peak Area	<i>J</i> (Hz)
a	8.928	d	2	6.9
b	8.363	d	2	6.9
c	8.439	d	2	7.9
d	8.046	d	2	7.9
e	4.992	t	2	5.8
f	3.930	t	2	5.8

3.2.4 Preparation of bis(4,4'-Bipyridinium *N*-Monoxide) Ethane [OTf]₂ (**3b**)

3a (5.00 g, 13.9 mmols) and **2a** (3.59 g, 20.9 mmols) were dissolved in MeCN (75 mL) and refluxed for 1 week. The light brown precipitate was filtered, dried and then dissolved in a minimum amount of H₂O. Five equivalents of [Na][OTf] were added and the mixture was heated until the solution was homogeneous. The solution was then cooled and the triflate salt of **3b** was isolated as a light tan powder. Yield (4.23 g) 45.4%.

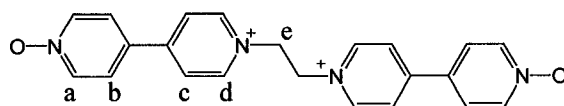


Table 3. 1

¹H NMR Spectroscopic Data (CD₃NO₂, 500 MHz) for **3b**.

Proton	δ (ppm)	Multiplicity	Peak Area	<i>J</i> (Hz)
a	8.892	d	4	6.9
b	8.449	d	4	6.9
c	8.305	d	4	7.4
d	7.965	d	4	7.4
e	5.417	s	4	

3.2.5 Preparation of $[\text{Cd}^{\text{II}}(\mathbf{3b})_2(\text{DB24C8})][\text{OTf}]_6$ (**3c**)

3b (15 mg, 0.02 mmols) and DB24C8 (30 mg, 0.06 mmols) were combined in 0.5 mL of MeNO₂. This solution was then added to a solution of $[\text{Cd}^{\text{II}}][\text{BF}_4]_2$ (4 mg, 0.01 mmols) in 0.5 mL of MeNO₂. *i*Pr₂O vapour was allowed to diffuse into the reaction mixture to produce orange, X-ray quality crystals. Yield (8.4 mg) 30.1%.

Table 3.3

Crystal data and details of structure solution and refinement for compound **3c**.

Formula	C ₇₈ H ₈₄ CdF ₁₈ N ₁₂ O ₃₈ S ₆	Collection Temp [K]	223(2)
Formula Weight	2444.33	ρ_{calcd} [g cm ⁻³]	1.630
Crystal System	Triclinic	μ (MoK α) [mm ⁻¹]	0.471
Space Group	<i>P</i> -1	Min/max trans	0.7034/1.0000
a [Å]	11.5792(10)	Unique data	19924
b [Å]	12.4592(11)	R(int)	0.1059
c [Å]	19.0001(17)	R1 [I > 2 σ I]	0.0988
α [°]	88.380(2)	R1 [all data]	0.1526
β [°]	84.943(2)	wR2 [I > 2 σ I]	0.2580
γ [°]	65.788(2)	wR2 [all data]	0.3022
V [Å ³]	2490.2(4)	Data/variables	8737/691
Z	1	Goodness-of-fit	1.003

3.2.6 Preparation of $[M^{III}(3b)_3(DB24C8)_3][OTf]_{8.5}[Cl]_{0.5}$ ($M^{III} = Sm^{III}(3d), Eu^{III}(3e), Gd^{III}(3f), Tb^{III}(3g)$)

3b (15 mg, 0.02 mmols) was combined with DB24C8 (30 mg, 0.06 mmols) in 0.5 mL of MeCN. This pseudorotaxane was then added to a solution of $[M^{III}][OTf]_3$ (4.5 mg, 0.01 mmols) in 0.5 mL of MeCN in a vial. Large orange crystals were observed to form upon standing for four days. Yield (10 mg) 51 %. TGA results for all four compounds are consistent and show loss of MeCN and water solvent to ~ 90 °C and thermal decomposition of the coordination framework occurring at ~ 250 °C.

Table 3.4

Crystal data and details of structure solution and refinement for **3d**.

Formula	$C_{152}H_{163.75}Cl_{0.5}F_{25.5}N_{14.75}$ $O_{64.09}S_{8.5}Sm$	Collection Temp [K]	100(2)
Formula Weight	4147.67	ρ_{calcd} [$g\ cm^{-3}$]	1.322
Crystal System	Triclinic	μ ($MoK\alpha$) [mm^{-1}]	0.476
Space Group	<i>P</i> -1	Min/max trans	0.8854/1.0000
a [\AA]	17.5661(13)	Unique data	66987
b [\AA]	23.4327(13)	R(int)	0.0483
c [\AA]	27.0910(17)	R1 [$I > 2\sigma I$]	0.1248
α [$^\circ$]	78.0860(10)	R1 [all data]	0.1421
β [$^\circ$]	80.5090(10)	wR2 [$I > 2\sigma I$]	0.3295
γ [$^\circ$]	74.0460(10)	wR2 [all data]	0.3524
V [\AA^3]	10421.2(12)	Data/variables	27216/3064
Z	2	Goodness-of-fit	1.576

3.2.7 Preparation of $[\text{Yb}^{\text{III}}(\mathbf{3b})_3(\text{DB24D8})_3][\text{OTf}]_8[\text{Cl}]$ (**3h**)

3b (15 mg, 0.02 mmols) was combined with DB24C8 (30 mg, 0.06 mmols) in 0.5 mL of MeCN to form the pseudorotaxane. This [2]pseudorotaxane solution was added to the bottom of a diffusion tube and 0.25 mL of MeCN was layered on top of this, followed by a solution of $[\text{Yb}^{\text{III}}][\text{OTf}]_3$ (4.7 mg, 0.01 mmols) in 0.5 mL of MeCN. Large yellow crystals grew at the metal and [2]pseudorotaxane solution interface after four days. Yield (5.2 mg) 17.0 %.

Table 3.5

Crystal data and details of structure solution and refinement for **3h**.

Formula	$\text{C}_{160}\text{H}_{175.5}\text{ClF}_{24}\text{N}_{19}\text{O}_{59.5}$ S_8Yb	Collection Temp [K]	100(2)
Formula Weight	4237.66	ρ_{calcd} [g cm^{-3}]	1.215
Crystal System	Triclinic	μ ($\text{MoK}\alpha$) [mm^{-1}]	0.579
Space Group	<i>P</i> -1	Min/max trans	0.7412/1.0000
a [\AA]	20.495(3)	Unique data	91905
b [\AA]	22.701(3)	R(int)	0.0980
c [\AA]	27.435(3)	R1 [$I > 2\sigma I$]	0.1417
α [$^\circ$]	84.146(3)	R1 [all data]	0.1841
β [$^\circ$]	78.935(3)	wR2 [$I > 2\sigma I$]	0.3729
γ [$^\circ$]	67.636(2)	wR2 [all data]	0.4003
V [\AA^3]	11579(3)	Data/variables	40594/2444
Z	2	Goodness-of-fit	1.426

3.3 Results and Discussion

3.3.1 Synthetic Design and Considerations

Previous work in the Loeb group has shown that in a non-coordinating solvent, a transition metal will coordinate four [2]rotaxane ligands forming two-dimensional grids with solvent and an anion in the apical coordination sites.⁶³ All attempts to replace these apical ligands with [2]rotaxanes in order to extend these grids into the third dimension were previously unsuccessful. As mentioned, it was theorized then that the steric bulk of the crown ether on the ligand prevented higher coordination numbers. In order to allow more ligands to coordinate to a metal node, thereby increasing the dimensionality, three possibilities were investigated: a larger cation (Figure 3.11) with a higher coordination number, extension of the length of the thread portion of the [2]pseudorotaxane, and a combination of both.

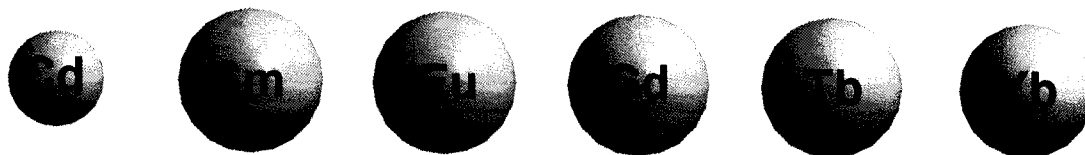


Figure 3.11

Relative sizes of the cations used in the construction of multi-dimensional polyrotaxanes. Atomic radii: 1.71 Å, 2.59 Å, 2.56 Å, 2.54 Å, 2.51 Å, and 2.40 Å for Cd to Yb respectively.

Several things must be considered when designing a synthetic protocol for these polyrotaxanes. First, the self-assembly of these solid state structures is inherently a dynamic process in which the intact [2]pseudorotaxane complex is in equilibrium with its

uncomplexed components. This is in addition to the complexation and decomplexation of metal coordinate bonds. Secondly, the linking of a [2]pseudorotaxane into a polyrotaxane network can be considered a special case of a capping reaction whereby the metal nodes act as a stopper preventing the crown ether from becoming unthreaded. With these processes in mind, a few guidelines were followed and a synthetic approach developed (Figure 3.12):

1. All reactions were carried out at room temperature.
2. The [2]pseudorotaxane was formed prior to addition of the metal salt.
3. Excess crown ether will help to ensure that the thread is completely complexed and that the species coordinating the metal centre is a [2]pseudorotaxane.
4. All components must be soluble in a solvent such as MeCN that is amenable to the formation of hydrogen bonds.
5. The coordinating, functional group on the thread must be a better donor than the solvent. (i.e., the appropriate solvent must be non- or weakly-coordinating).
6. X-ray quality, single crystals must be isolated as crystallography will be the only technique capable of unambiguous structural characterisation.

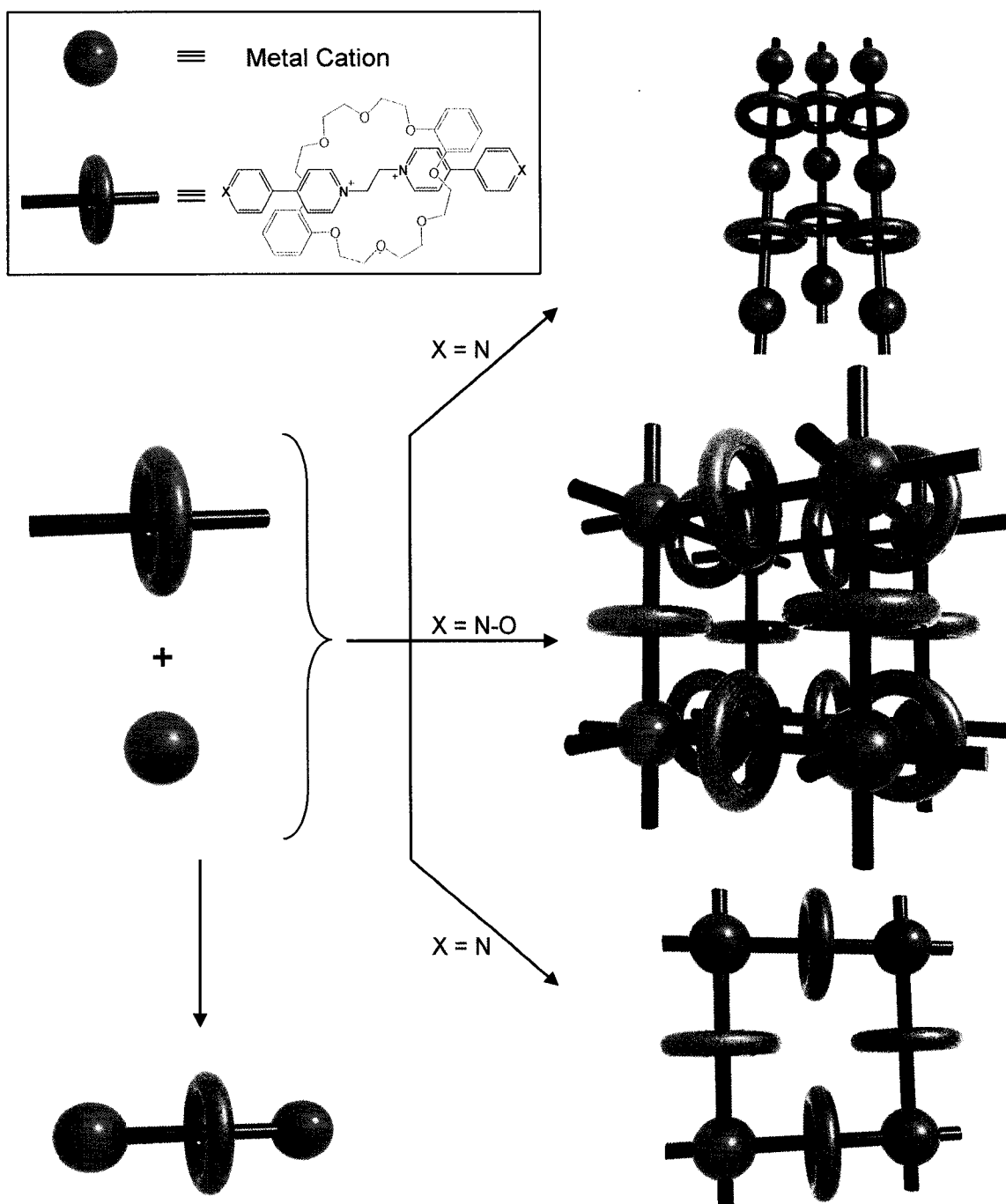


Figure 3.12

The synthetic protocol for the preparation of polyrotaxanes. Starting with a [2]pseudorotaxane (red and blue) and a suitable metal cation (green) multi-dimensional polyrotaxanes are easily prepared through self-assembly.

3.3.2 Synthesis of a [2]Pseudorotaxane and its Components

The synthesis of thread, **3b**, was completed in two steps from the previously synthesised, **2a**, following the method of Wisner.⁴⁰ In order to increase the solubility of the thread in less competitive, less polar solvents suitable for the formation of hydrogen bonded [2]pseudorotaxanes such as MeCN and MeNO₂, the hard bromide ions were exchanged for triflate anions. In MeCN, **3b** has an association constant, K_a , of 1125 M⁻¹ with DB24C8 as measured by ¹H NMR spectroscopy at 298 K. This compares well to DED which, in MeCN, has a K_a of 878 M⁻¹ with DB24C8.⁶⁴ The K_a was calculated by comparing the relative peak areas between the complexed and uncomplexed forms in the ¹H NMR spectra using the single point method.

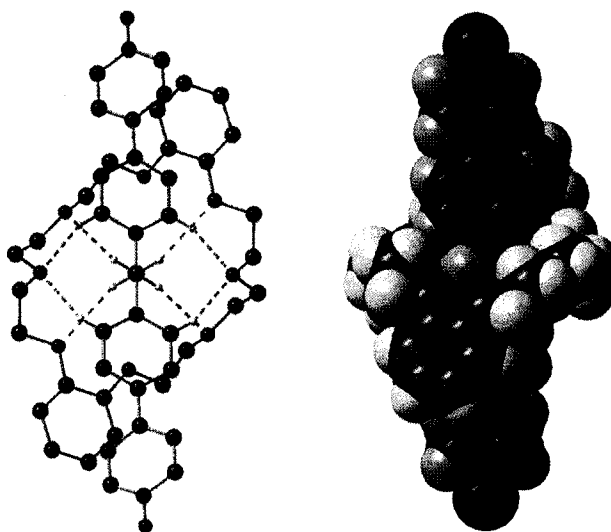


Figure 3.13

Ball and stick and space-filling models of **3b** ⊂ DB24C8. Key: blue = N, black = C; red = O; white = H. Anions and selected hydrogen atoms have been removed for clarity.

Table 3.6Selected hydrogen bond distances and angles in **3b** ⊂ DB24C8.

Hydrogen Bonded Atoms	C-H...O Distances (Å)	C-H...O Angles (°)
H8A...O3	2.560(2)	147.03(1)
H9A...O3	2.377(1)	156.47(1)
H11A...O2	2.777(1)	155.84(1)
H11B...O4	2.433(1)	166.63(2)

The solid state structure of the **3b** ⊂ DB24C8 (Figure 3.13) complex clearly shows the intermolecular interactions that exist between the thread and the crown. There are eight C-H...O hydrogen bonds, as well as ion-dipole interactions between the electronegative oxygen atoms in the crown and the positively charged pyridinium nitrogen atoms of the thread (Table 3.6). Molecules of **3b** ⊂ DB24C8 align in the solid state to maximise intermolecular π -stacking interactions.

Due to the dynamic nature of a [2]pseudorotaxane, a large excess of DB24C8 (~ 3 equivalents) was used in the preparation of **3b** ⊂ DB24C8 in order to ensure that the equilibrium was in favour of the complexed form. This is a necessary consideration in order to ensure that it is the [2]pseudorotaxane that is being converted to a [2]rotaxane through coordination of a metal cation, and not simply the uncomplexed thread.

Table 3.7

Crystal data and details of structure solution and refinement for **3b** \subset DB24C8.

Formula	$C_{104}H_{116}F_{12}N_{12}O_{32}S_4$	Collection Temp [K]	223(2)
Formula Weight	2402.33	ρ_{calcd} [g cm ⁻³]	1.433
Crystal System	Monoclinic	μ (MoK α) [mm ⁻¹]	0.190
Space Group	<i>P2(1)/c</i>	Min/max trans	0.6819/1.0000
a [Å]	10.8524(14)	Unique data	15730
b [Å]	19.706(3)	R(int)	0.0287
c [Å]	13.0660(17)	R1 [I > 2 σ I]	0.1204
α [°]	90.00	R1 [all data]	0.1219
β [°]	95.073(2)	wR2 [I > 2 σ I]	0.2996
γ [°]	90.00	wR2 [all data]	0.3009
V [Å ³]	2783.3(6)	Data/variables	3622/370
Z	1	Goodness-of-fit	1.115

3.3.3 Two-Dimensional Polyrotaxane Based on a Cd^{II} Cation

Continuing from the two-dimensional polyrotaxanes previously synthesised in the Loeb group, a Cd^{II} metal node was employed in combination with the new longer thread, **3b**. It was thought that the lessened steric requirements of the *N*-oxide donor would increase the ligand coordination number on the Cd^{II} centre from four to six, effectively increasing the dimensionality of the polyrotaxane topology. However, only two [2]rotaxanes are coordinated in the resultant structure, with the remaining ligands being two uncomplexed threads and two triflate anions (Figure 3.14). The two dimensional, square grids layer in an offset ABA pattern which eliminates any possible void space (Figure 3.15).

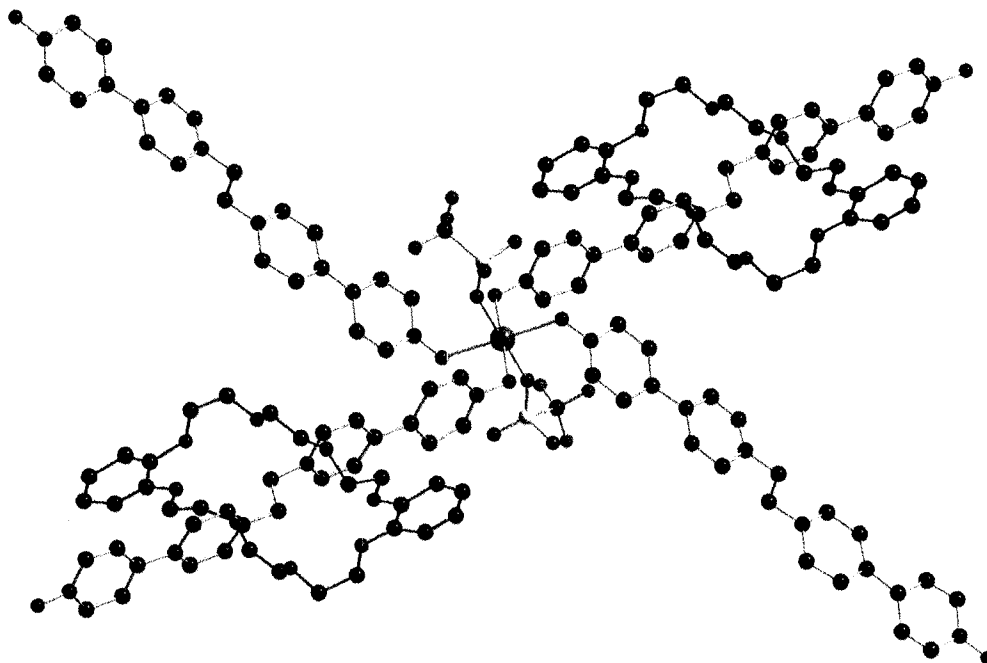


Figure 3.14

Ball and stick model of the Cd^{II} coordination sphere showing the *trans* arrangement of the ligands. Key: bronze = Cd^{II}; blue = N, black = C; red = O; green = F; yellow = S. Hydrogen atoms, solvent molecules and some anions, have been omitted for clarity.

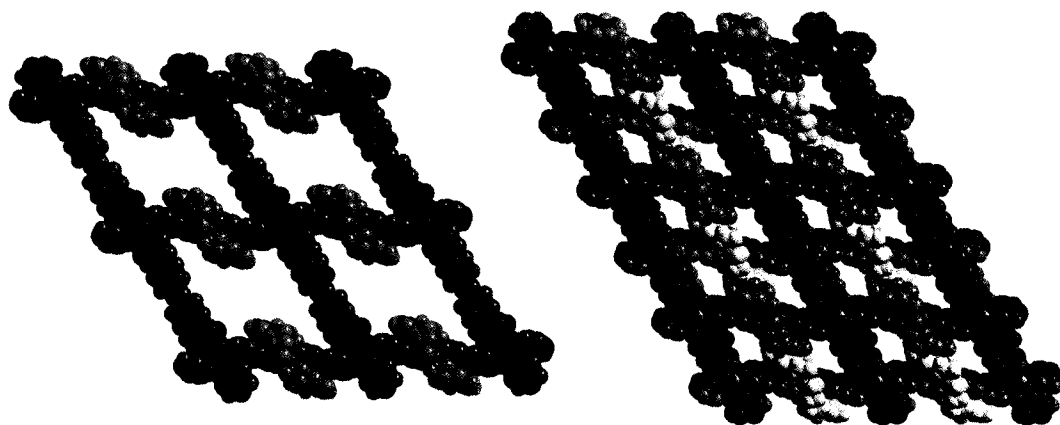


Figure 3.15

Space-filling views of **3c**. Left: a single net showing complexed and uncomplexed ligands. Right: Depiction of how one net (green and orange) fills the cavity of an adjacent net (blue and red). Solvent and anions have been omitted for clarity.

This network is reminiscent of the one-dimensional Co^{II} structure, and can be thought of as a pillared one-dimensional polyrotaxane (Figure 3.16). The two [2]rotaxanes coordinate to the Cd^{II} centre in one dimension while two uncomplexed threads *cis* to each [2]rotaxane unit pillar the polyrotaxane stands in the second dimension.

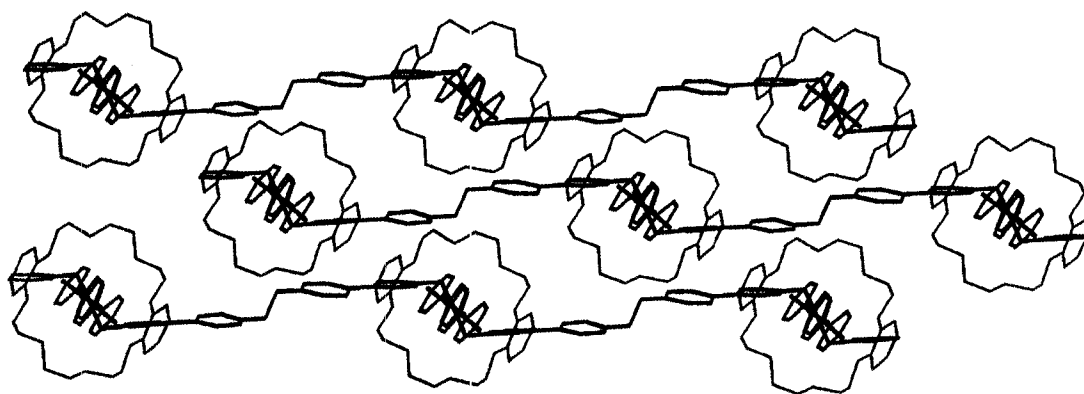


Figure 3.16

Line drawing of **3c** depicting the pillared nature of the polyrotaxane. It is also possible to see how the individual layers close pack, eliminating void space. Hydrogen atoms, anions, and solvent molecules have been omitted for clarity.

In the two-dimensional **3c** structure it was postulated that no interpenetration was observed due to the dynamic nature of the crown ether. During the self-assembly procedure the macrocycle is continually “flipping” and rotating about the thread, thus occupying a much larger volume than is observed in the solid-state picture. The increased length of **3b** had an interesting, unforeseen effect on the topology of the new two-dimensional network. While not interpenetrated, the individual nets close pack with the crown ether of one layer filling the void space in an adjacent layer. Now that the [2]pseudorotaxane ligand is slightly longer, the cavity is also increased in size thus allowing for the “inclusion” of another net.

3.3.4 Three-Dimensional Polyrotaxanes Based on Sm^{III}, Eu^{III}, Gd^{III}, Tb^{III} Cations

Since it was not possible to saturate the coordination sphere of a Cd^{II} centre with [2]rotaxanes following the aforementioned guidelines, a larger cation with more available coordination sites was used in the preparation of a three-dimensional polyrotaxane. The result (using four different lanthanides) was a three dimensional, “cubic” architecture in which all linkers are [2]rotaxanes. It is interesting to note that the complexes were still not homoleptic, with two coordination sites on the metal occupied by one triflate anion and one molecule of water respectively (Figure 3.17).

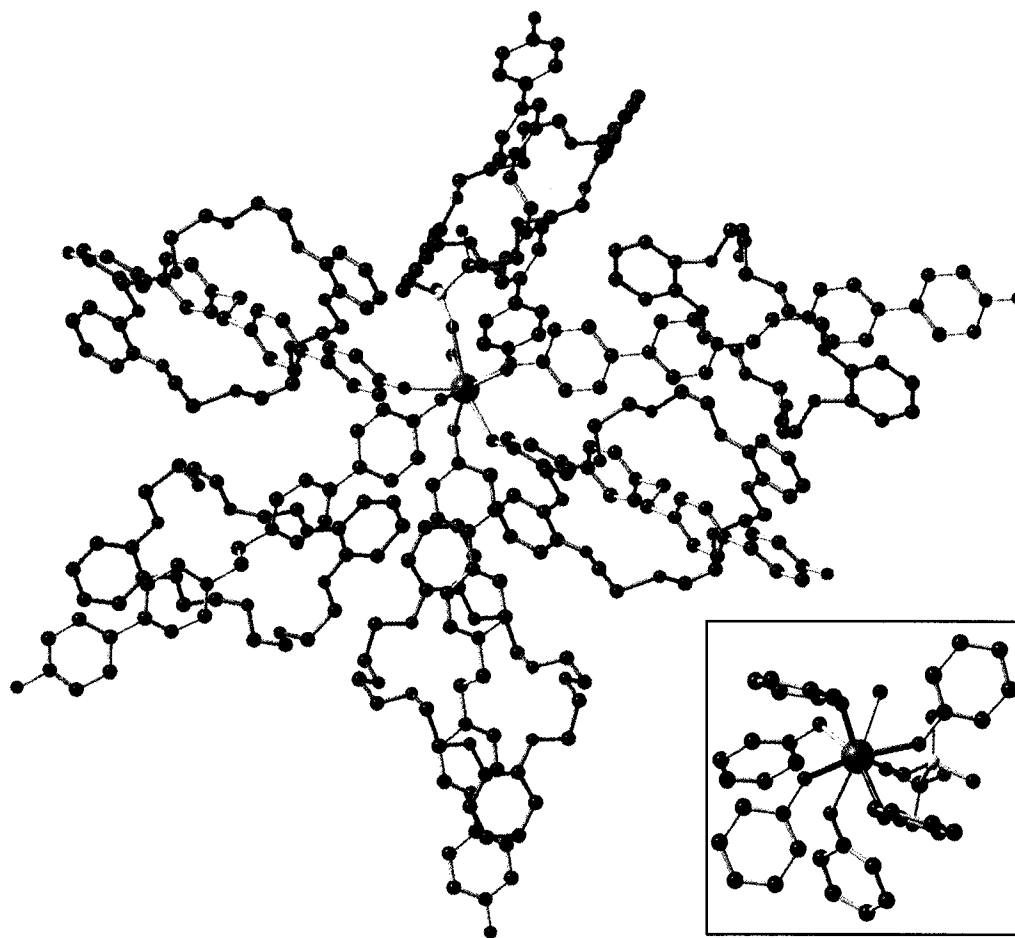


Figure 3.17

Ball and stick representation of the Sm^{III} centre with six coordinated [2]rotaxanes. Inset: primary coordination sphere of the Sm^{III} cation showing the distorted square anti-prism geometry. Key: bronze = Sm^{III} ; blue = N, black = C; red = O; green = F; yellow = S. Hydrogen atoms, anions, and solvent molecules have been omitted for clarity.

Single crystals, suitable for X-ray analysis, of **3d-g** are readily prepared from an MeCN solution over a few days. The large crystals readily desolvate at room temperature and become opaque, amorphous solids, but will retain their crystallinity for extended periods of time when maintained in MeCN. Single crystal data have been collected for complexes containing Sm^{III} , Eu^{III} , Gd^{III} , and Tb^{III} and preliminary analysis has shown them to be isomorphous. A full solution of the Sm^{III} data was performed and the same

treatment of the other datasets was deemed redundant. All structural diagrams in this section are generated from the Sm^{III} structure and are assumed to represent all four polyrotaxane complexes.

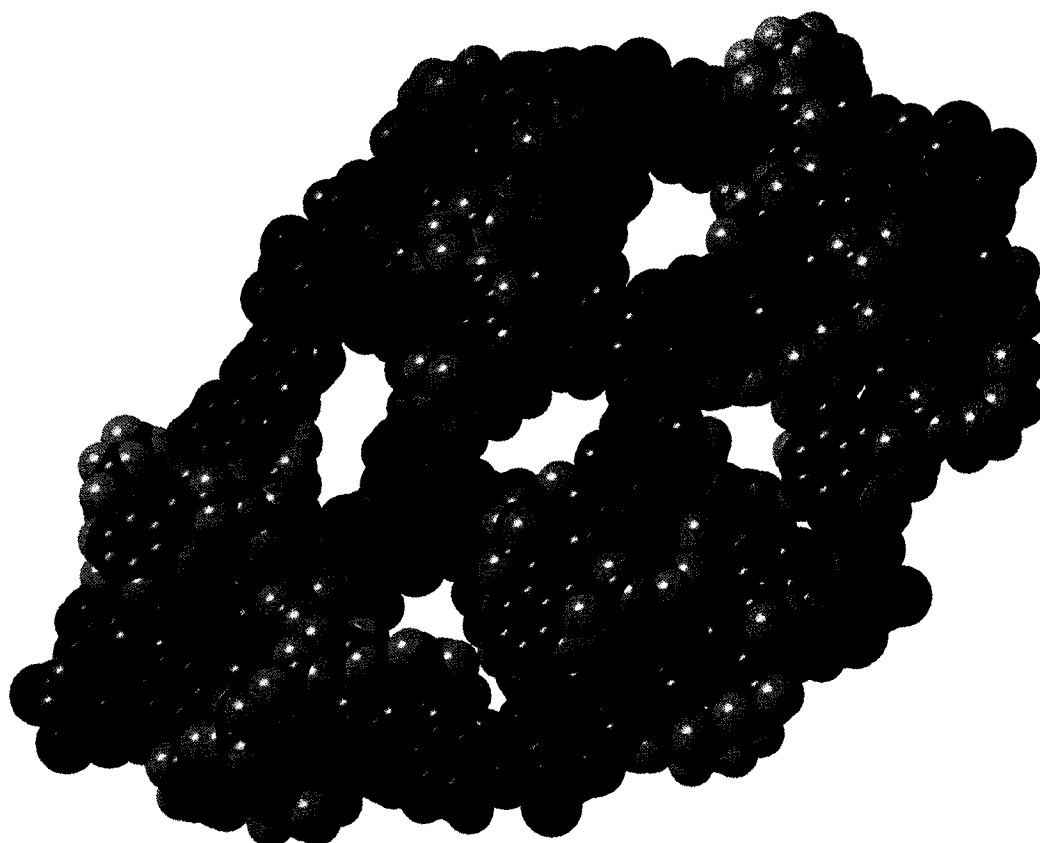


Figure 3.18

Space-filling model depicting a single, cubic unit of the Sm^{III} structure. Metal–metal distances are $\sim 24 \text{ \AA}$. The volume is $\sim 10,000 \text{ \AA}^3$. Hydrogen atoms, anions, and solvent molecules have been omitted for clarity. Also, extraneous ligands and the interpenetrated net has been removed for clarity.

The primary coordination sphere has a distorted square anti-prism geometry (Figure 3.17), while the terminal oxygen atoms on the six [2]rotaxane ligands propagate in a distorted octahedral geometry. It is this geometry that propagates the polyrotaxane network in a “cubic” fashion (Figure 3.18). Despite the fact that these structures display single interpenetration, there is still some available void space which is occupied by

anions and solvent. There are nine triflate anions, seven molecules of MeCN, and twelve molecules of water present in the asymmetric unit. As a result of the longer ligand dimensions, the cubes defined by twelve [2]rotaxanes and eight metal nodes at the corners have become large enough for interpenetration to occur as compared to $\text{Cd}^{\text{II}}(\text{DED} \subset \text{DB24C8})_2$ (Figure 3.19). Considering Van der Waals radii, the width of **3b** \subset DB24C8 is $\sim 11.6 \text{ \AA}$. Therefore the necessary cavity dimensions (metal–metal distance) required for interpenetration of a polyrotaxane network is estimated to be $\sim 23.2 \text{ \AA}$ (Figure 3.20).

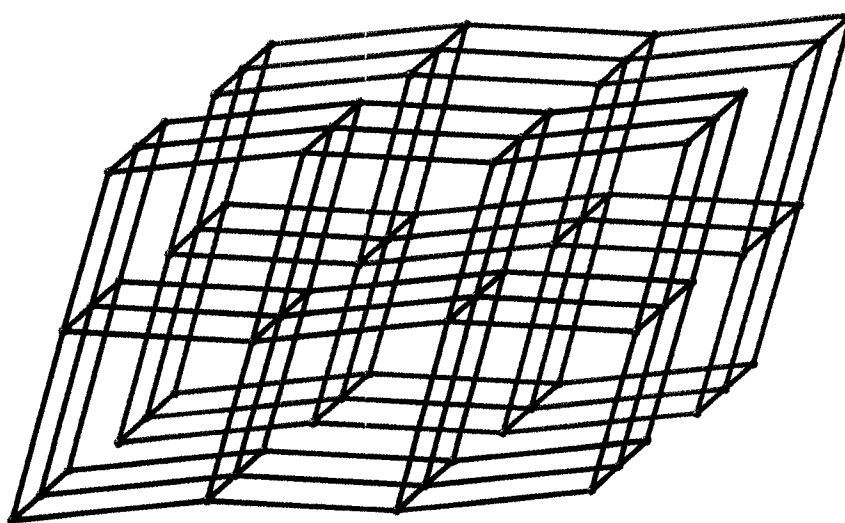


Figure 3.19

Line drawing showing the twofold interpenetrated nature of the Sm^{III} , Eu^{III} , Gd^{III} , and Tb^{III} polyrotaxane networks.

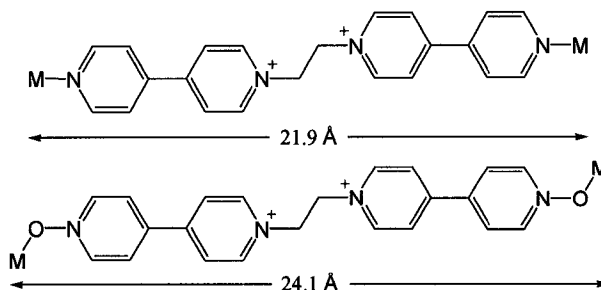


Figure 3.20

Comparison of the metal–metal distances in the DED and **3b** polyrotaxanes.

3.3.5 Three Dimensional Polyrotaxane Based on a Yb^{III} Cation

Upon switching to a slightly smaller cation, Yb^{III} , another three-dimensional polyrotaxane was synthesised. These large crystals are easily isolated in acceptable yield by slow diffusion of a solution of $\text{Yb}^{\text{III}}[\text{OTf}]_3$ into a solution of **3b** \subset DB24C8 at room temperature (Figure 3.21).



Figure 3.21

Diffusion tube used in the preparation of **3h**.

Instead of having a coordination number of eight, the Yb^{III} cation is seven coordinate; six ligands are [2]rotaxanes with coordination of an ancillary triflate anion occupying an apical position. The primary coordination sphere is a slightly distorted pentagonal bipyramid (Table 3.8), that is, five ligands in a planar, pentagonal arrangement with two apical ligands normal to the face of the pentagon (Figure 3.22 and Figure 3.23).

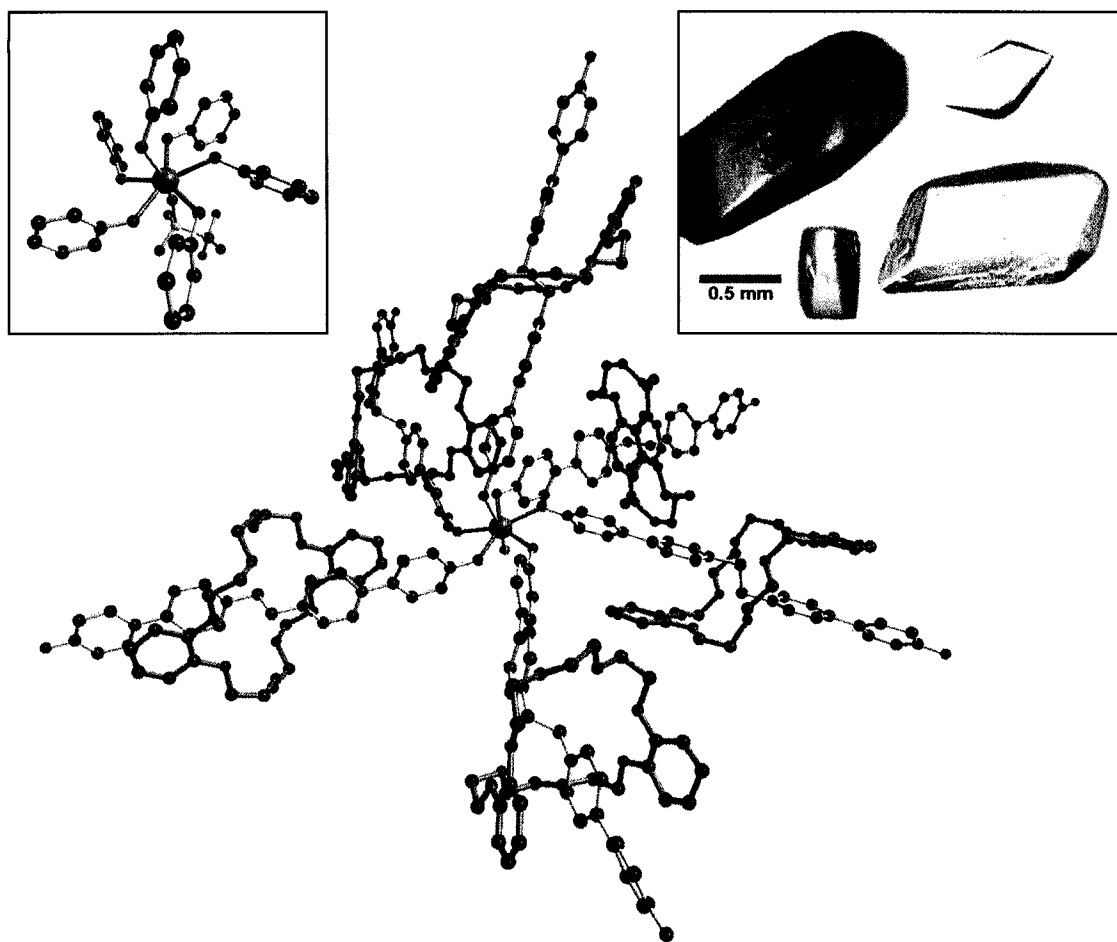


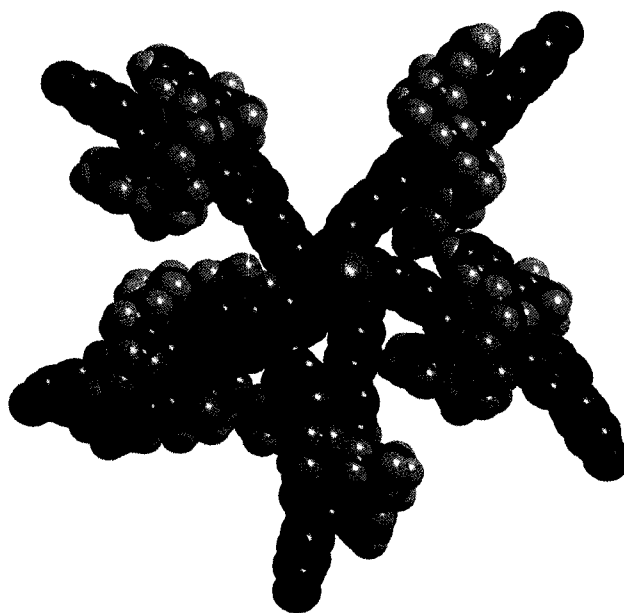
Figure 3.22

Ball and stick illustration of the coordination environment around the Yb^{III} centre. The **3b** threads are depicted with silver bonds and the crown ether molecules are connected by gold bonds. Inset (left): primary coordination sphere of the Yb^{III} cation displaying the pentagonal bipyramidal geometry. Inset (right): micrograph showing the colour and size of the Yb^{III} crystals. Key: bronze = Yb^{III} ; blue = N, black = C; red = O; green = F; yellow = S. Hydrogen atoms, anions, and solvent molecules have been omitted for clarity.

Table 3.8

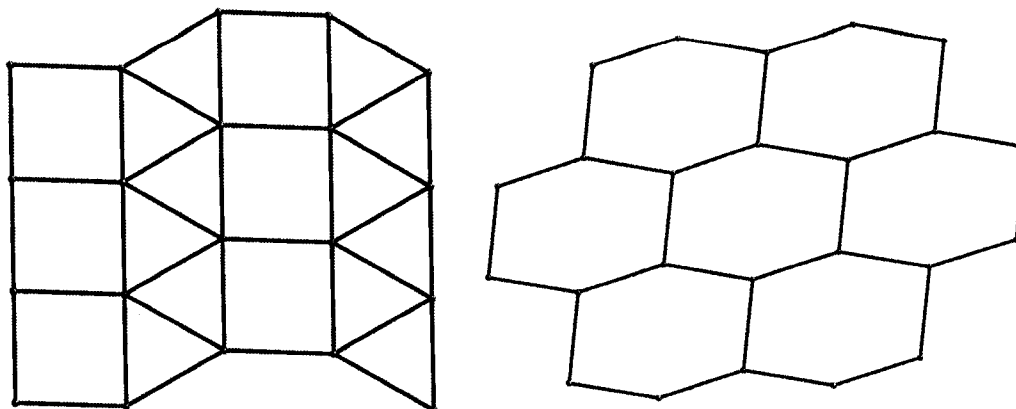
Selected angles from **3h**. The coordination angles show the near perfect pentagonal symmetry while the terminal O–Yb–O angles are close to expected angles for an equilateral triangle (60°) and a rectangle (90°).

Coordination Angles		Terminal Angles	
	Angle (°)		Angle (°)
O1–Yb1–O3	71.48	O1–Yb1–O3	57.13
O3–Yb1–O2	74.12	O3–Yb1–O4	63.73
O2–Yb1–O6	73.25	O4–Yb1–O6	85.68
O6–Yb1–O4	71.49	O6–Yb1–O2	91.71
O4–Yb1–O1	71.49	O2–Yb1–O1	61.26

**Figure 3.23**

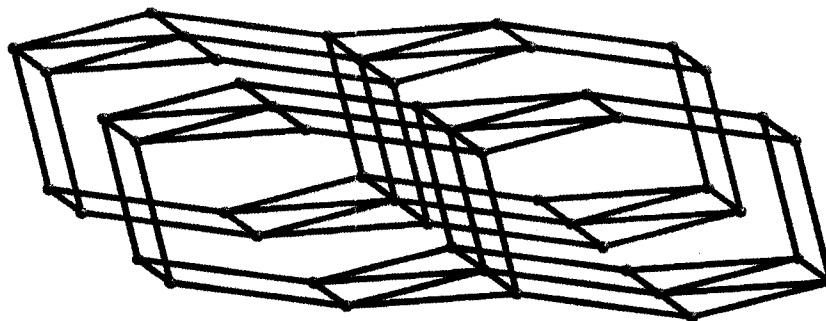
Space-filling model of Yb^{III} coordination sphere demonstrating the pentagonal symmetry and packing of five [2]rotaxanes around a single metal node. The apical ligands are removed for clarity.

With respect to the [2]rotaxane ligands, the Yb^{III} centre has *pentagonal pyramidal* geometry, while the terminal *N*-oxide oxygens diverge from the pentagonal symmetry and allow for the planar tessellation of a five-connected node. Following the system for naming periodic, three-dimensional nets by Wells⁶⁵, the network can be fully described as a $\left(\begin{smallmatrix} 3 \\ 4,6 \end{smallmatrix}\right)$ net, which is a previously unknown topology. The numbering scheme can be explained as follows: (n, p) , or in this case $\left(\begin{smallmatrix} l \\ m, p \end{smallmatrix}\right)$, where n is the number of edges of a polygon and p is the number of edges meeting at a vertex, such that a $\left(\begin{smallmatrix} 3 \\ 4,6 \end{smallmatrix}\right)$ net is comprised of triangles ($l = 3$), rectangles (squares) ($m = 4$) and hexagons ($n = 6$) all meeting at a six-connected node ($p = 6$). The structure can also be characterised as a pillared, $\left(\begin{smallmatrix} 3 \\ 4,5 \end{smallmatrix}\right)$ two dimensional, plane net (Figure 3.24). The $\left(\begin{smallmatrix} 3 \\ 4,5 \end{smallmatrix}\right)$ net, comprised of alternating triangles and squares (five-connected), was until recently,^{66,67} unknown in chemical systems.

**Figure 3.24**

Plane tessellations observed in the **3h** structural motif. Left: $\left(\frac{3}{4}, 5\right)$, as observed down the crystallographic *c* axis. Right: hexagonal (6,3) pattern as viewed down the crystallographic *b* axis..

Similar to the other three dimensional structures, **3h** is singly interpenetrated (Figure 3.25). Despite the interpenetration, there is still available void space which is occupied by anions and solvent molecules.

**Figure 3.25**

Line drawing of showing the interpenetrated nature of **3h** and the propagation of the $\left(\frac{3}{4}, 6\right)$ net.

3.4 Conclusions

In an attempt to organise [2]rotaxanes into a three-dimensional, regular solid, a new thread was synthesised which is sterically less-demanding and has good donor properties for the oxophilic lanthanide cations. A [2]rotaxane ligand containing the **3b** thread was coordinated to a Cd^{II} centre forming a two-dimensional polyrotaxane square grid. The Cd^{II} network is similar to other two-dimensional polyrotaxanes previously synthesized, indicating that a larger cation with a higher coordination number is necessary in order to self-assemble a three-dimensional solid.

Two different three-dimensional polyrotaxane topologies were self-assembled at room temperature incorporating several different lanthanide cations as nodes and **3b** \subset DB24C8 as a linker. The Yb^{III} network topology is previously unreported and is unique in that it is based upon a pentagonal geometry. The observed interpenetration was unexpected and generation of a non-interpenetrated, three-dimensional solid is the next challenge.

Now that a procedure for self-assembling ordered, three-dimensional motifs incorporating a mechanical linkage has been determined, the next challenge is to add functionality. In order to avoid interpenetration of the nets a larger crown, such as DN24C8, might be employed. Functionality may be incorporated into the crystal lattice by using a “molecular shuttle” or “flip switch” as a ligand instead of the [2]rotaxane.

Chapter Four - Electrostatics in Pseudorotaxane Formation

4.1 Introduction

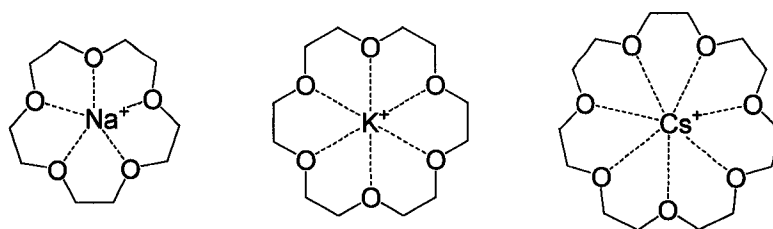
Pleasantest of all ties is the tie of host and guest.

Aeschylus⁶⁸

4.1.1 Supramolecular Cation Complexation

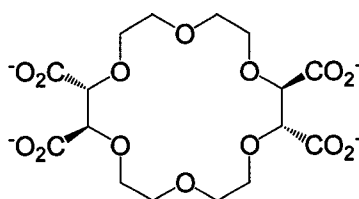
With his seminal paper in 1967, Pedersen,⁶⁹ showed that cyclic polyethers, which he termed crown ethers due to their solid state architecture, form stable complexes with metal and ammonium cations.

Typically, ethers are poor ligands. However, crown ethers are well suited to complex a variety of cations, making use of chelate and macrocyclic effects. Indeed, the interest in crown ether chemistry lies in their ability to selectively bind cations. This selectivity for a particular cation is a direct function of the size of the cavity within the macrocycle. The size–selectivity relationship of some example crown ethers are shown in Figure 4.1.¹

**Figure 4.1**

Cation selectivity as a function of cavity size in various crown ethers; the cavity of 15C5 is complementary to the Na^+ cation, while 18C6 and 21C7 are selective towards K^+ and Cs^+ , respectively.¹

One of the tenets of supramolecular chemistry is that although a single intermolecular interaction may be weak, the cooperation of several such non-covalent interactions can be significant. That is, the larger the number of interactions present between a substrate and receptor, the stronger the association. With this in mind, different crown ethers have been designed to interact with a cation not only through the electronegative oxygen atoms but also through anionic groups placed on the periphery of the macrocycle. For example, the tetra-anion shown in Figure 4.2 displays a 4000-fold increase in the stability of the K^+ complex over 18C6.⁷⁰

**Figure 4.2**

The incorporation of electrostatic components onto the crown ether moiety greatly increases the stability of the cation complex.⁷⁰

4.1.2 Sulfonated Crown Ethers

Sulfonated crown ethers have received relatively little attention in the literature and have primarily been used in analytical sciences for the sequestration of alkali, alkaline earth, and lanthanide cations from aqueous solution.⁷¹⁻⁷⁴ In this study, several mono- and di-sulfonated crown ethers were synthesised, and their binding constants with the aforementioned cations were compared (Figure 4.3).

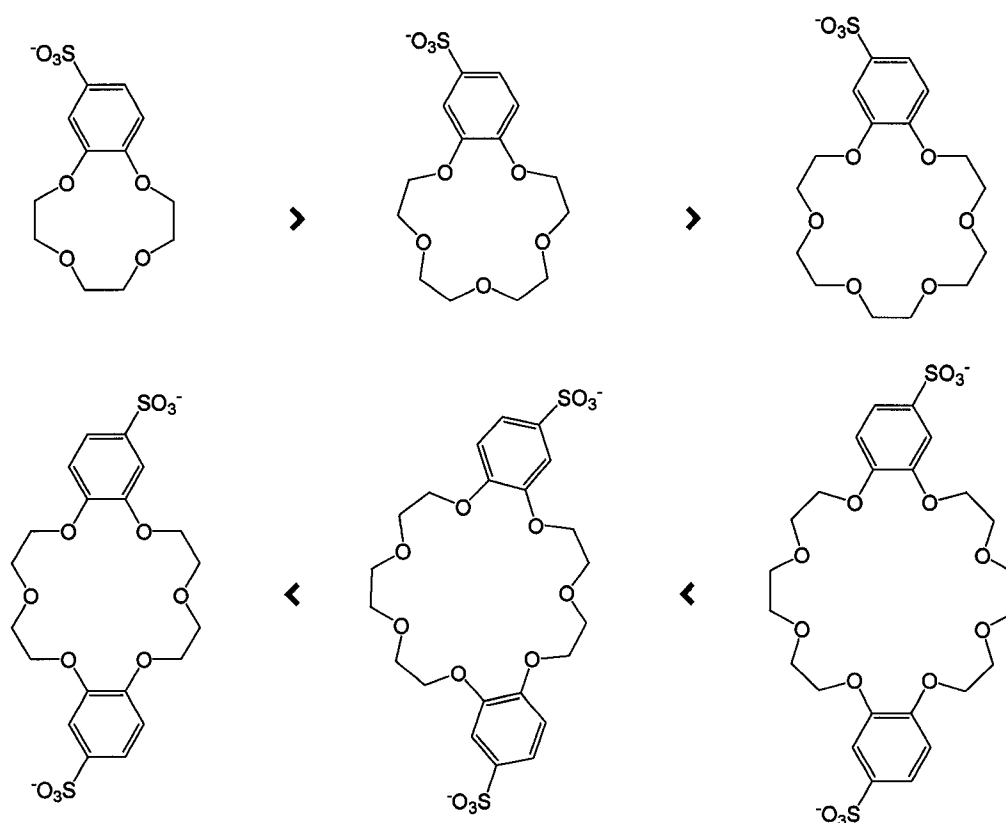
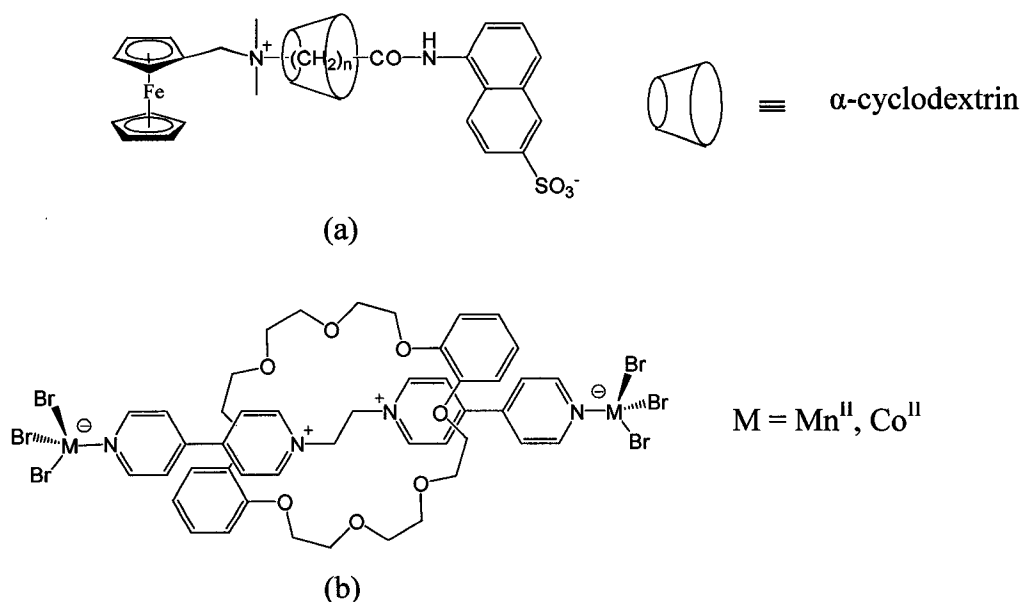


Figure 4.3

Relative lanthanide complex stabilities as a function of cavity size and charge for some sulfonated crown ethers. The dianionic crowns have higher complex stabilities than the monosulfonated corollaries.⁷¹

4.1.3 Zwitterionic Rotaxanes

Many rotaxane or pseudorotaxane motifs involve a cationic component and thus, there is always the requisite counter ion. In some cases, the counter ion can compete for the recognition site via ion-pairing effectively decreasing the observed K_a or destroying the complex completely. From a crystal engineering/materials perspective the counter ions occupy valuable void space, hence removing them would increase the available porosity. For example, following the previous chapter, for the solid state application of molecular machinery it would be advantageous to remove any counter ions from the respective system. Some neutral motifs are known, amongst these the most notable being amide based rotaxanes.⁷⁵ However, to-date, only two examples^{43,76} (Figure 4.4) of a zwitterionic rotaxane have appeared in the literature. Both examples also involve a neutral macrocycle and a zwitterionic thread, and furthermore involve the capping of a cationic thread with a anionic end group. In one case the end group was organic⁷⁶ while in the other, the end group was a metal fragment.⁴³ There have not been any zwitterionic pseudorotaxanes or rotaxanes reported in the literature in which a cationic charge on a thread is compensated for by the anionic charge on the macrocycle or *vice versa*. These supramolecules are not formally zwitterionic, as the two charges are not covalently connected, but for the purposes of this thesis will be referred to as such.

**Figure 4.4**

Two examples of zwitterionic rotaxanes: (a) Kaifer's⁷⁶ naphthalene sulfonate capped rotaxane, (b) Loeb's⁴³ metal-bromide capped zwitterionic rotaxane.

4.1.4 Scope

In this chapter a dianionic crown ether has been combined with four different cationic threads to form the first two examples of a zwitterionic [2]pseudorotaxane and two positively charged [2]pseudorotaxanes. The solution thermodynamics and the solid state structure of these new [2]pseudorotaxanes will be discussed. This study will serve as a model for the reduction of charged molecules (counter ions) in the formation of interlocked molecular species. Furthermore, it will also serve as a model for the effects of crown ether modification on the preparation of [2]pseudorotaxanes.

4.2 Experimental

4.2.1 General Comments

All chemicals were purchased from Aldrich Chemicals and were used as received except 4,4'(5')-diformyldibenzo-24-crown-8 (DFDB24C8), which was prepared by literature methods.⁷⁷ All deuterated solvents were purchased from Cambridge Isotope Laboratories. All solvents were purchased from EM Science. ¹H NMR spectra were recorded on a Brüker Avance 500 instrument locked to the deuterated solvent at 500.1 MHz. All peak positions are listed in ppm relative to TMS.

4.2.2 General Methods for X-ray Crystallography

The crystal was coated in paratone oil inside a cryoloop to prevent loss of solvent. A matrix was run and a unit cell determined prior to collection. A full hemisphere was collected in each case. Reflection data were integrated from frame data obtained from hemisphere scans on a Brüker Apex diffractometer with a CCD area detector with Mo-K_α radiation ($\lambda = 0.71073 \text{ \AA}$). Diffraction data and unit cell parameters were consistent with assigned space groups. The structure was solved direct methods, completed by subsequent Fourier syntheses and refined with full-matrix least-squares methods against $|F^2|$ data. All non-hydrogen atoms were refined anisotropically. All hydrogen atoms were calculated and treated as idealised contributions. Scattering factors and anomalous

coefficients are contained in the SHELXTL 5.03 software package (Sheldrick, G.M., Madison, WI).²⁸ All crystallographic figures were prepared using DIAMOND.²⁹

4.2.3 Preparation of 4,4'(5')-Dibenzylalcohol-24-crown-8 (4a)

NaBH₄ (115 mg, 3.0 mmol) was slowly added to a stirred solution of DFDB24C8 (250 mg, 0.5 mmol) in a 1:1 mixture of CH₂Cl₂:EtOH (100 mL) at 0°C, stirred for 1 hr and then brought to 25 °C over 2 hrs. The mixture was then acidified with HCl (1 M) and extracted with CH₂Cl₂ (3 x 100 mL). The organic layer was washed with NaHCO₃ (1 M) (3 x 50 mL), H₂O (2 x 50 mL), and then dried over MgSO₄. The solvent was removed under vacuum and the off-white solid dried at room temperature. Yield (210 mg) 83 %.

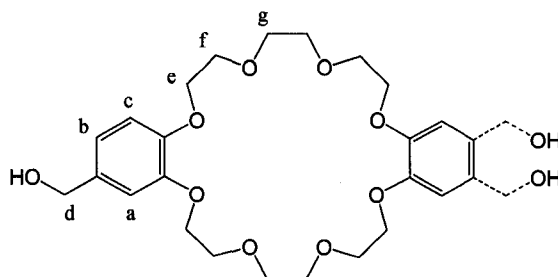


Table 4.1

¹H NMR Spectroscopic Data (CDCl₃, 500 MHz) for **4a**.

Proton	δ (ppm)	Multiplicity	Peak Area	J (Hz)
a	6.916	s	2	
b, c	6.831 – 6.871	m	4	
d	4.593	s	4	
e	4.143 – 4.176	m	8	
f	3.908 – 3.925	m	8	
g	3.828	s	8	

4.2.4 Preparation of 4,4'(5')-Dibromomethyl dibenzo-24-crown-8 (4b)

PBr₃ (70 μL, 0.6 mols) was added to a solution of **4a** (175 mg, 0.3 mols) in dry THF (50 mL) at 0 °C under an atmosphere of N₂. The reaction was stirred for 1 hr after which time CH₂Cl₂ (10 mL) was added to keep the solution homogeneous. After 2 hrs the mixture was warmed to 25 °C and the solvent was removed under vacuum. The resulting white solid was washed with cold EtOH and dried. Yield (188 mg) 88 %.

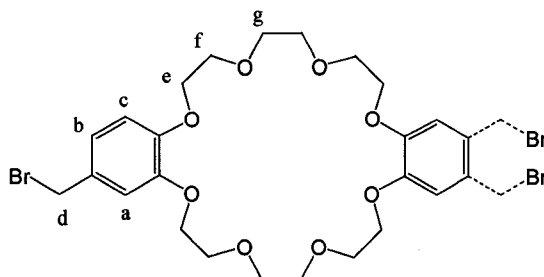


Table 4.2

¹H NMR Spectroscopic Data (CDCl₃, 500 MHz) for **4b**.

Proton	δ (ppm)	Multiplicity	Peak Area	<i>J</i> (Hz)
a, b	6.914 – 6.932	m	4	
c	6.798	d	2	8.0
d	4.466	s	4	
e	4.139 – 4.175	m	8	
f	3.902 – 3.928	m	8	
g	3.821 – 3.827	m	8	

4.2.5 Preparation of the disodium salt of 4,4'(5')-Disulfomethyl dibenzo-24-crown-8 (4c)

An aqueous solution (5 mL) of Na₂SO₃ (310 mg, 2.5 mmol) was added to a solution of **4b** (770 mg, 1.2 mmol) in MeCN (45 mL) and stirred at room temperature for 48 hrs. The precipitate was filtered, washed with cold MeOH and the filtrate collected. The solvent was removed under vacuum and the white solid dried *in vacuo*. Yield (550 mg) 67 %

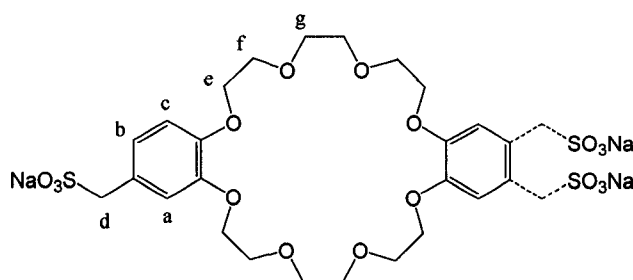


Table 4.3

¹H NMR Spectroscopic Data (D₂O, 500 MHz) for **4c**.

Proton	δ (ppm)	Multiplicity	Peak Area	J (Hz)
a, b, c	7.060 – 7.150	m	6	
d	4.638	s	4	
e	4.283 – 4.314	m	8	
f	3.999 – 4.010	m	8	
g	3.890	s	8	

4.2.6 Preparation of the tetramethylammonium salt of 4,4'(5')-Disulfodibenzo-24-crown-8 (4d)

Concentrated sulfuric acid (0.7 mL, 12.3 mmol) was added to a solution of DB24C8 (2.5 g, 5.6 mmol) in MeCN (40 mL) and then refluxed for 45 min. The solvent was removed under vacuum and an excess of $[\text{Me}_4\text{N}^+][\text{OH}^-]$ (25% in MeOH) was then added to the resulting pink oil. The white precipitate was collected by filtration and recrystallised from MeOH. Yield (3.8 g) 90 %.

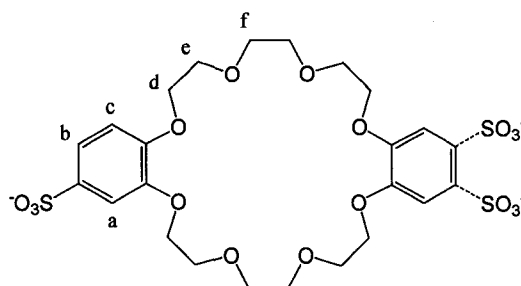


Table 4.4

^1H NMR Spectroscopic Data ($(\text{CD}_3)_2\text{SO}$, 500 MHz) for **4d**.

Proton	δ (ppm)	Multiplicity	Peak Area	J (Hz)
a, b	7.118 – 7.130	m	4	
c	6.867	d	2	8.8
d	4.040 – 4.072	m	8	
e	3.748 – 3.772	m	8	
f	3.664	s	8	
$[\text{N}(\text{CH}_3)_4]^+$	3.090	s	24	

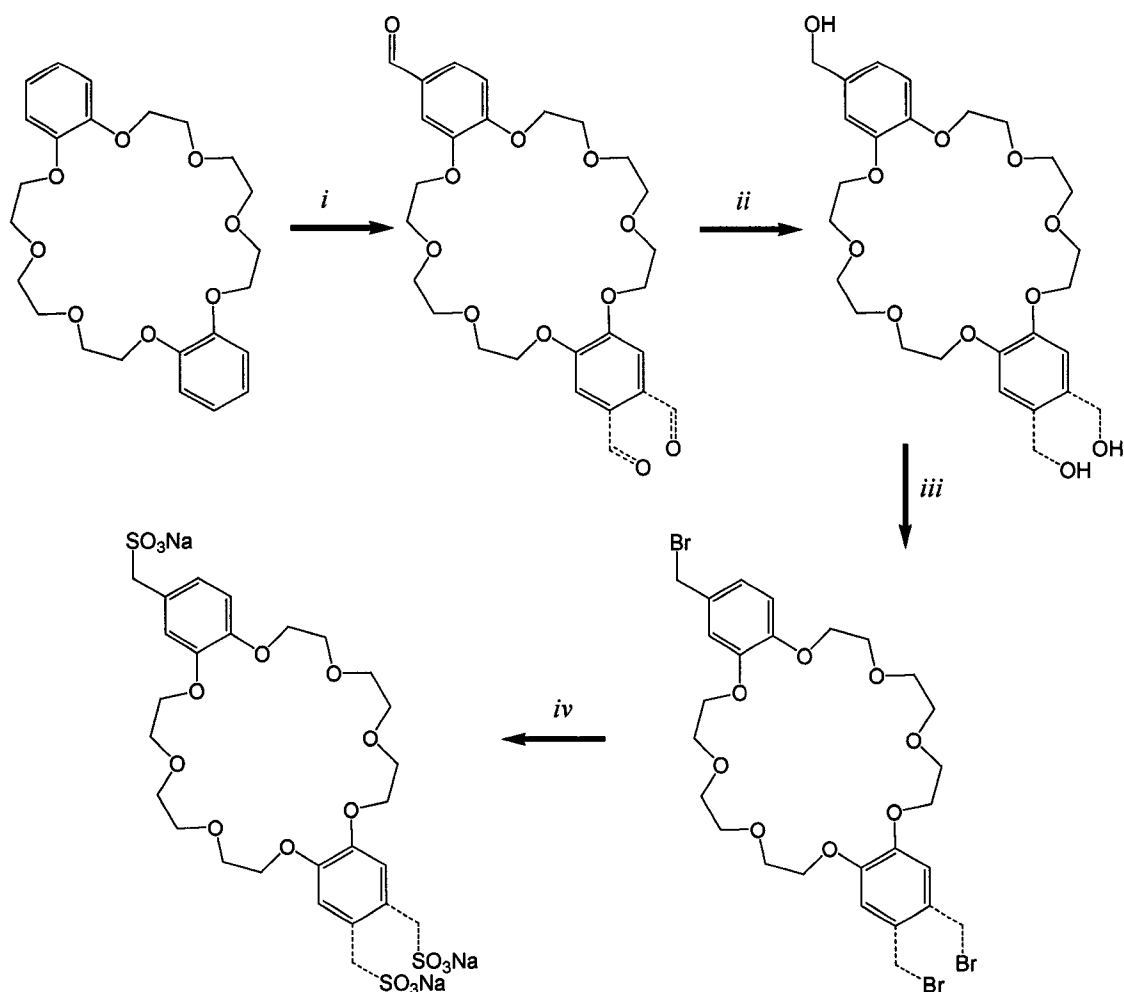
4.2.7 Formation of [2]Pseudorotaxanes

In all cases, except for DED, the thread and **4d** were mixed in a 1:1 ratio at a concentration of 2×10^{-3} M in aqueous deuterated acetic acid (75% CD₃COOD in D₂O). A 2×10^{-3} M solution of DED in aqueous deuterated acetic acid (75% CD₃COOD in D₂O) was titrated with a 0.1 M solution of **4d** from 0.1 equivalents to 3.0 equivalents.

4.2 Results and Discussion

4.3.2 Synthesis of Sulfonated Crown Ethers

4d was synthesised in a single step from DB24C8 (Figure 4.6)⁷¹ while **4c** was prepared in four steps from DB24C8 (Figure 4.5). In each case, the exact conformation of the final product is unknown and is assumed to be a statistical mixture of both the *syn* and *anti* isomers. Any attempt to isolate one conformer or to separate the two was unsuccessful. Due to the symmetrical nature of the ¹H NMR spectra, it was assumed that the two conformers would not greatly affect the recognition site and would not hinder the formation of a [2]pseudorotaxane.

**Figure 4.5**

Synthesis of **4c**: *i*) trifluoroacetic acid, hexmethylenetetramine, 85 – 90 °C, 16 hrs, *ii*) NaBH₄, 0 °C, 3 hrs, *iii*) PBr₃, 0 °C, 3 hrs *iv*) Na₂SO₃, RT, 48 hrs.

4c was the initial dianionic crown synthesised in this project with the idea that the methylene group would give the sulfonate more structural freedom compared to **4d**, while at the same time increasing the solubility in more organic solvents. Preliminary experiments showed that there was a competition between the sodium counter ion and the desired thread. Despite the perceived advantages of **4c**, **4d** was used for all further experiments due to its simple preparation and isolation as the tetramethylammonium salt, a non-competitive counter cation.

The sulfonation of DB24C8 is straight forward through treatment with concentrated sulphuric acid (Figure 4.6). This generates the sulfonic acid, which is converted to the tetramethylammonium salt *in situ* by the addition of tetramethylammonium hydroxide. Sulfonation occurs on only one position of the aromatic ring, it is surmised that sulfonation in a second position does not occur due to the steric hindrance of the triethylene glycol chains of the crown ether.

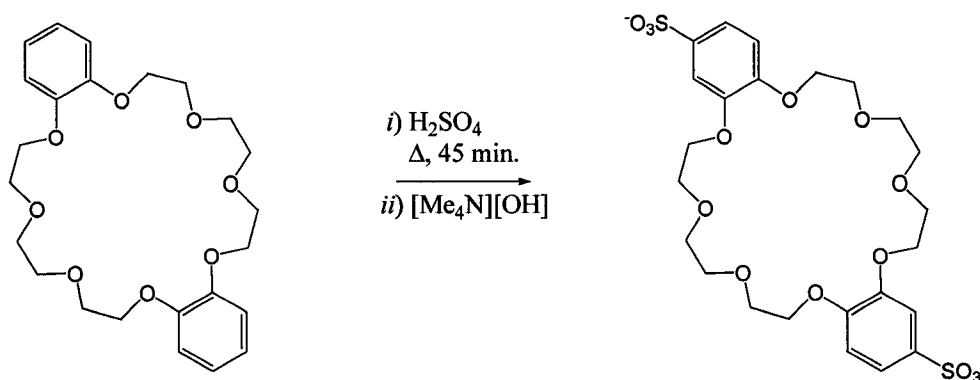


Figure 4.6
Synthesis of **4d**.

The synthesis of all threads has been either previously reported⁶⁴ or described in the previous chapter.

4.3.2 Solution Behaviour of [2]Pseudorotaxanes

The [2]pseudorotaxanes studied herein were prepared by simply combining the desired thread with the appropriate crown in a suitable solvent. Figure 4.7 shows the four [2]pseudorotaxanes that were prepared in this study. Typically, a non-polar solvent such as CH_2Cl_2 or toluene that promotes hydrogen bonding is ideal. However, in this case,

due to the insolubility of the [2]pseudorotaxane complex in such solvents, an aqueous solution of acetic acid was found to be suitable.

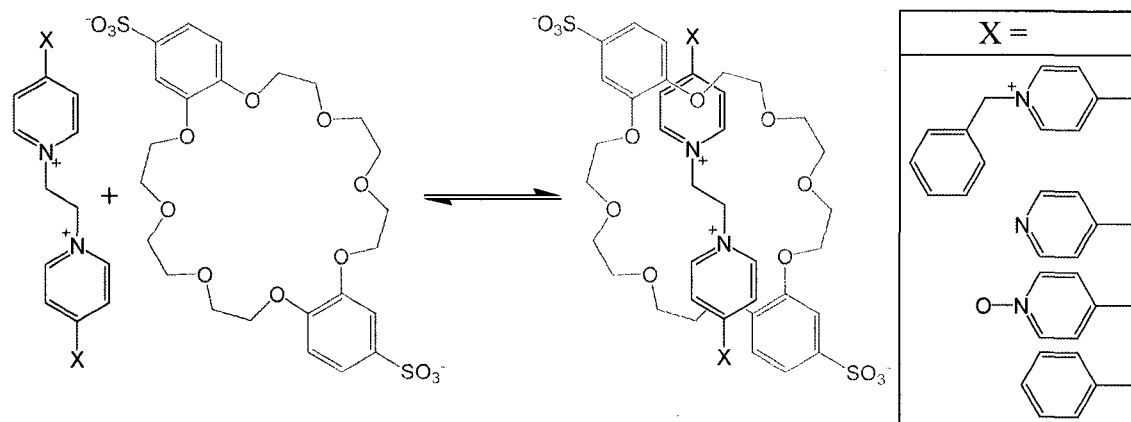


Figure 4.7

Synthetic protocol for the preparation of [2]pseudorotaxanes used in this study.

The formation of a [2]pseudorotaxane is an equilibrium process and as such, the stability of the complex or the association constant, K_a , can be calculated in the following manner:

$$K_a = \frac{[\text{Thread} \subset \text{Crown}]}{[\text{Thread}][\text{Crown}]} \quad \text{Eqn. 4.1}$$

This method works well when the equilibrium process is slow enough that it is possible to see peaks in the ^1H NMR spectrum that can be assigned to both the complexed and uncomplexed forms. In this situation, the solution concentration of all species can be determined by the relative peak areas. However, if the process is fast on the NMR timescale, only a single peak will be observed at a weight averaged chemical shift. In this case, the K_a can be calculated by a non-linear least-squares refinement program such as EQNMR which uses NMR titration data and the following equation:⁷⁸

$$\delta_{\text{calc}} = \frac{\delta_{\text{uc}}[\text{Thread}]_{\text{uc}}}{[\text{Thread}]_{\text{total}}} + \frac{\delta_{\text{c}}K_a[\text{Thread}]_{\text{uc}}[\text{Crown}]_{\text{uc}}}{[\text{Thread}]_{\text{total}}} \quad \text{Eqn. 4.2}$$

Of the four [2]pseudorotaxanes presently studied, only the formation of DED \subset **4d** was fast on the NMR timescale. The titration data used to calculate the association constant is represented graphically in Figure 4.8.

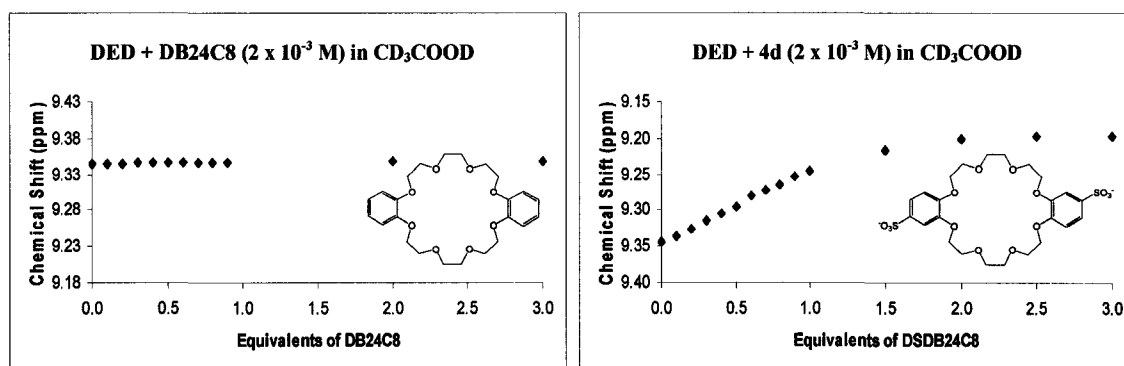


Figure 4.8

Graphical representation of the change in chemical shift of the α -pyridinium hydrogen as a function of crown ether concentration in CD₃COOD_{aq} at 500 MHz.

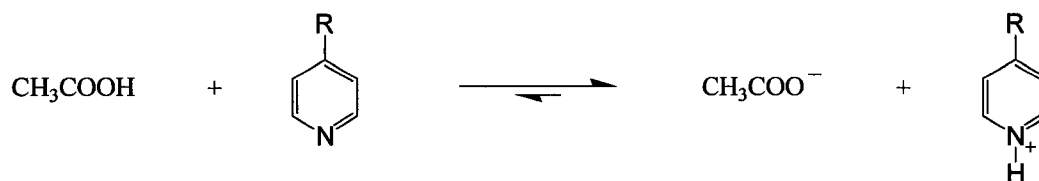
Due to solvent effects, it is difficult to directly compare the association constants between similar threads and either DB24C8 or **4d** (Table 4.5). With the idea that the added electrostatic component would greatly increase the solution stability of the [2]pseudorotaxane complex, a method of comparing the stabilities between the “standard” [2]pseudorotaxane complex, DED \subset DB24C8, and the new series of [2]pseudorotaxanes incorporating the sulfonated crown, **4d**, was needed. In CD₃COOD_{aq}, there is no association between DB24C8 and DED as is evidenced in Figure 4.8. Although this still does not allow for a direct comparison, it does show that in CD₃COOD_{aq} any observable association is a considerable improvement.

Table 4.5

Comparison of association constants for [2]pseudorotaxanes containing **4d** and DB24C8.

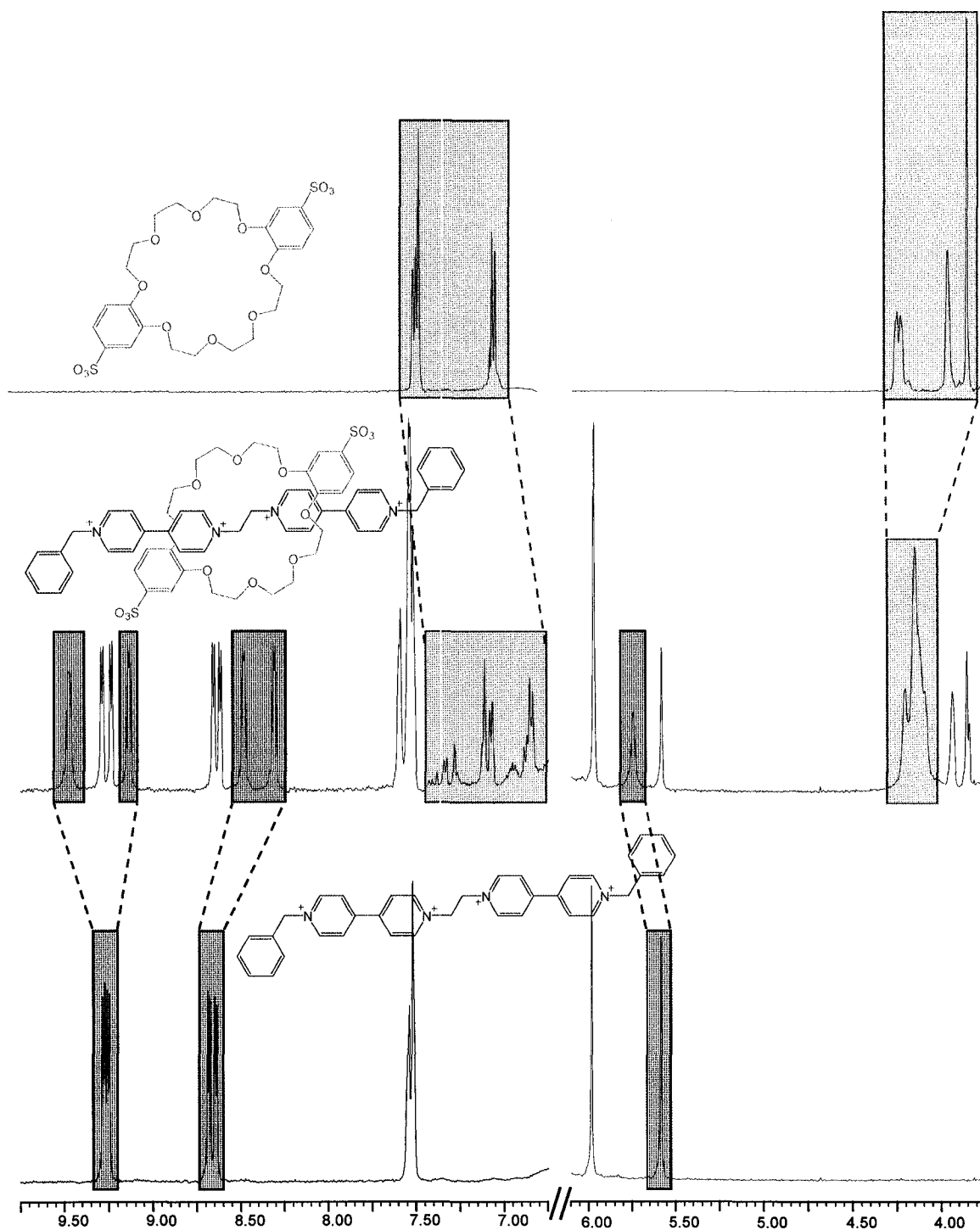
4d		DB24C8	
Thread in CD ₃ COOD	K_a (M ⁻¹)	Thread in CD ₃ CN	K_a (M ⁻¹)
(PhPy) ₂ Et	31	(PhPy) ₂ Et	387
O2DED	N/A	O2DED	1125
DED	1301	DED	878
Bz ₂ DED	1870	Bz ₂ DED	1256

There are several necessary considerations when using acetic acid as a solvent. First, the pK_a of CH₃COOH is 4.76 and the pK_a of an aryl sulfonic acid is ~ -6.5 .⁷⁹ Hence, the sulfonate is expected to remain unprotonated and continue to act as an anion in the [2]pseudorotaxane complex. However, the nitrogens on the terminal pyridines of DED will tend to be in the protonated form as the pK_a of the pyridinium cation is ~ 5.2 (Figure 4.9). Therefore, in acetic acid, DED \subset **4d** is not zwitterionic as the thread is 4⁺ while the crown is 2⁻. However, it was thought that the extra positive charges on the thread would increase the electrostatic association. Indeed, (4-PhPy)₂Et \subset **4d** has a K_a of 31 M⁻¹; much lower than expected when considering the difference between DED \subset DB24C8 and (PhPy)₂Et \subset DB24C8, indicating that the 4⁺ charge on the thread helps to stabilise the [2]pseudorotaxane complex. Along these lines of reasoning, it was expected that Bz₂DED would also have an increased K_a due to the four pyridinium cations present in the thread.

**Figure 4.9**

The acid/base equilibrium that exists between acetic acid and a pyridine. Given that the concentration of CH_3COOH is much larger than the concentration of the pyridine and that the $\text{p}K_a$ of acetic acid is lower than that of pyridinium the equilibrium is shifted to the right.

Despite the high polarity and competitive nature of acetic acid, hydrogen bonding between the acidic α -pyridinium and ethylene hydrogens on the thread and the oxygen atoms of the crown exist as evidenced by the downfield shift of these peaks in the ^1H NMR spectra. The upfield shifts of the other aromatic thread and crown protons and the observed yellow colour in solution indicate that there is a π -stacking component to the complex formation. Figure 4.10 shows the observed changes in chemical shift between the “free” components and the “complexed” supramolecule.

**Figure 4.10**

^1H NMR spectra showing the uncomplexed crown (top) and thread (bottom) and $\text{Bz}_2\text{DED} \subset \mathbf{4d}$ (middle) at 500 MHz in $\text{CD}_3\text{COOD}_{aq}$. In the [2]pseudorotaxane spectrum, the peaks due to the complexed form are highlighted.

By calculating the association constants at various temperatures the thermodynamic parameters ΔG° , ΔH° , and ΔS° can be extracted by a van't Hoff analysis:

$$\Delta G^\circ = -RT \ln K_a = \Delta H^\circ - T\Delta S^\circ \quad \text{Eqn. 4.3}$$

The van't Hoff plot given in Figure 4.11 shows a linear fit following equation 4.3 and over a small temperature range, can be assumed to be correct. However, there is a slight variation with temperature of the association constant resulting in a non-linear relationship. In this case, there is a non-negligible heat capacity and can be modeled following the method of Dougherty⁸⁰ in which the standard van't Hoff analysis is modified to consider this effect:

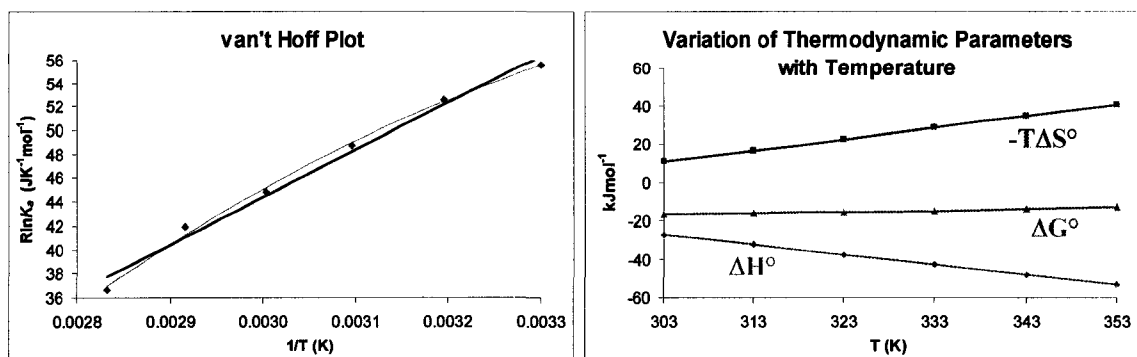
$$\Delta H^\circ = \Delta H_0 + T\Delta C_p^\circ \quad \text{Eqn. 4.4}$$

$$\Delta S^\circ = \Delta S_0 + \Delta C_p^\circ \ln T \quad \text{Eqn. 4.5}$$

Substituting equation 4.4 and 4.5 into equation 4.3 gives:

$$R \ln K_a = -\left(\frac{\Delta H_0}{T}\right) + \Delta C_p^\circ \ln T + (\Delta S_0 - \Delta C_p^\circ) \quad \text{Eqn. 4.6}$$

This modified equation now fits the data better ($R = 0.9963$) compared to the standard van't Hoff analysis ($R = 0.9873$). Considering heat capacity, the thermodynamic parameters can be plotted against temperature as in Figure 4.11, the resulting plot shows that in the available temperature range, dependent upon the solvent, the formation of $\text{Bz}_2\text{DED} \subset \mathbf{4d}$ is enthalpic in nature.

**Figure 4.11**

Van't Hoff plot with a linear fit (dark blue) and Dougherty's⁸⁰ best fit (pink) and a plot of the thermodynamic parameters for the [2]pseudorotaxane formation of $\text{Bz}_2\text{DED} \subset \mathbf{4d}$. In the experimental temperature range, the [2]pseudorotaxane formation is primarily enthalpic in nature.

4.3.3 Solid State Structure of $\mathbf{3b} \subset \mathbf{4d}$

If the two components are combined in a 1:1 ratio in H_2O , the [2]pseudorotaxane will crystallise overnight in *quantitative* yields. Single crystals suitable for X-ray diffraction were grown by combining $\mathbf{3b}$ and $\mathbf{4d}$ in H_2O at 40°C .

Table 4.6Crystal data and details of structure solution and refinement for **3b** \subset **4d**.

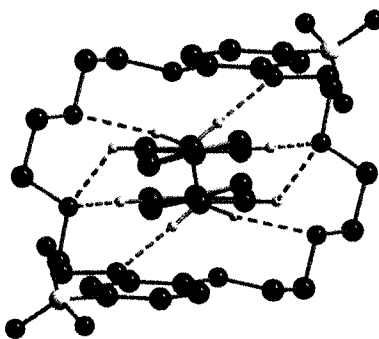
Formula	C ₄₆ H ₇₀ N ₄ O ₂₆ S ₂	Collection Temp [K]	273(2)
Formula Weight	1159.18	ρ_{calcd} [g cm ⁻³]	1.397
Crystal System	Monoclinic	μ (MoK α) [mm ⁻¹]	0.186
Space Group	<i>P2(1)/n</i>	Min/max trans	0.8995/1.0000
a [Å]	12.191(6)	Unique data	21721
b [Å]	18.702(9)	R(int)	0.0466
c [Å]	13.087(6)	R1 [I > 2 σ I]	0.0593
α [°]	90	R1 [all data]	0.0752
β [°]	112.518(9)	wR2 [I > 2 σ I]	0.1620
γ [°]	90	wR2 [all data]	0.1741
V [Å ³]	2756(2)	Data/variables	4853/352
Z	2	Goodness-of-fit	1.040

The solid state structure (Figure 4.12) clearly shows the interpenetrated nature of the [2]pseudorotaxane complex, providing evidence for the observed solution state behaviour. Also evident are all of the intermolecular, non-covalent interactions between the thread and the crown, including eight C–H...O hydrogen bonds (Table 4.7) and the two N⁺...O^{δ-} ion dipole interactions.

Table 4.7Hydrogen bond distances and angles in **3b** \subset **4d**.

Hydrogen Bonded Atoms	C–H...O Distances (Å)	C–H...O Angles (°)
H8A...O6	2.351(3)	154.94(21)
H9A...O6	2.687(8)	135.37(21)
H11A...O7	2.575(5)	163.15(19)
H11B...O5	2.776(3)	150.88(20)

It was thought that addition of the sulfonate group directly to the aromatic ring of the crown, as compared with removal of the sulfonate group from the ring by a methylene carbon, might, through sterics, hinder the penetration of the crown by a *bis*-pyridinium dication. As is evident from the X-ray structure, this is not the case as the sulfonate functionalities are directed away from the interior of the crown and hence penetration by the thread is not impeded (Figure 4.12).

**Figure 4.12**

Ball and stick depiction of **3b** \subset **4d** as viewed down the thread axis. The sulfonate groups do not sterically interfere with recognition site. Key: blue = N, black = C; red = O; yellow = S; white = H. Selected hydrogen atoms have been omitted for clarity.

In the solid state structure of **3b** \subset **4d** the thread is slightly offset from the axis of the crown so as to maximise the hydrogen bonding interactions between the α -pyridinium

hydrogens on the thread and the oxygen atoms of the crown. The structure of **3b** \subset **4d** has the same conformation (Figure 4.13), thus supporting the suggestion that the sulfonate group does not sterically interfere with the formation of a [2]pseudorotaxane.

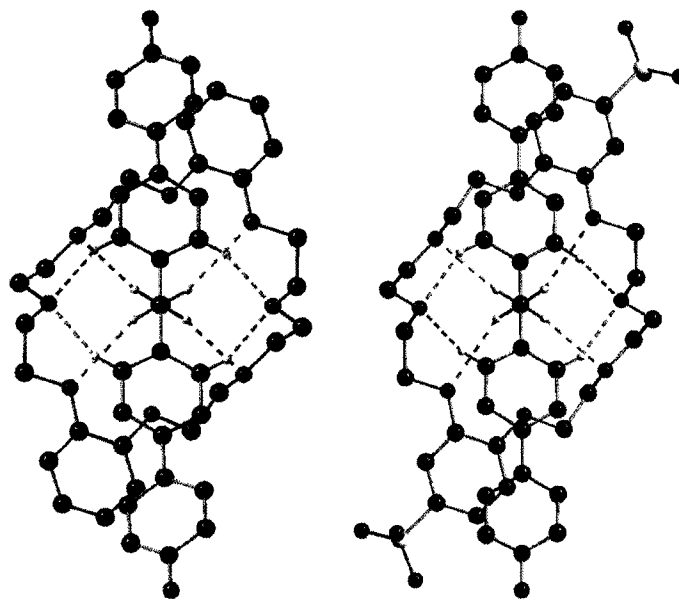


Figure 4.13

Comparison of the solid state structures of **3b** \subset DB24C8 and **3b** \subset **4d**, showing the eight hydrogen bonds between the crown and the thread. Key: blue = N, black = C; red = O; yellow = S; white = H. Selected hydrogen atoms and anions are omitted for clarity.

A major impetus for the use of a negatively charged crown ether was the formation of a formally neutral [2]pseudorotaxane. The anionic, terminal sulfonate groups on the crown ether balance the cationic charge of the pyridinium nitrogens. The packing diagram (Figure 4.14) shows that the sulfonate of one [2]pseudorotaxane interacts with the pyridinium nitrogen of an adjacent [2]pseudorotaxane.

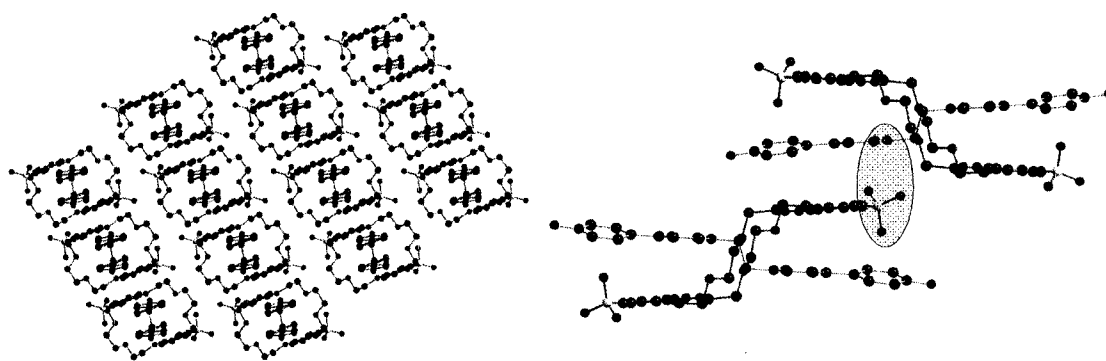


Figure 4.14

Packing diagrams of **3b** \subset **4d**. Highlighted is the intermolecular ion pairing (~ 3.5 Å). Key: blue = N, black = C; red = O; yellow = S; white = H. Hydrogen atoms and solvent molecules omitted for clarity.

4.4 Conclusions

An extra supramolecular interaction has been successfully added to the pseudorotaxane motif currently being used in the Loeb group. The added electrostatic component increases the K_a relative to the corresponding system in which there are no electrostatic considerations. Furthermore, the addition of an anionic component to the crown ether has allowed for the first observation of a zwitterionic [2]pseudorotaxane complex.

The solid state structure is in agreement with the observed shifted resonances in the ^1H NMR and confirms the solution evidence that the bis(pyridinium) thread penetrates the cavity of the 24 membered crown ether. Also evident, in the solid state, are all of the non-covalent interactions that allow for the formation of the [2]pseudorotaxane complex, namely, eight C–H \cdots O hydrogen bonds, two N $^+$ \cdots O $^{\delta-}$ ion dipole interactions, and the electrostatic attraction between the sulfonate anions and the pyridinium cations.

The use of a sulfonated crown ether in combination with the bis(pyridinium) thread expands the scope and utility of this supramolecular motif. It is now possible to self-assemble these [2]pseudorotaxanes in competitive, polar solvents (such as CH₃COOH and H₂O), allowing for application in a increased array of further chemical transformations. In addition, the removal of ancillary anions is attractive from a crystal engineering/materials perspective in that solids can now be generated in which accessible void space would not be occupied by required counter ions.

References

1. Steed, J. W.; Atwood, J. L. *Supramolecular Chemistry*; John Wiley and Sons: New York, 2000
2. Pedersen, C. J. *Angew. Chem. Int. Ed.* **1988**, *27*, 1021
3. Lehn, J. M. *Angew. Chem. Int. Ed.* **1988**, *27*, 89.
4. Cram, D. J. *Angew. Chem. Int. Ed.* **1988**, *27*, 1009.
5. Yaghi, O. M.; O'Keefe, M.; Ockwing, N. W.; Chae, H. K.; Eddaoudi, M.; Kim, J. *Nature* **2003**, *423*, 705.
6. Results from a search using the Cambridge Structural Database on July 9, 2004 using CONQUEST v. 1.6.
7. Khlobystov, N. A.; Blake, A. J.; Champness, N. J.; Lemenovskii, D. A.; Majouga, A. G.; Zyk, N. V.; Schröder, M. *Coord. Chem. Rev.* **2001**, *222*, 155.
8. Kitagawa, S.; Kitaura, R.; Noro, S. *Angew. Chem. Int. Ed.* **2004**, *43*, 2334.
9. Roesky, H. W.; Andruh, M. *Coord. Chem. Rev.* **2003**, *236*, 91.
10. Su, C. Y.; Kang, B. S.; Yang, Q. C.; Mak, T. C. W. *J. Chem. Soc. Dalton Trans.* **2000**, *12*, 1857.
11. Gillon, A. L.; Lewis, G. R.; Orpen, A. G.; Rotter, S.; Starbuck, J.; Wang, X. M.; Rodriguez-Martin, Y.; Ruiz-Pérez, I. C. *J. Chem. Soc. Dalton Trans.* **2000**, *21*, 3897.
12. *Sulfoxides, Amines, Amine Oxides and Related Ligands*; Goggin, P. L. Comprehensive Coordination Chemistry Series; Wilkinson, G. Ed. Pergamon: New York, 1987, Vol. 2.

-
13. Long, D.; Blake, A. J.; Champness, N. R.; Wilson, C.; Schröder, M. *J. Am. Chem. Soc.* **2001**, *123*, 3401.
 14. Long, D.; Blake, A. J.; Champness, N. R.; Schröder, M. *Chem. Commun.* **2000**, *15*, 1369.
 15. Tanase, S.; Andruh, M.; Müller, A.; Schmidtman, M.; Mathonière, C.; Rombaut, G. *Chem. Commun.* **2001**, *12*, 1084.
 16. Long, D.; Blake, A. J.; Champness, N. R.; Wilson, C.; Schröder, M. *Chem. Eur. J.* **2002**, *9*, 2026.
 17. Long, D.; Blake, A. J.; Champness, N. R.; Wilson, C.; Schröder, M. *Angew. Chem. Int. Ed.* **2001**, *13*, 2443.
 18. Long, D.; Hill, R. J.; Blake, A. J.; Champness, N. R.; Hubberstey, P.; Proserpio, D. M.; Wilson, C.; Schröder, M. *Angew. Chem. Int. Ed.* **2004**, *43*, 1851.
 19. Long, D.; Blake, A. J.; Champness, N. R.; Schröder, M. *Chem. Commun.* **2000**, *22*, 2273.
 20. Ma, B.; Gao, S.; Sun, H.; Xu, G. *J. Chem. Soc. Dalton Trans.* **2001**, *2*, 130.
 21. Brunner, H.; Störiko, R.; Rominger, F. *Eur. J. Inorg. Chem.* **1998**, *6*, 771.
 22. Lin, W.; Evans, O. R.; Xiong, R.; Wang, Z. *J. Am. Chem. Soc.* **1998**, *120*, 13272.
 23. Lin, W.; Wang, Z.; Ma, L. *J. Am. Chem. Soc.* **1999**, *121*, 11249.
 24. Lin, W.; Ma, L.; Evans, O. R. *Chem. Commun.* **2000**, *22*, 2263.
 25. Evans, O. R.; Lin, W. *Inorg. Chem.* **2000**, *39*, 2189.

-
26. Evans, O. R.; Xiong, R.; Wang, Z.; Lin, W. *Angew. Chem. Int. Ed.* **1999**, *38*, 536.
27. Lu, T.; Luck, R. L. *Inorg. Chim. Acta.* **2003**, *351*, 345.
28. SHELXTL 5.03 Program Library, Siemens Analytical Instrument Division, Madison, WI, USA, **1997**.
29. DIAMOND–Visual Crystal Structure Information System CRYSTAL IMPACT, Postfach 1251, D-53002 Bonn.
30. (a) Calculation completed using HF/6-31G(d) level of theory. (b) Spartan'02 Wavefunction, Inc. Irvine, CA. (c) Kong, J.; White, C. A.; Krylov, A. I.; Sherrill, C. D.; Adamson, R. D.; Furlani, T. R.; Lee, M. S.; Lee, A. M.; Gwaltney, S. R.; Adams, T. R.; Ochsenfeld, C.; Gilbert, A. T. B.; Kedziora, G. S.; Rassolov, V. A.; Maurice, D. R.; Nair, N.; Shao, Y.; Besley, N. A.; Maslen, P. E.; Dombroski, J. P.; Daschel, H.; Zhang, W.; Korambath, P. P.; Baker, J.; Byrd, E. F. C.; Van Voorhis, T.; Oumi, M.; Hirata, S.; Hzu, C.-P.; Ishikawa, N.; Florian, J.; Warshel, A.; Johnson, B.G.; Gill, P. M. W.; Head-Gordon, M.; Pople, J.A. *J. Computational Chem.* **2000**, *21*, 1532.
31. Eddaoudi, M.; Moler, D. B.; Li, H.; Chen, B.; Reineke, T. M.; O'Keefe, M.; Yaghi, O. M. *Acc. Chem. Res.* **2001**, *34*, 319.
32. Guo, D.; Duan, C.; Lu, F.; Hasegawa, Y.; Meng, Q.; Yanagida, S. *Chem. Commun.* **2004**, *13*, 1486.
33. Albrecht, M.; Lutz, M.; Spek, A. L.; van Koten, G. *Nature* **2000**, *406*, 970.
34. Harrison, I. T.; Harrison, S. J. *J. Am. Chem. Soc.* **1967**, *89*, 5723.
35. Rowan, S. J.; Stoddart, J. F. *Polym. Adv. Technol.* **2002**, *13*, 777.

-
36. Consuelo-Jiménez, M.C.; Dietrich-Buchecker, C.; Sauvage, J. P.; De Cian, A. *Angew. Chem. Int. Ed.* **2000**, *39*, 1295.
37. Ashton, P.R.; Baxter, I.; Fyfe, M. C. T.; Raymo, F. M.; Spencer, N.; Stoddart, J. F.; White, A. J. P.; Williams, D. J.; *J. Am. Chem. Soc.* **1998**, *120*, 2297.
38. Gibson, H. W.; Bheda, M. C.; Engen, P. T. *Prog. Polym. Sci.* **1994**, *19*, 843.
39. Ashton, P. R.; Grognoz, M.; Slawin, A. M. Z.; Stoddart, J. F.; Williams, D. J. *Tetrahedron Lett.* **1991**, *32(43)*, 6235.
40. Loeb, S. J.; Wisner, J. A. *Angew. Chem. Int. Ed.* **1998**, *37*, 2838.
41. Loeb, S. J.; Wisner, J. A. *Chem. Commun.* **1998**, *24*, 2757.
42. Solladié, N.; Chambron, J. C.; Sauvage, J. P. *J. Am. Chem. Soc.* **1999**, *121*, 3684.
43. Davidson, G. J. E.; Loeb, S. J.; Parekh, N. A.; Wisner, J. A. *J. Chem. Soc., Dalton Trans.* **2001**, *21*, 3135.
44. Lyon, A. P.; Macartney, D. H. *Inorg. Chem.* **1997**, *36*, 729.
45. Chambron, J. C.; Collin, J. P.; Dalbavie, J. O.; Dietrich-Buchecker, C. O.; Heitz, V.; Odobel, F.; Solladié, N.; Sauvage, J. P. *Coord. Chem. Rev.* **1998**, *178-180*, 1299.
46. Baer, A. J.; Macartney, D. H. *Inorg. Chem.* **2000**, *39*, 1410.
47. Chichak, K.; Walsh, M. C.; Branda, N. R. *Chem. Commun.* **2000**, *10*, 847.
48. Ogino, H.; Ohata, K. *Inorg. Chem.* **1984**, *23*, 3312.
49. Ogino, H. *J. Am. Chem. Soc.* **1981**, *103*, 1303.
50. Chambron, J. C.; Heitz, V.; Sauvage, J. P. *J. Am. Chem. Soc.* **1993**, *115*, 12378.

-
51. Wylie, R. S.; Macartney, D. H. *J. Am. Chem. Soc.* **1992**, *114*, 3136.
 52. Macartney, D. H.; Waddling, C. A. *Inorg. Chem.* **1994**, *33*, 5912.
 53. Gunter, M. J.; Bampos, N.; Johnstone, K. D.; Sanders, J. K. M. *New J. Chem.* **2001**, *25*, 166.
 54. Moulton, B.; Zaworotko, M. J. *Chem. Rev.* **2001**, *101*, 1629.
 55. Kidd, T. J.; Loontjens, T. J. A.; Leigh, D. A.; Wong, J. K. *Angew. Chem. Int. Ed.* **2003**, *42*, 3379.
 56. Whang, D.; Kim, K. *J. Am. Chem. Soc.* **1997**, *119*, 451.
 57. Kim, K. *Chem. Soc. Rev.* **2002**, *31*, 96.
 58. Lee, E.; Kim, J.; Heo, J.; Whang, D.; Kim, K. *Angew. Chem. Int. Ed.* **2001**, *40*, 399.
 59. Lee, E.; Heo, J.; Kim, K. *Angew. Chem. Int. Ed.* **2000**, *39*, 2699.
 60. Park, K. M.; Whang, D.; Lee, E. Heo, J.; Kim, K. *Chem. Eur. J.* **2002**, *8*, 498.
 61. Hoskins, B. F.; Robson, R.; Slizys, D. A. *J. Am. Chem. Soc.* **1997**, 2952.
 62. Batten, S. R.; Robson, R. *Angew. Chem. Int. Ed.* **1998**, *37*, 1460.
 63. Davidson, G. J. E.; Loeb, S. J. *Angew. Chem. Int. Ed.* **2003**, *42*, 74.
 64. Loeb, S. J.; Tiburcio, J.; Wisner, J. A. *Chem. Eur. J.* in press.
 65. Wells, A. F. *Three-Dimensional Nets and Polyhedra*, Wiley, New York, **1977**.
 66. Bu, X. H.; Weng, W.; Li, J. R.; Chen, W.; Zhang, R. H. *Inorg. Chem.* **2002**, *41*, 413
 67. Li, J. R.; Bu, X. H.; Zhang, R. H. *Inorg. Chem.* **2004**, *43*, 237
 68. Aeschylus (525-456 v. Chr.): *Choephoren*.
 69. Pedersen, C. J. *J. Am. Chem. Soc.* **1967**, *89*, 7017.

-
70. Dietrich, B.; Viout, P.; Lehn, J. M. *Macrocyclic Chemistry*, VCH, New York, **1993**.
71. Sasaki, T.; Umetani, S.; Matsui, M.; Tsurubou, S.; Kimura, T.; Yoshida, Z. *Bull. Chem. Soc. Jpn.* **1998**, *71*, 371.
72. Umetani, S.; Sasaki, T.; Matsui, M.; Tsurubou, S.; Kimura, T.; Yoshida, Z. *Anal. Sci.* **1997**, *13*(Suppl., Asianalysis IV), 123.
73. Sasaki, T.; Umetani, S.; Le, Q. T. H.; Matsui, M.; Tsurubou, S. *Analyst* **1996**, *121*, 1051.
74. de Jong, F.; van Zon, A.; Reinhoudt, D. N.; Torny, G. J.; Tomassen, H. P. M. *Recl. Trav. Chim. Pays-Bas* **1983**, *102*, 164.
75. Vögtle, F.; Dünwald, T.; Schmidt, T. *Acc. Chem. Res.* **1996**, *29*, 451.
76. Isnin, R.; Kaifer, A. *J. Am. Chem. Soc.* **1991**, *113*, 8188.
77. Wada, F.; Hirayama, H.; Namiki, H.; Kikukawa, K.; Matsuda, T. *Bull. Chem. Soc. Jpn.* **1980**, *53*, 1473.
78. Hynes, M. J. *J. Chem. Soc., Dalton Trans.* **1993**, 311.
79. March, J. *Advanced Organic Chemistry* John Wiley & Sons, New York, **1992**.
80. Stauffer, D. A.; Barrans Jr., R. E.; Dougherty, D. A. *J. Org. Chem.* **1990**, *55*, 2762.

Curriculum Vitae

Name	Dennis J. Hoffart
Date of Birth	November 15, 1978
Place of Birth	Calgary, Alberta, Canada
Education	B.Sc., Chemistry, 2002 University of Calgary
	M.Sc., Chemistry, 2004 University of Windsor
Professional Work History	Teaching Assistant University of Windsor, Windsor, Ontario, Canada Sept., 2002 – April, 2004
	Research Assistant University of Windsor, Windsor, Ontario, Canada Sept., 2002 – Sept. 2004
	Research Assistant University of Calgary, Calgary, Alberta, Canada April 2000 – July 2002
Scholarships And Awards	University of Windsor Tuition Scholarship (2004) CCMR Fellowship (2002 -2004)
Publications in Refereed Journals	D. J. Hoffart, A. P. Côté, and G. K. H. Shimizu*, “An Adamantane-Based Coordination Framework with the First Observation of Discrete Metal Sulfonate Clusters.”, <i>Inorg. Chem.</i> 2003 , (43), 8603-8605.

-
- Conference Presentations
- D. J. Hoffart and S. J. Loeb*, *Coordination Chemistry of a Pyridine-Pyridine N-oxide Ligand*, Inorganic Discussion Weekend, Hamilton, ON, October 2003.
- D. J. Hoffart and S. J. Loeb*, *The Design of Multi-Dimensional, Metal-Based Polyrotaxanes*, CIC 2003, Ottawa, ON, August 2003.
- A. P. Côté, D. J. Hoffart, and G. K. H. Shimizu*, *Ligand Directed Dimensionality in Barium Sulfonate Coordination Networks*, CIC 2003, Ottawa, ON, August 2003.
- D. J. Hoffart and G. K. H. Shimizu*, *Hybrid Inorganic-Organic Architectures Based Upon a Tetrahedrally Symmetric, Poly-Sulfonated Ligand*, CIC 2002, Vancouver, BC, June 2002.
- D. J. Hoffart and G. K. H. Shimizu*, *Porous Networks Based on a Tetrahedrally Symmetric Ligand*, Western Canadian Undergraduate Chemistry Conference, Calgary, AB, May 2002.
- D. J. Hoffart and G. K. H. Shimizu*, *Tetra-anionic Ligand in the Design of Extended Metal – Organic Frameworks*, Alberta, and British Columbia Inorganic Discussion Weekend 2001, Prince George, BC, July 2001.